Muscle Fatigue in Musculoskeletal Numerical Models

Dissertation
zur Erlangung des Doktorgrades
der Humanwissenschaften
(Dr. sc. hum.)

der
Fakultät für Medizin
der Universität Regensburg

vorgelegt von
Simon J. Groß
aus
Straubing

im Jahr
2018

Muscle Fatigue in Musculoskeletal Numerical Models

Dissertation
zur Erlangung des Doktorgrades
der Humanwissenschaften
(Dr. sc. hum.)

der
Fakultät für Medizin
der Universität Regensburg

vorgelegt von
Simon J. Groß
aus
Straubing

im Jahr
2018

Dekan:	Prof. Dr. Dr. Torsten E. Reichert
Betreuer:	Prof. Dr.-Ing Sebastian Dendorfer
Tag der mündlichen Prüfung:	

Abstract

The investigation of the musculoskeletal system is a challenging task, since comprehensive knowledge of muscle and joint forces within the human body is required. Therefore, in recent years numerical models have been developed for a better understanding of the musculoskeletal system. Especially for the investigation of long-term effects, the issue of muscle fatigue needs to be taken into consideration in these models.

The objectives of this thesis was to develop a novel EMG based muscle fatigue algorithm and the implementation into a state-of-the-art musculoskeletal modelling system. This included the investigation of the progress of muscle fatigue of single muscles, as well as the behaviour of muscle recruitment pattern when experiencing fatigue.

Therefore, two experimental studies were conducted in the course of this thesis, in order to analyse the progress of muscle fatigue of single muscles in correlation with relative muscle loadings and to study the behaviour of muscle recruitment pattern of thorax muscles when experiencing fatigue. Based on the results of the first study a fatigue algorithm was developed and implemented to the AnyBody Modeling System^{TM} (AMS). Both experimental studies were simulated in the altered AMS to validate the fatigue algorithm and to analyse the behaviour of the muscle recruitment solver of the modified system.

The results show a good correlation between the simulated muscle fatigue and the experimental data. Furthermore, it revealed a reduction of maximum force capacity of the muscles of about 10-15 % compared to the non-fatigued condition. The analysis of the muscle recruitment pattern indicated an additional activation of muscles in the upper back as well as the abdomen. The numerical simulation of these exercises in the AMS revealed a shift of muscle activity to the upper back.

Kurzfassung

Die Untersuchung des muskuloskeletalen Apparates ist eine große Herausforderung, da hierzu möglichst genaue Kenntnisse von Muskel- und Gelenkkräften benötigt werden. Daher wurden in den letzten Jahren numerische Modelle entwickelt, um einen genaueren Einblick in das muskuloskeletale System zu erhalten. Insbesondere um eine Aussage über Langzeiteffekte machen zu können, muss die Ermüdung von Muskeln berücksichtigt werden.

Ziel dieser Arbeit war die Entwicklung eines neuartigen Ermüdungsalgorithmus basierend auf EMG Messungen. Dies beinhaltete die Untersuchung des Verlaufs der Ermüding einzelner Muskeln, sowie deren Einflusses auf Rekrutierungsmuster. Des Weiteren wurde dieser Algorithmus in ein modernes muskuloskeletales Berechnungssystem implementiert.

Im Zuge dieser Arbeit wurden zwei experimentelle Studien durchgeführt, um den Verlauf von Muskelermüdung einzelner Muskeln in Korrelation mit deren relativen Belastung zu ermitteln, sowie das Verhalten von Muskelrekrutierungsmustern der Thoraxmuskulatur während ermüdender Übungen zu untersuchen. Basierend auf den Ergebnissen der ersten Studie wurde ein Ermüdungsalgorithmus entwickelt und in das AnyBody Modeling System™ (AMS) implementiert. Beide experimentellen Studien wurden mit dem modifizierten AMS simuliert um den Algorithmus zu validieren und das Verhalten des Rekrutierungssolvers zu untersuchen.

Die Ergebnisse der simulierten Muskelermüdung korrelierten gut mit den Daten aus der experimentellen Studie. Außerdem ergab sich eine Reduktion der maximalen Muskelkraft der belasteten Muskulatur um 10-15 % durch die Ermüdung. Die Analyse der Rekrutierungsmuster ergab eine zusätzliche Aktivierung entweder der oberen Rückenmuskulatur oder der Bauchmuskulatur bei den meisten Probanden. Die numerischen Simulationen der Übungen im modifizierten AMS ergab eine Verschiebung der Muskelaktivität hin zu der oberen Rückenmuskulatur.

Contents

1. Introduction 9
   - 1.1. Objectives of the Thesis . . . 10
     - 1.1.1. Experimental Quantification of Muscle Fatigue . . . 10
     - 1.1.2. Experimental Study of Muscle Recruitment Pattern Under the Influence of Fatigue . . . 11
     - 1.1.3. Development of a Novel Fatigue Algorithm and Implementation to the AMS . . . 11
     - 1.1.4. Validation of the AMS Muscle Recruitment with Included Muscle Fatigue . . . 11
   - 1.2. Outline of This Thesis . . . 12
   - 1.3. AnyBody Modeling System™ . . . 12
     - 1.3.1. AnyBody™ Managed Model Repository . . . 13
     - 1.3.2. Scaling . . . 17
     - 1.3.3. Muscle Recruitment . . . 19
     - 1.3.4. Muscle Models . . . 21
   - 1.4. Muscle Physiology . . . 22
     - 1.4.1. Structure of Human Skeletal Muscles . . . 23
     - 1.4.2. Process of Muscle Activation and Force Generation in Human Skeletal Muscles . . . 25
     - 1.4.3. Muscle Fatigue Mechanisms . . . 28
     - 1.4.4. Measurement of Muscle Fatigue . . . 30
   - 1.5. Electromyography (EMG) . . . 31
     - 1.5.1. Signal Emergence . . . 31
     - 1.5.2. Influencing Factors on the EMG Signal . . . 33
     - 1.5.3. Surface EMG Measurement . . . 35
     - 1.5.4. Surface EMG - Force Relationship . . . 38

1.5.5. EMG Signal Normalization 40
1.5.6. Manifestation of Muscle Fatigue in the EMG signal 46

2. Material and Methods 49
2.1. Investigation of Fatigue Progress of m. Biceps Brachii and m. Triceps Brachii 50
2.1.1. Experimental Set-up 50
2.1.2. Summary Investigation of Fatigue Progress 60
2.2. Development of Fatigue Algorithm, Implementation to AMS and Validation 60
2.2.1. Fatigue Algorithm 63
2.2.2. Recovery Model 64
2.2.3. Endurance Time Model 65
2.2.4. AnyBody Model^{TM} Set-up 65
2.2.5. Summary Modified AMS Model of Upper Extremities 67
2.3. Experimental Study to Investigate Muscle Recruitment Pattern of the Back Muscles 67
2.3.1. Experimental Set-up 68
2.3.2. Subject Description 69
2.3.3. Study Protocol 69
2.3.4. Anthropometric Data 71
2.3.5. Reference Values for Normalization and Relative Muscle Loading 72
2.3.6. Isometric Fatigue Protocol 73
2.3.7. Dynamic Fatigue Protocol 73
2.3.8. Data Processing 73
2.3.9. Summary Experimental Study Muscle Recruitment Pattern . 76
2.4. Investigation of AMS Recruitment Algorithm with Implemented Fatigue 76
2.4.1. AnyBody^{TM} Model to Investigate Muscle Recruitment Pattern 77
2.4.2. Summary Recruitment Pattern of modified AMS Model . . . 80

3. Results 81
3.1. Experimental Study of Muscle Fatigue Progress 81
3.1.1. Results from Isometric Fatigue Protocol 82
3.1.2. Results from Dynamic Fatigue Protocol 88
3.2. Results of the Developed Novel Fatigue Algorithm and Its Validation 90
3.2.1. Model Parameters for the AMS Model and the Implemented Fatigue Algorithm 90
3.2.2. Validation of the Fatigue Algorithm in the AMS Model . . . 91
3.3. Experimental Study of Muscle Recruitment Pattern 95
3.3.1. Results from Isometric Fatigue Protocol 96
3.3.2. Results from Dynamic Fatigue Protocol 98
3.4. Recruitment Pattern Modified AMS Model 100
3.4.1. Model Parameters for the Simulation and Validation of the Muscle Recruitment Pattern 101
3.4.2. Results from Simulated Muscle Recruitment 101

4. Discussion 107
4.1. Fatigue Progress of Single Muscles 108
4.2. Fatigue Algorithm and Implementation to AMS Model 111
4.3. Muscle Recruitment Pattern - Experimental Study 114
4.4. Muscle Recruitment Pattern - AMS 117

5. Conclusion 119

A. Work Packages of the Thesis 142

B. Additional AnyBody^{TM} Source Code of Upper Limb Model 147

C. Segments and Muscles of the AMS Model to Simulate Fatigue of Shoulder and Arm Muscles 151

D. Segments and Muscles of the AMS Model to Study Muscle Recruitment Pattern 154

E. Additional Results of Experimental Study of Muscle Fatigue Progress 161

List of Acronyms and Symbols

Acronyms and symbols used in this thesis are listed subsequently.

Acronyms

AMS	AnyBody Modeling System^{TM}
AAU	Aalborg University
ADP	Adenosine diphosphate
AMMR	AnyBody managed model repository
AP	Action potential
ATP	Adenosine triphosphate
BMI	Body mass index
CNS	Central nervous system
CT	Computed tomography
DoF	Degree of freedom
ECG	Electrocardiographic
EMG	Electromyographic
FDK	Force-dependent kinematics
FFT	Fast Fourier transform
MET	Maximum endurance time
MPF	Median power frequency
MSD(s)	Musculoskeletal disorder(s)
MU(s)	Motor unit(s)
MUAP	Motor unit action potential
MVC	Maximum voluntary contraction
PCSA	Physiological cross-sectional area
RMS	Root-mean-square
SD	Standard deviation
SENIAM	Surface EMG for a non-invasive assessment of muscles
TELEM	Twente lower extremity model
TKE	Teager-Kaiser-Energy

1. Introduction

Analyses of the musculoskeletal system are challenging tasks since measurements of joint and muscle forces within the human body are not or hardly possible at all. Therefore, in recent years numerical models have been developed to enhance the knowledge about the musculoskeletal system and to calculate the muscle and joint forces based on subject-specific data. The Anybody Modeling System^{TM} (AMS) (AnyBody Technology A/S, Aalborg, Denmark) is a system for generating highly developed musculoskeletal models with a realistic level of complexity [1]. These models are validated and work well to analyse single motions or short motion cycles with relatively low intensity and allow the investigation of muscle and joint reaction forces. Therefore, these models are a useful tool when studying the musculoskeletal system and musculoskeletal disorders (MSDs). MSDs were the most common cause of work-related absence in 2016 [2] and often muscle fatigue is involved in these disorders [3]. In most cases, these MSDs are progressive disorders, as a result of muscles being loaded over a long period of time. The symptoms vary from discomfort followed by pain up to invalidity [4]. Therefore, a good understanding of the mechanics of the human body is required to be able to analyse long-term effects properly. However, when investigating long-term effects with numerical models, the issue of muscle fatigue needs to be taken into consideration, which is not yet represented in the AMS.

Different algorithm have been proposed in the last years to describe muscle fatigue. When experiencing fatigue, the maximum force capacity of a muscle is reduced over time. The algorithm published by Ma et al., 2009b [5], for example, describes this. The model though is validated against the maximum endurance time of the exercises and thereby, total exhaustion is reached when the muscle can no longer produce the required force. This means that the model overestimates the reduction

of maximum force capacity during fatigue, since the contribution of central fatigue and peripheral fatigue are not considered [6, 7]. Another example for a numerical fatigue model was published by Silva et al., 2011 [8], in which the central fatigue was also excluded from the study.

Electromyographic (EMG) measurements are the most common tool to investigate muscle fatigue. Furthermore, the myoelectric signal is influenced not only by the fatigue of the muscle itself, but by central fatigue and peripheral fatigue as well. Therefore, the development of a fatigue algorithm based on EMG measurements is required for a realistic assessment of its influence on muscle force generation. To gain a closer insight into the musculoskeletal system when experiencing fatigue, it is necessary, to implement this novel fatigue algorithm to a state-of-the-art simulation tool.

1.1. Objectives of the Thesis

In this thesis, fundamental research regarding the simulation of the effect of muscle fatigue on the musculoskeletal system is presented. The workflow conducted throughout the study can be grouped into four different work packages which are described in the following. A detailed overview of the work packages is shown in tables A.1 - A.4.

1.1.1. Experimental Quantification of Muscle Fatigue

The first step was the quantification of muscle fatigue based on EMG measurements. The study was designed to investigate the progress of muscle fatigue of single muscles during isometric and dynamic contraction in relation to the relative muscle loading. This novel approach was required for the development of the fatigue algorithm, which was based on the results from this experimental study. The progress of muscle fatigue was estimated with the maximum voluntary contraction (MVC) normalized root mean square (RMS) of the EMG signal. Furthermore, the median power frequency (MPF) was analysed in order to verify the muscle fatigue during the recorded exercises. The recorded data was also used to validate the modified AMS model including the fatigue algorithm which was developed in

work package three.

1.1.2. Experimental Study of Muscle Recruitment Pattern Under the Influence of Fatigue

The second work package aimed to investigate the influence of muscle fatigue on the recruitment pattern of muscles. Therefore, an experimental study was designed, where the EMG signals of 16 muscles of the back and abdomen were collected during exhausting isometric and dynamic exercises. This data was evaluated for potential changes in the global muscle recruitment of back and abdominal muscles when experiencing fatigue. The data was also used to validate the recruitment algorithm of the modified AMS model including the novel fatigue algorithm.

1.1.3. Development of a Novel Fatigue Algorithm and Implementation to the AMS

The aim of the third work package was the development of a novel fatigue algorithm based on the results from the first work package. Furthermore, the implementation to the AMS was also part of this work package, including the validation of the developed model against measured data. The designed algorithm allowed the estimation of the current maximum muscle force capacity of single muscles when experiencing fatigue and therefore provides an insight into the musculoskeletal system during long-term loadings.

1.1.4. Validation of the AMS Muscle Recruitment with Included Muscle Fatigue

The modified AMS model developed in the third work package was extended to simulate the exercises from the experimental muscle recruitment study. Additionally, all exercises were simulated with the generic AMS model without any modifications to analyse the behaviour of the muscle recruitment algorithm of the AMS. The calculated muscle forces were investigated focusing on global muscle recruitment of back and abdominal muscles.

1.2. Outline of This Thesis

The thesis is structured in four major chapters. In the first chapter, basic information about the AMS, muscle physiology, muscle fatigue in general and electromyographic measurements is provided. The second chapter is complemented with information about the set-up of the conducted experimental studies, as well as the development of the fatigue algorithm. Furthermore, the structure of the modified AMS models for the validation of the fatigue and recruitment algorithm is described. In the third chapter, the results from the experimental studies and from the validation simulations are presented. These results are discussed in chapter 4, followed by a brief summary in chapter 5.

1.3. AnyBody Modeling System^{TM}

AnyBody Technology A/S is a spin-off from the University of Aalborg, Denmark where the AMS was originally developed. In this chapter the AMS is described in detail with a special focus on the recruitment of muscles.
According to Damsgaard et al., 2006 [1] the AMS was developed as a tool to create musculoskeletal models from scratch or to modify existing models. It should also allow the exchange of models and the cooperation on model development. Another aim when designing the AMS was to allow ergonomic design optimization studies. Furthermore, the system should be able to handle models with a level of detail as high as possible.
The models in the AMS are based on the methods of multi-body modelling systems. Therefore, the generic model consists of rigid-bodies as bones connected by joints, ligaments and muscle-tendon units. Drivers for each joint restrict the degrees of freedom of each segment, allowing time depending kinematics. External loads and forces can also be applied in the AMS as time dependent boundary conditions. To calculate the variables like muscle force, joint reaction forces, etc. inverse dynamic routines are applied. Therefore, the motion of the body needs to be specified. In comparison to forward dynamic models, this method is much more efficient [1].
Since the development of a whole human body model is a very challenging and elaborating task, the AMS provides a model repository, the so called AnyBody^{TM}

Managed Model Repository (AMMR). The AMMR consists of several different body models and application models like for example the 'HumanStanding' model which is shown in figure 1.1. The models from the AMMR can be adjusted by the

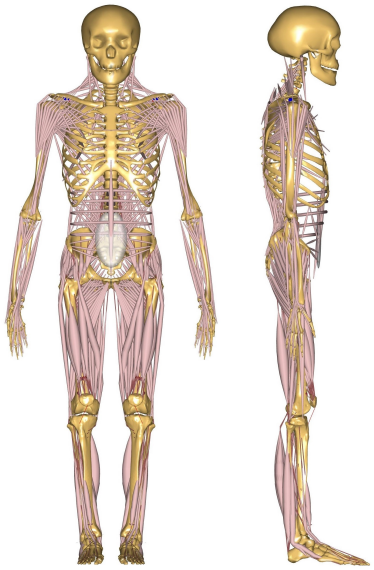

Figure 1.1.: Full body human standing model from the AMMR (v.2.1.1)

user so that the development of an entirely new model is not required.
The following chapters give a brief overview of the model set-up and mechanisms. Furthermore, the validation of the models is described.

1.3.1. AnyBody™ Managed Model Repository

The generic model for the AMMR was developed at Aalborg University (AAU) and is therefore called AAUHuman full body model. The information about this model is taken from the documentation of the AMMR v2.1.1 [9]. Since then, many different research facilities have developed different body parts for this model and increased the level of detail progressively. The most important models are presented in the following.

Lumbar Spine

The lumbar spine model consists of five vertebrae which are connected by three DoF joints. The lumbar muscles are represented by a total of 188 muscle fascicles, which do not consider the force-length-velocity relation. Additionally, a model to calculate the intra-abdominal pressure is applied. In this model two assumptions were made. The first one is that only the transversus muscles contribute to the abdominal pressure. The second assumption is that the pressurized column is idealized as a cylinder. The abdominal model includes five artificial segments (disks) which are connected to one vertebra each (see figure 1.2). Furthermore, a reaction force between the buckle segment and each of these disks is modelled. The transversus muscles are placed around these disks and are connected to the buckl segment. As the transversus muscles change length, the cross sectional area of the artificial disks, which are idealized as a circle change size. The force of the transversus muscles on the disks are balanced by the abdominal pressure which affects the reaction force on the lumbar spine. This allows the transversus muscles to function as an indirect spine extensor. The inter-vertebrae motions are considered by kinematic rhythms as a function of overall lumbar curvature. The facet joints are not represented in the model.

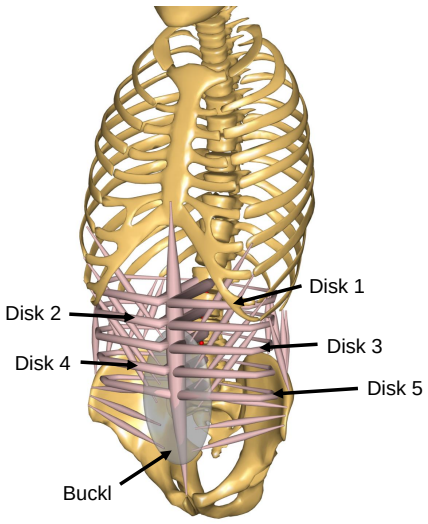

Figure 1.2.: Abdominal model of the AMS

Cervical Spine

The model of the cervical spine consists of seven vertebrae which are connected with three DoF joints, except for the joint between the C2 and the skull which only has one DoF. The muscles are represented by 136 muscle fascicles. The centre of rotation between vertebrae is modelled according to Amevo et al., 1991 [10].

Arm Model

The arm model was developed using data based on two cadaver studies. The joints and kinematic constrains of the arm model are shown in table 1.1.

Table 1.1.: Joints and kinematic constrains of the arm model [9]

Name	**Description**	**Joint/Construction Type**
SC	SternoClavicular	Spherical Joint
AC	AcromioClavicular	Spherical Joint
GH	Glenohumeral Joint	Spherical Joint
AI		One DoF constraint requiring the bony landmark AI on the scapula to stay in contact with the thorax
AA		One DoF constraint requiring the bony landmark AA on the scapula to stay in contact with the thorax
Conoideum-Ligament		The length of this ligament is driven to always remain constant
FE	Flexion-extension of the elbow	Revolute Joint
PS	Pronation-supination joint for the forearm	Combination of joints at the distal and proximal end of the radius bone that leaves one DoF free which is pronation/ supination of the forearm
Wrist Joint		Two successive revolute joints where the axes of rotations are not coincident

Leg Model

The basic leg model includes the pelvis, thigh, shank and the foot which is represented by one segment. Furthermore, 35 muscles are defined. A spherical joint is used to model the hip joint, while the knee and ankle are specified as hinges.

A more detailed leg model is the so called *Twente lower extremity model* (TELEM) which is available in two versions.
The version 1.2 contains 159 muscles and has six joint degrees. It is based on a published anatomical dataset [11] and validated against literature with a focus on biomechanical performances.
The version 2.1 (TELEM2) includes 169 muscles. The model is based on a single consistent anatomical dataset which was derived at the University of Twente, The Netherlands [12]. In the new version, the surface wrapping of several muscles has been updated and the muscle attainment points and bone surfaces origin from a single subject which makes it more consistent.

Other Body Models

The body models also include two different mandible models. The *symmetric mandible model* is based on a CT scan of a 30-year-old male subject and contains 24 hill-type muscles and four DoF [13]. The second model is the so called *Aalbor mandible*. This model is based on the CT scan of a 40-year-old male subject. It features force-dependent kinematics (FDK) for the temporomandibular joint [14]. The *detailed hand model* is a model only designed for dynamic analysis, since there are no muscles included. The carpal bones are represented by 17 DoF.

Application Examples

The AMMR provides many different application examples. Starting from the 'StandingModel' to 'CrossTrainer' or 'BikeModel' to 'AirlinePassenger' model only to mention some examples, the user can choose which model fits closest to the motion of interest and modify this model. Furthermore, the AMMR includes different motion capture models. These models provide the opportunity to use C3D files from motion capture measurements as boundary conditions to drive the model which allows a very high kinematic accuracy. Models like the 'Spine Fixation Model' are included mainly for studies in the area of orthopaedics and rehab.

A detailed list of all available models is available on `https//anyscript.org` [9].

1.3.2. Scaling

Since the basic generic model represents the 50^{th} percentile European male human, scaling of the model is required to allow subject-specific modelling. A list of scaling laws that are available in the AMS is given in table 1.2.

Table 1.2.: Scaling laws available in the AMS [9]

Scaling law	**Description**
ScalingStandard	Scale to a standard size; i.e. use 50^{th} percentile sizes for a European male
ScalingNone	Do not scale; i.e. use underlying cadaveric dataset as it is
ScalingUniform	Scale segments equally in all directions; input is joint to joint distances
ScalingLengthMass	Scale taking mass into account; input is joint to joint distances and mass
ScalingLengthMassFat	scale taking mass and fat into account; input is joint to joint distances
ScalingUniformExt	Scale equally in all directions; input is external measurements
ScalingLengthMassExt	Scale taking mass into account; input is external measurement
ScalingLengthMassFatExt	Scale taking mass and fat into account; input is external measurements
ScalingXYZ	Scale taking mass and fat into account; scale segments along X, Y, Z axes; input is scale factors along X, Y, Z axes

Details about the scaling in the AMS are described by Rasmussen et al., 2005 [15]. The following information is taken from the aforementioned. The basic equation for linear scaling is defined as:

$$s = S \cdot p + t_r \tag{1.1}$$

where s is the position of a local node on the scaled segment, p is the original position of the node, t_r is the translation and S is the 3 x 3 scaling matrix defined

as:

$$S = \begin{bmatrix} S_{11} & 0 & 0 \\ 0 & S_{22} & 0 \\ 0 & 0 & S_{33} \end{bmatrix} \tag{1.2}$$

The scaling law mostly used in the AMS is the Length-Mass Scaling with fat percent. The parameters of the main diagonal of equation 1.2 are calculated as:

$$S_{22} = k_L = \frac{L_1}{L_0} \tag{1.3}$$

where L_1 is the new length of the scaled segment and L_0 is the initial length. The ratio of masses of the segment is described by:

$$k_m = \frac{m_1}{m_0} \tag{1.4}$$

S_{11} and S_{33} are defined as:

$$S_{11} = S_{33} = \sqrt{\frac{k_m}{k_L}} \tag{1.5}$$

This formulation allows an inclusion of the fat percent for the scaling the strength of the model. The percent of muscle tissue is calculated by the equation:

$$R_{muscle} = 1 - R_{fat} - R_{other} \tag{1.6}$$

with R_{other} is the percent of skeleton, organs, blood, etc. The strength scale model is estimated by the function:

$$F = F_0 \frac{k_m}{k_L} \frac{R_{muscle,1}}{R_{muscle,0}} = F_0 \frac{k_m}{k_L} \frac{1 - R_{other,1} - R_{fat,1}}{1 - R_{other,0} - R_{fat,0}} \tag{1.7}$$

When no measurement of the fat percent is available, [16] proposed a method to calculate the R_{fat} for women and men.
For women:

$$R_{fat} = -0.08 + 0.0203 \cdot BMI - 0.000156 \cdot BMI^2 \tag{1.8}$$

For men:

$$R_{fat} = -0.09 + 0.0149 \cdot BMI - 0.00009 \cdot BMI^2 \tag{1.9}$$

1.3.3. Muscle Recruitment

The AMS allows the estimation of joint and muscle force in the human body. The algorithms which need to be solved for this are described in the following chapter. The information presented is from the documentation of the AMS and the provided tutorials (Anybody Tutorials v7.1.2). Inverse dynamic is used in the AMS to calculate joint reactions and muscle forces in the AMS. Compared to the forward dynamic approach, this allows the analysis of large musculoskeletal systems with a relatively low computational effort. A simplified model of the forearm is shown in left figure 1.3.

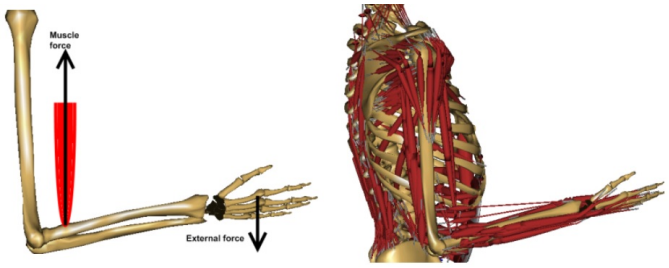

Figure 1.3.: Simplified arm model (left); anatomical realistic model of human upper extremity (right)

The known magnitude of the external load combined with the length of the forearm and the insertion point of the muscle allows the estimation of the muscle force by solving the momentum equilibrium about the elbow. The reaction force within the elbow joint can also be estimated by equilibrium equations.
When calculating a realistic musculoskeletal system as shown on the right side of figure 1.3 the complexity of equilibrium equations increases with each additional muscle. Further complications come with inertia terms which need to be considered during dynamic motion a well as the wrapping of muscles around bones and joints. In addition, the human body has more muscles than required to balance all DoFs. The AMS therefore provides different muscle recruitment algorithms which will be shown in the next paragraphs. Rasmussen et al., 2001 [17] describes how the

muscle forces are calculated. A brief overview is given in this paragraph. The muscle recruitment in the AMS determines which set of muscle forces is used to balance a certain external load. The basic equilibrium equations can be written as:

$$Cf = r \tag{1.10}$$

where C is the coefficient matrix, f contains the muscle and joint forces and r is the vector containing the external loads and inertia forces. This linear system of equations is usually easy to solve. However, due to muscles only producing force in one direction and the former mentioned muscle redundancy, there are more unknowns than equations in the system which leads to infinitely many possible solutions. Experimental studies have shown that the recruitment of muscles tend to be systematically. This consideration leads to the following optimization problem:

$$\begin{aligned} &minimize\ G(f^{(M)}) \\ &subject\ to\ Cf = r \\ &\qquad f_i^{(M)} \geq 0, i = 1...n^{(M)} \end{aligned} \tag{1.11}$$

$G(f^{(M)})$ represents the body loads and $n^{(M)}$ is the number of muscles. The constrains only apply to the muscles to ensure only forces in one direction. [17] distinguishes two different objective functions. The polynomial criteria (1.12) is the most popular objective function.

$$G(f^{(M)}) = \sum_{i=1}^{n^{(M)}} \left(\frac{f_i^{(M)}}{N_i} \right)^p \tag{1.12}$$

N_i are normalization factors or functions like assumed maximum muscle strength, physiological cross-section area (PCSA), or the strength of the muscle at time instant. Polynomial objective functions require additional constraints to prevent single muscles to exceed their physiological maximum force with increasing external load.

The objective function includes a variable power p. This parameter controls how fast muscles are activated and deactivated. A value of $p = 1$ leads to a recruitment of only the stronger muscles which is agreed to be non-physiological. Increasing

the power leads to a more realistic reflection of the human muscle recruitment, hence to an increasing degree of synergism. Too high values for p result in a very quick, non-physiological activation and deactivation of muscles. Furthermore, high values of p can lead to numerical instabilities.
With increasing order of the objective function the solution converges with the so-called min/max objective function:

$$G(f^{(M)}) = max\left(\frac{f_i^{(N)}}{N_i}\right),\ i = 1, ..., n^{(M)} \tag{1.13}$$

This criterion results in a relative muscle force that is as small as possible. This means that the activation of all muscles contributing to balancing the external load is identical. This criterion has not only numerical advantages but is also physiological interesting, since maximum synergism leads to minimum fatigue of the muscles. Disadvantages of this criterion are that muscles are switched in and out very abruptly. Furthermore, muscles with only marginally positive contribution are also fully activated.

1.3.4. Muscle Models

In this chapter the different muscle models which are available in the AMS are described. The information is taken from the documentation AnyBody Tutorials v.7.1.2.
Basically, there are two different approaches to describe muscle behaviour. The first approach is based on the work of Hill, 1938 [18]. In this model, the muscle is represented as a contractile element, combined with elastic elements. The model is proven to represent the behaviour of muscles quite well and has the advantage of being very efficient in numerical simulations.
The second approach is based on the work of Huxley, 1957 [19]. This model describes the cross bridge activity during muscle contraction by differential equations and is therefore much more demanding to compute.
Classic numerical muscle model need to be adjusted to be used in inverse dynamic computation since usually these models need the activity of the muscle as input to calculate the muscle force. The AMS provides four different muscle models.

AnyMuscleModel The simplest muscle model is the so-called AnyMuscleModel. The only required input variable is the strength of the muscle at its optimal length. Therefore, the contraction velocity or length of the muscle is not considered in this model. Although it is known that muscles do not behave this way, it provides good results for many cases. Different studies describe the correlation between the strength of the muscle and the cross-sectional area [20–23] which are reported for the major muscles from cadaver studies.

AnyMuscleModel3E The AnyMuscleModel3E in the AMS is Hill-model-based on the model published by Zajac, 1989 [24]. This model considers parallel passive elasticity of the muscle, serial elasticity of the tendon pennation angle of the fibres and other parameters. Furthermore, the model applies non-linear force-length and force-velocity relationship.

AnyMuscleModel2ELin The AnyMuscleModel2ELin is also a multi-element model. The strength is proportional to the length of the muscle and the contraction velocity at time instant. The tendon is modelled as a linear-elastic element. The disadvantage of this model is that in some cases, if the muscle is stretched far enough, the active muscle force can be switched off entirely since the passive elements always produce force while the muscle is elongated.

AnyMuscleModelUsr1 The AnyMuscleModelUsr1 provides the opportunity for the user to define a muscle model. The strength of the muscle can be defined as a function of different variables, including isometric strength, volume or PCSA, fibre length, kinematic measures and time.

1.4. Muscle Physiology

In this section, the basic physiology of human muscles is explained. Most information is taken from Schmitt, 1993 [25]. Basically three different types of muscles are distinguished in the human body:

- cardiac muscle
- smooth muscles

- skeletal muscles

The cardiac muscle is a muscle type which is only found in the heart. Smooth muscles are found in the walls of hollow organs like the uterus, stomach, urinary bladders or in the walls of arteries, veins and the respiratory system. The function of the skeletal muscles is mainly the voluntary active motion of the human body. Therefore, in the following the structure and processes of skeletal muscles are described in more detail.
Skeletal muscles represent about 40 % of the body weight. Overall more than 400 different muscles are distinguished. Each muscle is connected to at least one of each of the following parts:

- artery for oxygen and nutrient delivery
- vein for removal of metabolic waste products
- efferent nerves
- afferent nerves from muscle tendon spindles
- fibres from automatic nervous system

1.4.1. Structure of Human Skeletal Muscles

Each human muscle is constructed from muscle fibres with a diameter of approximately 50 μm and a length of up to several centimetres. Skeletal muscles consist mostly of water (about 80 %). The main solid component are proteins, of which about 50 % are the contractile proteins myosin (35 %), actin (15 %) and tropomyosin-troponin (10 %). The contractile fibres are mainly constructed by myofibrils, from which each one is surrounded by the sarcoplasmatic reticulum. Furthermore, mitochondria, glycogen granules and nuclei are embedded. The mitochondria are important for the generation of adenosine triphosphate (ATP), which is necessary in the process of the cross-bridge formation (see section 1.4.2). Figure 1.4 shows the construction of a skeletal muscle.

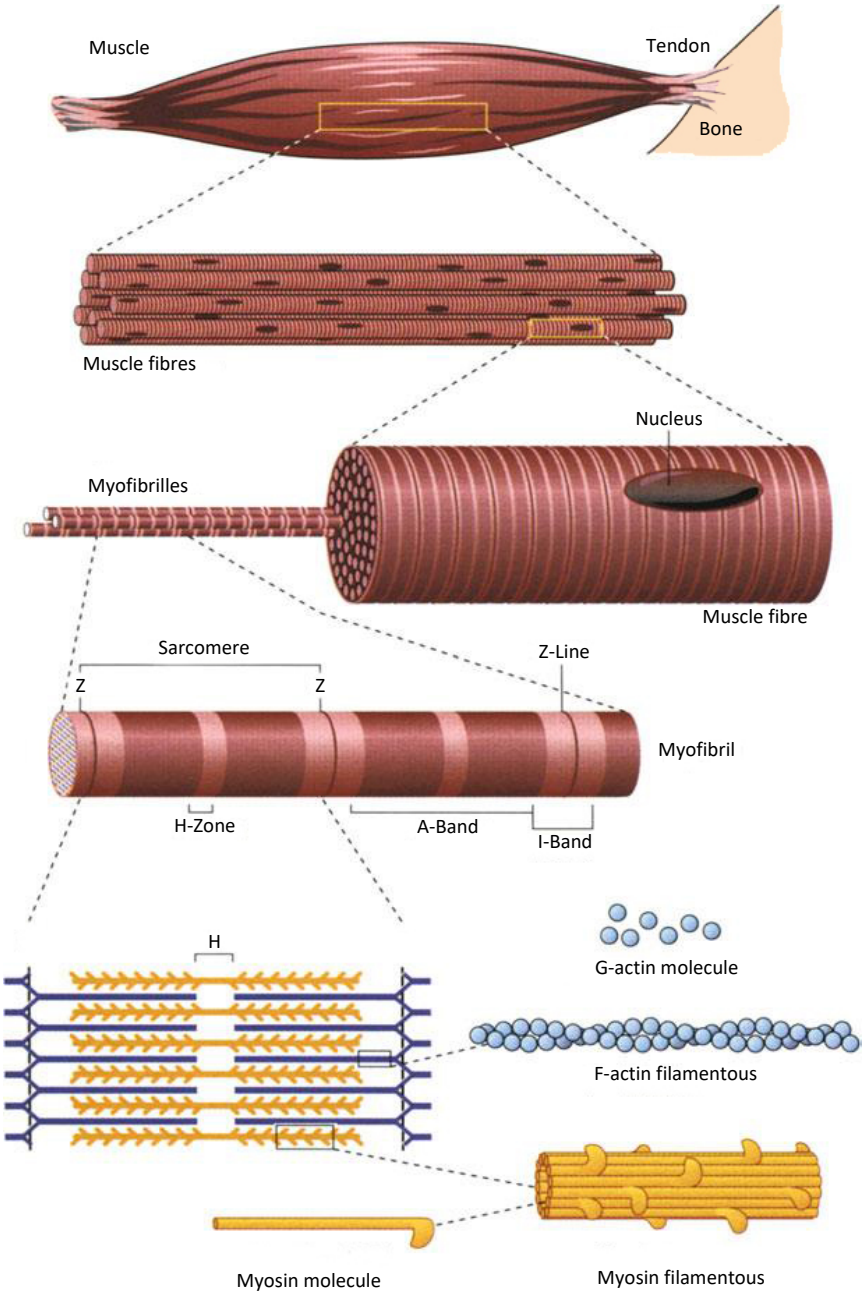

Figure 1.4.: Construction of a human skeletal muscle (modified after Bloom & Fawcett, 1986 [26])

1.4.2. Process of Muscle Activation and Force Generation in Human Skeletal Muscles

The motor unit is the smallest functional unit to describe the neural control of muscle contraction and consists of the motor neuron with its dendrites and axon, together with the muscle fibres which are innervated by the axon [27]. The motor neuron receives its input from the central nervous system (CNS) and is located in the spinal cord or the brain stem. The axon connects the motor neuron and the muscle fibres, which it innervates [28]. All motor neurons that are connected to a muscle are known as a motor nucleus or motor neuron pool [29].
While in resting condition, the muscle fibre membrane has a potential of approximately -80 to -90 mV, which is maintained by the so-called ion pump [30]. The activation of a motor neuron results in the conduction of the excitation along the axon, which leads to the release of transmitter substances at the motor endplates. The resulting endplate potential causes a slight modification of the diffusion characteristics of the muscle membrane and allows Na^+ ions to flow into the muscle cell, which leads to a depolarisation of the transverse tubular system and sarcoplasmic reticulum. When exceeding a certain threshold, the action potential (AP) changes from about -80 mV to +30 mV and is reversed instantly. A hyperpolarization phase is following the repolarisation phase during which the muscle fibre cannot be activated for a short time. The AP is schematically shown in figure 1.5 and is often referred to as the motor unit action potential (MUAP).

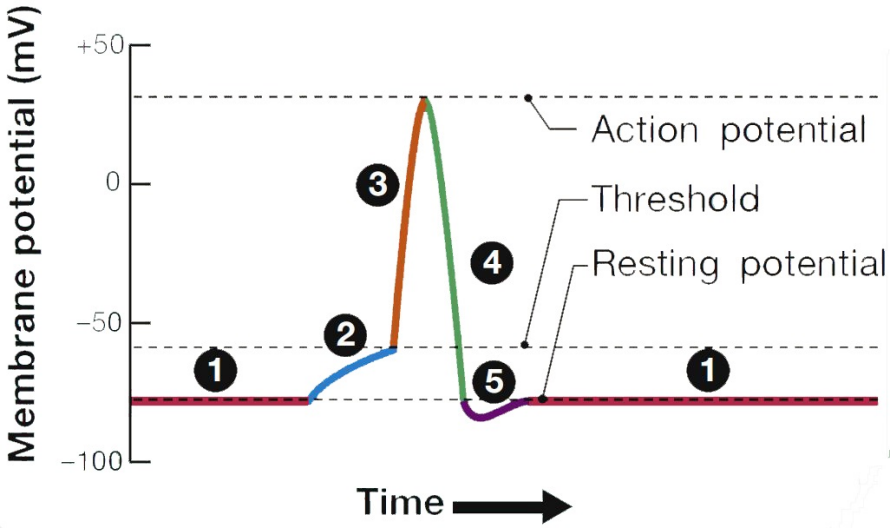

Figure 1.5.: Action potential; Phase 1: Resting phase of AP, Phase 2: Depolarization, Phase 3: Rising phase of AP, Phase 4: Falling phase of AP, Phase 5: Undershoot (hyperpolarisation) [31]

The depolarization and repolarisation of the transverse tubular system and sarcoplasmic reticulum moves in a wave (electrical dipole) [32] across the muscle fibre bidirectionally starting from the endplates with a speed of about 2 - 6 m/s [30] and causes a release of Ca^{2+} in the sarcoplasmic reticulum. The shortening of a sarcomere is initiated by the release of this Ca^{2+}, which spreads over the contractile filaments of actin and myosin. The binding of Ca^{2+} with tropin changes its shape by moving tropomyosin away from the binding sites of actin. This allows the myosin head to bind to actin and to form a cross-bridge. Adenosine diphosphate (ADP) is released from the myosin head which causes its rotation and a force generation towards the middle of the sarcomere. When ATP binds to the myosin head, the cross-bridge is detached. The ATP is hydrolysed to ADP and organic phosphate which causes the myosin head to return to its initial position so that it can form another cross-bridge. The cross-bridge cycle repeats as long as the binding sites of actin are exposed. The muscles relaxes when intracellular calcium ($[Ca^{2+}]_i$) is actively returned to the sarcoplasmic reticulum which causes the recuperation of the blockade of the cross-bridge cycle and therefore a reduction of the produced force. The process of activation, contraction and relaxation can be described by 15 steps, where steps 1-6 describe the excitation, 7-10 the contraction

and 11-15 the relaxation of the muscle:

1. Depolarization of end-plate membrane
2. Triggering of AP outside of end-plates and transmitting the AP across fibre surface
3. AP spreading into the fibre through tubular system
4. Release of Ca^{2+} from terminal cisterns of sarcoplasmatic reticulum, leading to an increase of $[Ca^{2+}]_i$ and diffusion of Ca^{2+} to the contractile filaments
5. Binding of Ca^{2+} to troponin of thin filaments
6. Lifting of the blockade of cross-bridge cycle due to changes of the shape of troponin
7. Formation of cross-bridge
8. Force towards the middle of the sarcomere caused by rotation of myosin head
9. Binding of the ATP causes detachment of myosin head from actin and a backwards rotation to the starting position
10. Hydrolysis of bound ATP
11. Absorption of Ca^{2+} by sarcoplasmic reticulum by decreasing $[Ca^{2+}]_i$
12. Releasing of Ca^{s+} from troponin, back diffusion and absorption by sarcoplasmic reticulum
13. Recuperation of blockade of cross-bridge cycle
14. Reduction of force by breaking cross-bridges without a new formation
15. Preparation of myosin heads for next contraction

1.4.3. Muscle Fatigue Mechanisms

Muscle fatigue is studied for various applications such as rehabilitation medicine, sports, occupational medicine, space medicine, prostheses control or oncology [33]. Furthermore, it plays an important role in the fields of ergonomics. There are different definitions of muscle fatigue. Edwards, 1981 [34] defined fatigue as failure to maintain required or expected force. Heimer states, that fatigue is a temporarily lowered capacity to perform work of a certain intensity caused by the work itself [35]. In general, fatigue is defined as any exercise-induced reduction in maximal capacity to generate force output [36]. According to Merletti et al. 2016, fatigue can be subdivided into fatigue of the CNS and the neuromuscular junction, or peripheral fatigue, describing changes of muscle force generating capability [33]. The generation of muscle force is influenced by different factors, which are explained in the following.

Contribution of the neural system

Changes in the CNS or proximal to the neuromuscular junction are referred to as central fatigue. Neurotransmitters play an important role during this fatigue. For example Serotonin has been proven to have a negative influence on the performance during an exercise [37]. As described in section 1.4.2, the activation of motor units (MUs) is triggered by an input from the CNS on the spinal motoneurons by neurotransmitters. The strength output and timing of the contraction of the muscle fibre is controlled by the firing rate of the MU which is approximately 50 Hz - 60 Hz in healthy humans during a non-fatigued contraction [38]. Since the firing rate of the MUs is directly related to the force output of the muscle, a slowing or cessation of the MUs firing contributes to muscle fatigue. The firing rate is influenced by intrinsic in motoneuron properties and influenced by different factors [39]. It was found by Taylor et al. 2016, that repetitive activation of motoneurons lead to a reduced excitability [40]. The excitatory drive from the motor cortex or the supraspinal areas to the motoneurons is also negatively affected by intensive exercise and therefore lower, which leads to reduced firing rate of MUs [40]. Another factor that influences the firing rate is the firing of group III (myelinated) / IV (unmyelinated) muscle afferents, which lead to decreasing firing

rate of the MUs when increased [41, 42]. Another factor is the firing rate of the muscle spindles. When decreased, the presynaptic inhabitation is increased which then leads to decreasing MU firing rate [43, 44].

Ca^{2+}

Calcium plays an important role during the process of muscle activation. Neural activation leads to a reveal of calcium from the sarcoplasmic reticulum into the cytosol. This leads to the generation of the AP as described in section 1.4.2. It was found that an affected calcium release contributes to muscle fatigue. Different mechanisms have been proposed to explain this contribution. One hypothesis is, that a high-frequency stimulation might lead to an accumulation of extracellular K^+ which may cause a decreased voltage sensor activation and therefore affect the amplitude of the AP.
As described in section 1.4.2, Ca^{2+} initiates the cross-bridge cycle, which leads to a contraction of the sarcomere and therefore, a contraction of the muscle fibre. Furthermore, ATP is required which activates the myosin head. In the resting fibre, most ATP is Mg^{2+} bound. Another hypothesis is that fatigue may lead to an increased intracellular ATP, which causes an increased concentration of free Mg^{2+}. This might cause an effectiveness of sarcoplasmic reticulum Ca^{2+} channel opening.[39]

Blood Flow and Oxygen

As described in section 1.4.2, ATP is required to activate the myosin head, which is a critical process for the contraction of a muscle. For the production of aerobic ATP, oxygen is required, which makes a satisfactory supply with blood necessary. Furthermore, blood flow is required, to remove metabolic waste products from this process. Wright et al. 1999 showed, that the contraction of a muscle leads to an increased mean arterial pressure [45], which causes a reduction of the net blood flow [46]. Several studies have shown that this causes a lowered endurance time during an exhausting task [47–49], and that it increases the decline of muscle force [50, 51].
Amann et al. 2007 have found that breathing hypoxic air significantly increases

muscle fatigue [52]. Grassi et al. 2011 reported a reduction of fatigue when increasing the O_2 level [53]. During a high-intensity exercise, the amount of oxygen consumption can be assumed as maximum (VO_{2max}). A further demand of ATP within the muscle can therefore not be satisfied which also contributes to muscle fatigue [54].

1.4.4. Measurement of Muscle Fatigue

During the last decades, different methods to measure muscle fatigue were developed. In this section a few of these methods are summarised and discussed.
In section 1.4.3, different definitions of muscle fatigue are described. Since fatigue can be described as the failure to maintain a required or expected force, the easiest way to measure muscle fatigue is by recording the time until failure occurs. However, the results depend on various psychological factors like motivation [55, 56]. Furthermore, no insight into fatigue as a continuous process is possible since it is not being detected before it occurs. Another limitation of this method is that the fatigue of a specific muscle cannot be determined.
A further method to evaluate muscle fatigue is by measuring the blood lactate concentration. This method is used in sport medicine and gives an insight into the global fatigue state of the whole organism. The limitations are that again no single muscle can be evaluated and that due to the manner of taking the blood sample and the way of determining the lactate concentration, the monitoring of fatigue in real-time is not possible.
An additional method is to monitor fatigue using EMG measurements. The advantage of this method is that biochemical and physiological changes in the muscles are reflected in the myoelectric signal [57]. Utilizing surface EMG electrodes is non-invasive and allows real-time fatigue monitoring even from single muscles. Limitations of this method are the so-called physiological cross talk and that the EMG signal is a stochastic signal and therefore, non-reproducible. Despite its limitations this method is most commonly used when studying muscle fatigue and will therefore be explained in detail in the following.

1.5. Electromyography (EMG)

According to Basmajianm & De Luca, 1953 [58] "Electromyography is the study of muscle function through the inquiry of the electrical signal the muscles emanate." The method of EMG traces back to Du Bois-Reymond, 1875 [59], who was the first to measure the electric signal generated by a muscle during voluntary contraction. It took until the beginning of the 20^{th} century that the recording equipment was sufficient enough to allow the development of clinical EMG. The first book on the topic of EMG was published by Piper, 1912 [60], who described his experimental studies. The further development was mainly made by physiologists. Later on, neurologists contributed to the evolution of EMG not only by describing electromyographic findings, but also by correlating clinical and pathological findings to these measurements [61].

1.5.1. Signal Emergence

As described in section 1.4.2, the activation of a MU leads to a MUAP. This MUAP can be measured with EMG sensors placed on the surface of the skin above the muscle or with fine wire electrodes placed inside the muscle. As described above, the AP moves in a wave (electrical dipole) [32] across the muscle fibre bidirectionally starting from the endplates with a speed of about $2 - 6\,ms^{-1}$ [30].

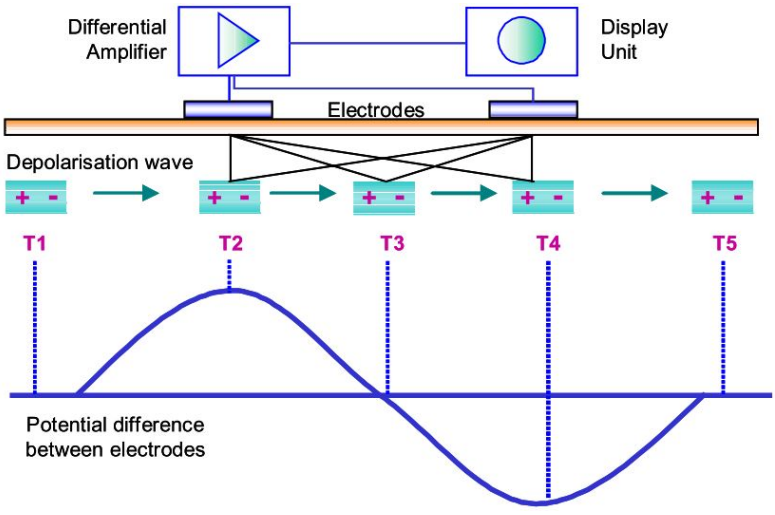

Figure 1.6.: Model of AP wave over time [30]

Electromyographic signals are usually measured with two electrodes in a certain distance to each other (bipolar) and a differential amplification. Figure 1.6 illustrates the measurement of a single muscle fibre. At time point T1, an AP is generated. When it travels towards the first EMG electrode, the potential difference between the two electrodes increases to a maximum at T2 and starting to decrease until position T4. Since the electrodes do not only measure a single muscle fibre, the recorded signal represents the algebraic sum of all MUAPs. Therefore, the EMG signal differs in size and shape depending on the fibre orientation and fibre distance to the electrodes.

The superposition of single MUAPs generates the EMG signal which is an interference signal that oscillates symmetrically about zero. Main influence factors of the shape of the signal are the recruitment and the firing rate of motor units. Since human tissue acts as a lowpass filter, the measured firing rate is not equal to the real frequency of the motor unit. Nevertheless, the EMG signal collected at the surface of the skin represents the firing rate and recruitment of underlying motor units. The composition of an EMG signal is illustrated in figure 1.7. It is shown, that the EMG signal consists of the sum of the single MUAPs.

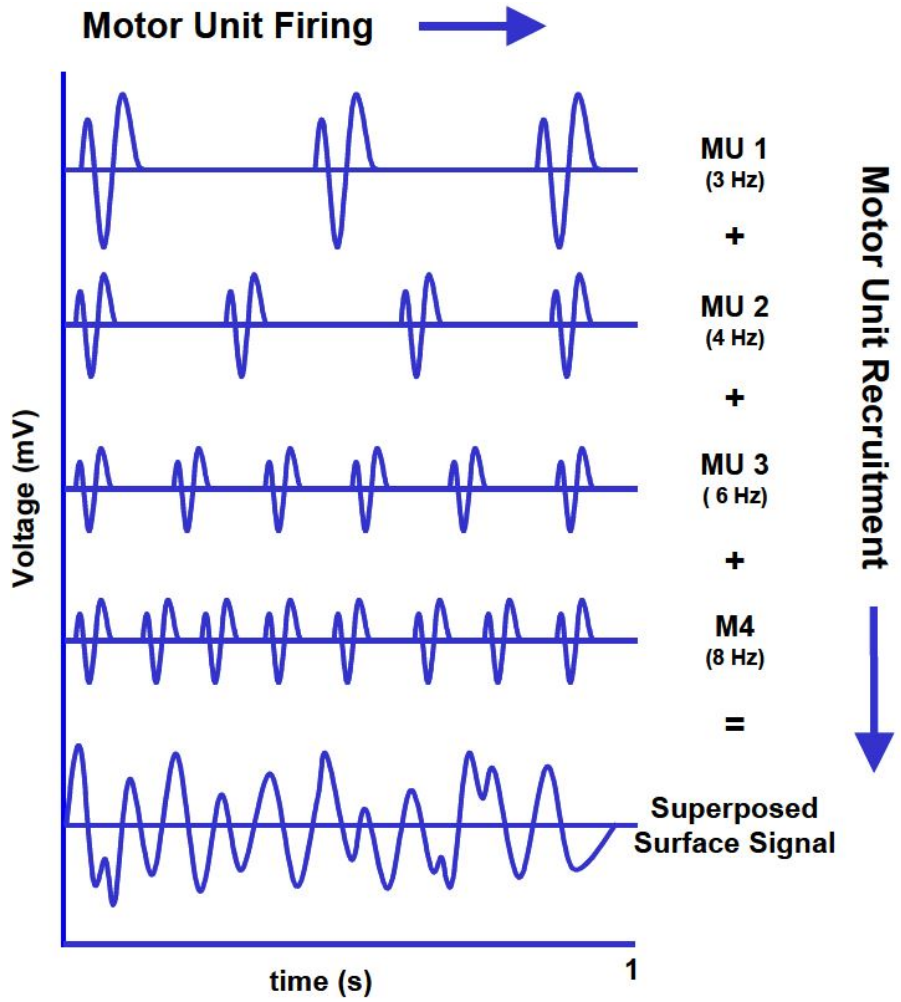

Figure 1.7.: Recruitment and firing rate of motor units result in superpositioned EMG signal [62]

1.5.2. Influencing Factors on the EMG Signal

The quality of the EMG signal is influenced by many different factors that can only partially be controlled. In this chapter, the most important factors are described. Most information is taken from Konrad, 2005 [30].

Tissue Properties

Generally speaking, the human body is a relatively good electrical conductor. However, the conductivity depends on different variables such as:

- type of tissue
- thickness of tissue
- physiological changes in tissue
- temperature

These factors vary considerably between subjects and even between different application positions at one subject. Therefore, no quantitative comparison between different EMG measurements is possible when investigating the raw signal.

Physiological Cross Talk

Since the EMG signal is the algebraic sum of all MUAPs in the range of the sensor, neighbouring muscles may contribute a significant quantity to the collected signal (up to 10 % - 15 % [30]). This phenomena is called cross talk and needs to be considered, especially when measuring muscle groups that are geometrically close. De Luca & Merletti, 1988 [63] recommended particular caution when interpreting EMG signals, especially when the activation of nearby muscles cannot be excluded. Therefore, the data collected with a surface EMG sensor cannot be assumed to originate from a single muscle. Furthermore, the EMG signal can be contaminated by electrocardiographic (ECG) signals which are emitted from the heart [64]; this occurs primarily when collecting data from muscles of the torso or the upper extremities.

External Noise

The EMG recording might also be contaminated electromagnetic radiation which originates from electrical devices, fluorescent lights and power lines (50 Hz).

Changes in Muscle-Electrode-Distance

The measurement of the EMG signal during dynamic motion involves another factor that influences the shape of the signal. The motion of the muscle belly underneath the sensor changes the distance to the electrode and therefore, influences the shape of the signal. Furthermore, the innervation zones of the muscle might move under the sensor so that no signal can be detected at all [65].
Pressure on the muscle or the sensor may also lead to artefacts in the collected signal.

1.5.3. Surface EMG Measurement

As described above, the EMG signal is influenced by many different factors. The placement of the sensor therefore is an important issue. Since the methodical developments have been made mostly locally by different research groups, a standardisation was required. In 1996 the so-called SENIAM (surface EMG for a non-invasive assessment of muscles) project was started to develop recommendations for the surface EMG sensors and the sensor placement procedure. Hermens et al., 2000 proposed six steps for a surface EMG measurement and described recommendations for each of these steps [66].

Step 1: Selection of the SEMG sensor

The shape and size of the sensor needs to be specified. Regarding the shape, there is no clear criteria as recommendation. The size of the electrodes should not exceed 10 mm.

Step 2: Preparation of the skin

The skin needs to be prepared carefully prior to the placement of the electrodes, since a good electrode-skin contact is required for a good signal quality. Therefore, it is recommended to shave the skin and to clean the sensor area with alcohol. It is also recommended to let the alcohol vaporize afterwards, so the skin area is dry before placing the sensor.

Step 3: Positioning the patient in a starting posture

During the SENIAM project, a starting posture was defined for each muscle. It is required, since the target muscle and the anatomical landmarks need to be determined clearly. The positions can be found on www.seniam.org [67].

Step 4: Determination of sensor location

The location of the sensor is a very important factor for the quality of the surface EMG signal. Therefore, 27 different recommendations for sensor placements have been proposed by the SEMIAM project. These proposals were based on two general points. With respect to the longitudinal positioning of the sensor on the muscle, the sensor should be placed halfway between the most distal endplate zone and the most distal tendon. Regarding the transversal location, the sensor should be placed in order to maximize the geometrical distance to other subdivisions or muscles.

Step 5: Placement and fixation of the sensor

When the location of the sensor is chosen, the orientation needs to be specified. It is recommended to orientate the sensor parallel to the muscle fibres. The sensor should be fixed with double-sided tape and the cables of the electrodes should be fixed on the skin as well. For the reference electrode, the wrist, ankle or processus spinosus of C7 are common standard positions.

Step 6: Testing the connection

When the sensor is placed on the skin, a test can be performed and the signal quality can be checked. After that, the measurement can be carried out.

There are different recommendations for the positioning of the sensors. In figure 1.8 and figure 1.9 the proposals from Peter Konrad's ABC of EMG are shown. These sensor locations are collected from the SENIAM project [67], from [68], Cram, 1998 [69] and Basmajian, 1989 [70].

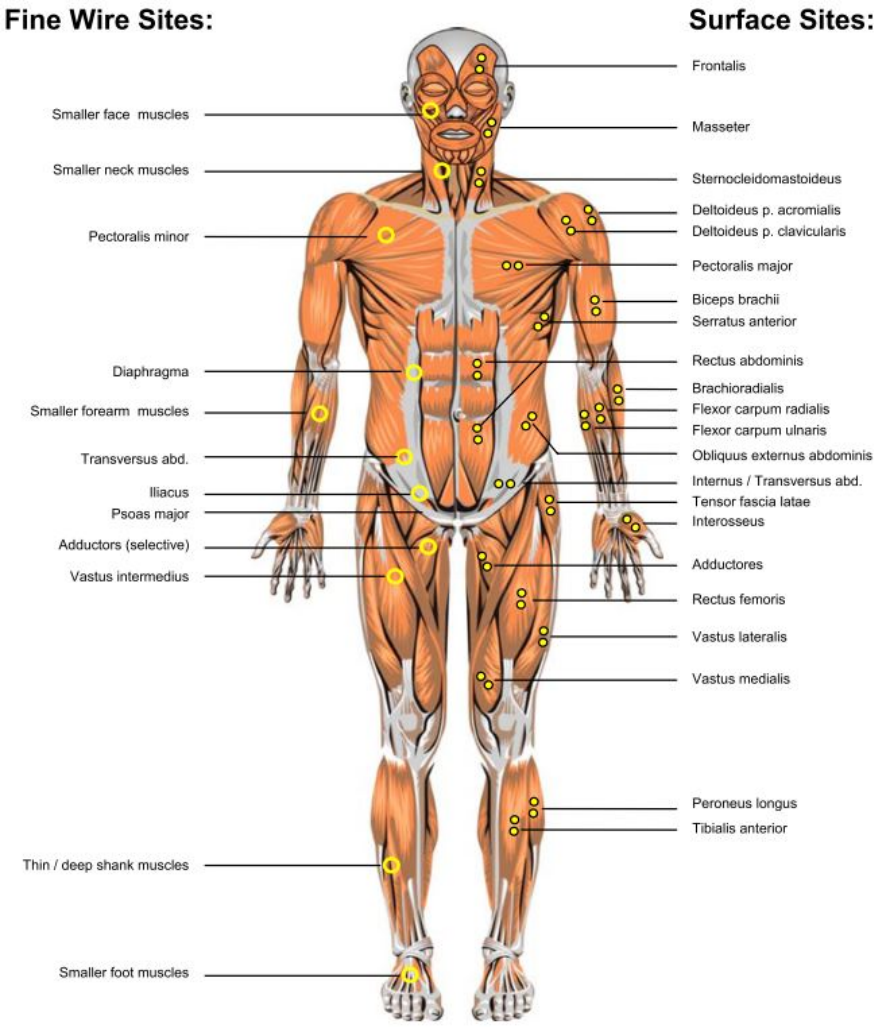

Figure 1.8.: Placement of sensors from Konrad, 2005 [30], frontal view

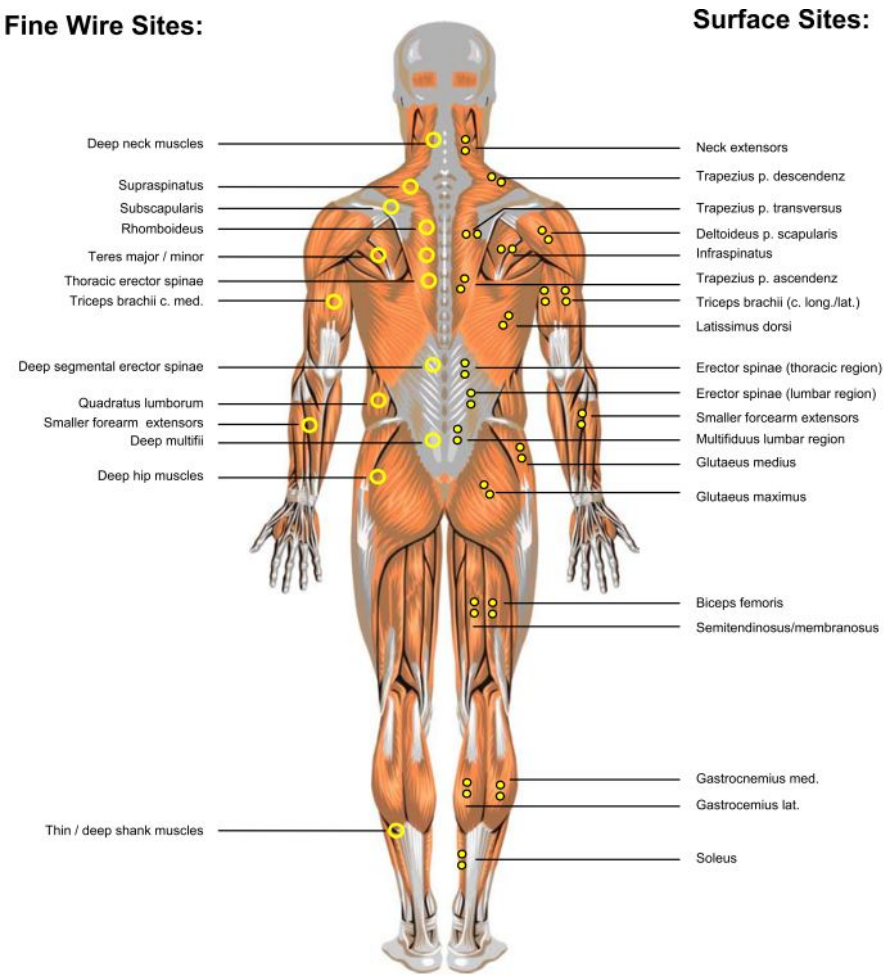

Figure 1.9.: Placement of sensors from Konrad, 2005 [30], back view

1.5.4. Surface EMG - Force Relationship

The insight in the muscle force of single muscles is an important factor in biomechanic research since the forces of muscles are the main determinants for joint loadings. Since the direct measurement of muscle force is only possible with invasive procedures and furthermore only for certain muscles [71, 72], the estimation of muscle forces based on EMG measurements is frequently used. Therefore, the relationship between the EMG signal and the generated muscle force needs to be clarified.

The force output of a muscle depends on the number of active MUs, their cross-

sectional area (size) and their firing rate [73]. Therefore, spatial and temporal information is required to estimate the muscle force. All three factors influence the EMG signal as described in chapter 1.5.2. Since the EMG signal is only one-dimensional it can only provide an imperfect representation of all three factors. To address the issue of spatial information, multi-channel EMG [74–78] have been confirmed to improve the EMG based force estimation [79].

It must also be considered, that the EMG signal is influenced by factors that are not relevant for the force production of the muscle like, for example, the wave shape of the MUAP [76, 80]. Furthermore, the muscle force is influenced by factors that are not represented in the EMG signal, such as the instantaneous muscle length, the rate of length [81] or the contraction history [82]. Other influencing factors on the quality of the EMG-based muscle force estimation are the quality of the instrumentation and the procedure of the signal acquisition [83–88].

The shape of the relationship has been investigated in several studies with different results. A linear relation was found for example by Bigland and Lippold, 1953 [89], DeJong and Freund, 1967 [90], DeVries, 1968 [91], Kroner et al., 1984 [92] or Milner-Brown and Stein 1975 [73]. A non-linear relation on the other hand was suggested for example by Alkner at al., 2000 [93], De Luca et al., 1997 [80], Komi and Buskirk, 1970 [94], Potvin, 1996 [95], Solomonow et al., 1886 [96], Vink et al. 1987 [97] or Zuniga and Simons, 1969 [98].

Animal models suggest that narrow recruitment ranges lead to a more linear relationship between the muscle force and the EMG signal [99, 100], which was also found in humans [101]. Therefore, a linear or non-linear relation depends on the fibre composition of the muscle, where a uniform composition leads to a linear relation, while non-uniform composition lead to non-linear relation. In conclusion, the relationship between muscle force and EMG signal is not trivial and might not necessarily be linear but as proven by several studies, reasonable results can be achieved assuming a linear description of the relationship between muscle force and EMG signal [102].

1.5.5. EMG Signal Normalization

The EMG signal is influenced by many different physiological and non-physiological factors as described in section 1.5.2. It has been shown, that when comparing different subjects, muscles or measurements on different days, a normalization of the raw EMG signal is required [69, 80, 103]. An interpretation of the raw signal is only possible when comparing signals qualitatively and therefore, the absolute values are irrelevant. Even then, certain circumstances need to be fulfilled, for example the data needs to be collected from one individual in one session. Furthermore, the set-up during the session such as sensor placement, the filtering of the signal or the amplification must not be changed. A constant temperature and humidity is also required during the session, when analysing the raw signal.[104]
There are also different analysis with the EMG signal that are not sensitive to the amplitude of the signal and therefore, do not require a normalization. For example when investigating the frequency of the signal using a Fast Fourier transform (FFT) no normalization needs to be done since the frequency is not sensitive to the amplitude. The shape of the signal frequency is often analysed when monitoring muscle fatigue.
Another method that can be done without normalization is the decomposition of the EMG signal into wavelets. This is often used when analysing firing patterns of the MUs or to investigate cross talk between muscles.
When the time of the muscle activation and deactivation is of interest, which is for example defined as a multiple of the standard deviation of mean above the base line level [105, 106], also the raw signal can be used without any normalization.
The described methods show that an interpretation of the raw EMG signal is only possible to a limited extend and usually does not allow the comparison between measurements of different individuals or sessions. To deal with this problem, Eberhart et al., 1954 [107] were the first to propose a normalization method. Since then, different methods have been developed. The signal is usually divided by a reference EMG value which is determined from the same muscle under the same conditions. In order to guarantee a high reliability, the reference value needs to fulfil certain conditions. First of all, the method of recording the reference value needs to be highly repeatable. Secondly, it needs to be assured, that the value

has similar meaning between subjects or muscles. The choice of the normalization method needs to be taken into consideration when interpreting measurements, since it influences the pattern and the amplitude of the results [108]. Over the last decades, different methods have been proposed to normalize the EMG signal. In the following, the most popular methods are described and discussed.
The most common method to normalize EMG signals, is by obtaining the reference EMG value during an isometric maximum voluntary contraction [101, 109–111]. Different tests have been proposed for different muscles where the muscle can produce maximum contraction while the EMG signal is recorded. Some examples are summarised by Halaki & Ginn, 2012 [104]. The different tests collected and proposed by Konrad, 2005 [30] are shown in figure 1.10 and figure 1.11. The procedure for these measurements is the following:

1. Fixate subject in position
2. Slowly begin to increase force level to the maximum within 3 - 5 s
3. Hold maximum force level for 5 s
4. Slowly calm down within 3 - 5 s

Matthiassen et al., 1995 [112] recommends at least three repetitions of this procedure with a recovery break of 120 s in between. Konrad, 2005 [30] recommends a resting period of 30 - 60 s and 2 repetitions. The recorded signal is high-pass filtered, rectified and smoothed. Alternatively, the root-mean-square of the signal is calculated. The maximum value is then obtained from all trials and used as reference value for the normalization. This method allows a comparison of activation levels during different tasks in reference to the maximum activation capacity [113–115].
However, this method is highly dependent on the test procedure that is used to obtain the reference value. Since the maximum activation of a muscle is required, a proper guidance of the subject is necessary. Furthermore, not for every muscle a test is known where maximum contraction can be achieved. Consequently, several studies report an activity level greater than 100 % [103, 116, 117].

Muscle group	Exercise	Comments
Forearm flexors / extensors	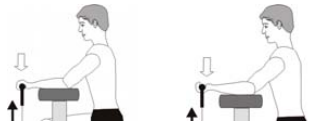	Select a seated or kneeling position (in front of a bench) and arrange a stable forearm support. Manual resistance, barbells or cable/belts can be used. Consider using the latissimus d. and pectoralis major MVC test as a control exercise
Biceps Brachii		A valid biceps b. MVC needs a very stable elbow and trunk fixation. This can best be arranged in a seated or kneeling position (in front of a bench). Consider using the latissimus d. MVC-test as a control exercise.
Triceps Brachii		Same instruction as biceps b.! Consider using the pectoralis major MVC-test as a control exercise.
Deltoideus	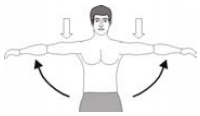	Select a seated position, if possible with fixated back. Fixate near the arms near the 90° position. The bilateral contractions guarantee a balanced force distribution for the trunk. The abduction works best for the pars acromialis of the deltoid muscle. Consider a flexion/extension position for the pars clavicularis.
Trapezius p. descendens	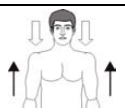	The MVC test can be performed with one side only. A static resistance can be arranged by manually fixating the arm or arrange a large enough load to press the shoulder down (difficult).
Pectoralis major		Numerous test positions can be used! However, all of them need a very good shoulder/back resistance. The prone lying position would best be performed with a (fixated) long bar. The push up may work as an easy to arrange alternative. Both positions should be performed in 90° elbow position.
Infraspinatus	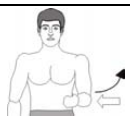	Being the most important outward rotator of the shoulder cuff, any related outward rotation may work. Good results are achieved with uni- or bilateral manual resistance against the forearm
Trapezius p. trans. / Rhomboideus	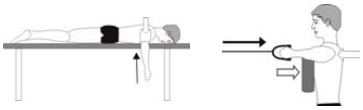	The horizontal abduction best addresses the shoulder stabilization muscles. In the prone laying position a barbell or bilateral manual resistance can be used. The seated position requires a good breast fixation and a cable or machine resistance (rowing machines).
Latissimus/Trapezius p. ascendence	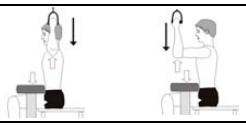	The simulation of a pull-up addresses the highest latissimus innervation. Consider/check a frontal and a lateral arm position at 90° elbow flexion. You may find MVCs for the biceps and the lower trapezius also.

Figure 1.10.: MVC tests proposed by Konrad, 2005 [30] for muscle groups in the upper body and the upper limbs. The black arrow indicates the movement direction of the subject, the white arrow indicates the resistance direction.

Muscle group	Exercise	Comments
Rectus abdominis Obliquus internus abdominis		A valid MVC test for the abdominals is difficult to arrange. Sit-up styled movements with very good leg fixation (!) work best. Let the spine flex by around 30° and use a belt or manual fixation for that position. The obliques may fire higher when an additional trunk rotation is added to the flexion
Obliquus externus abdominis	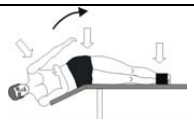	This MVC test needs good coordinative skill. A side laying position with leg and hip fixation is a good start position. Let the subject flex up and fixate early in the flexion position. An important check exercise is the MVC test for the rectus abdominis
Erector spinae / Multifidii	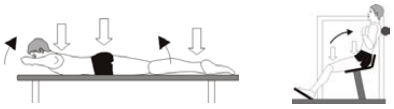	The prone laying position on a bench is a very productive MVC test position. Because all back muscles are facilitated within a muscle chain, MVCs for the erector spinae, the gluteus and the hamstrings can be found here. A check exercise is the isolated back extension at a machine
Glutaeus maximus	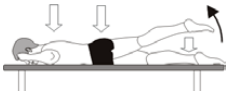	A control exercise for the gluteus maximus muscle! It should be performed both in extended and flexed knee position with slightly outward rotated legs. The hyperextension position (~20°) is important.
Glutaeus medius	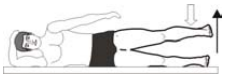	The hip abduction can be performed in fixated side laying position or supine position. Some subjects show higher EMGs in standing position
Mm. adductores		A big and stiff roll cushion is pressed between the flexed legs
Rectus femoris		An easy and beneficial exercise for all quadriceps muscles! A single leg knee extension between 90 and 70° knee flexion position is performed
Mm ischiocrurales	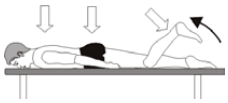	Isolated test for the hamstrings. Arrange a very good fixation of the hip (belt/heavy person) and perform a unilateral knee flexion at ~ 20-30° knee flexion. An important check exercise is the prone laying MVC test for the erector spinae
Gastrocnemius		Being one of the strongest human muscles, the triceps surae group needs very rigid (machine) resistance against the fixated hip. Perform an unilateral plantar flexion at 90° ankle position
Soleus		This is an important check exercise for the soleus muscle because the gastrocnemius is at a difficult work position. Perform a unilateral plantar flexion. A very rigid fixation of the knee is needed due to high forces
Tibialis anterior	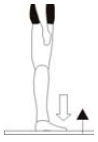	The tibialis anterior usually can be fixated by manual resistance, work unilateral

Figure 1.11.: MVC tests proposed by Konrad, 2005 [30] for muscle groups in the back, abdomen and the lower extremities. The black arrow indicates the movement direction of the subject, the white arrow indicates the resistance direction.

This indicates, that the MVC test does not necessarily reveal the maximum activation capacity of individual muscles. The consequence of this is an overestimation of the activity level [118]. For a valid comparison of activation levels, the test for maximum capacity needs to be reliable [119]. Several studies are concerned with the investigation of test procedures to estimate maximum voluntary activation level. Nevertheless, no single test procedure is valid for all test subjects to reveal maximum activation [120–130]. It is therefore recommended to use different exercises to measure the maximum activation level of a single muscle.

Another similar method to obtain the reference value for normalization is to measure the EMG signal while the subject is conducting the requested task with maximum effort, for example during maximum sprinting [131, 132], or maximum cycling [133]. This method was proven to have high reliability between trials and reduces the chances of obtaining results greater than 100 % [131, 132]. However, as already discussed, the maximum activation level of the investigated muscle might not be achieved during the task [108]. Furthermore, this method of normalization is highly dependent on the task and does not allow comparison of measurements from different tasks. Different test subjects might also have different activation patterns when conducting the same exercise which also leads to various activation levels.

Since there is a contrary discussion whether or not the EMG signal is dependent [134–137] or independent [138–140] of the muscle length, it is questioned if isometric measurements are suitable for determining the reference value for dynamic contractions [114]. Therefore, Mirka et al., 1991 [141] proposed a method where the maximum activation level is recorded during a maximum isokinetic contraction that is conducted with same speed as the measured task. The activation level vs joint angle curve from this is used for normalization. This method is not reliable within a test subject [142]. Furthermore, the EMG signal is dependent on the contraction velocity for a given force level [143], which makes recordings for different velocities necessary.

The methods described above have in common, that maximum effort is required to determine the reference value for the normalization. Since it is often difficult to voluntarily activate a muscle to its full magnitude or not possible at all due to injuries or pain [108, 144], different methods have been proposed using activation

levels during sub-maximal contraction [113, 115, 145–147]. Relative or absolute muscle loadings are used to measure the activation level. The normalization of the signal to a value from sub-maximal contraction however has different drawbacks. At first, the comparison of activity levels between muscles is not valid, since the reference value is not relative to the maximum length. When using absolute weights, the comparison between subjects is also not valid. Since the length of the moment arm of the muscles varies between subjects, and the EMG signal is related to the muscle force and not the torque of the joint, the normalization to sub-maximal contraction does not allow comparison between individuals. [104]
The normalization using the peak or mean activation level obtained during the investigated task is another method that does not require maximum contraction. This method was first proposed by Eberhart et al., 1954 [107], where the EMG signal was normalized to the peak muscle activity during a gait cycle and afterwards used in various studies [113, 114, 146, 148, 149]. It has been shown that this method decreases the variability between subjects compared to raw signal analysis or normalization to the MVC [113, 114, 146, 148]. However, the variability between different days is higher compared to MVC normalization [150]. Furthermore, the activity level for a specific task is dependent on the strength of the subject and therefore no comparison between muscles, tasks or individuals is possible when using the peak or mean activation level obtained during the task that is investigated as reference value.
The estimation of the reference value using the maximum peak to peak amplitude (M-max) of the M-wave is also a further method. Therefore, the $\alpha-$motor neuron is externally stimulated and the EMG answer (M-wave) is recorded. The stimulus is increased until the peak to peak amplitude does not further increase. To measure the reference value, the stimulus is then increased another 30 % [151]. Since the repeatability of M-max is problematic due to factors like its dependence on muscle length [152–154], this method is questioned at the moment [104].

In conclusion, the normalization to a reference value obtained during maximum isometric contraction can be used to compare muscle activity levels between different tasks, individuals or muscles, presupposed that the exercise is suitable to reveal maximum activation level of the muscle. The normalization to the peak or

mean activity recorded during the task is useful when comparing muscle activation pattern between individuals. A reliable comparison between muscles, tasks, or individuals is not possible. Both the normalization to a sub-maximal contraction and to the maximum activation during task conducted with maximum effort are not valid when comparing activity levels between individuals, muscles, or tasks. The normalization to the M-max cannot be recommended due to its low inter-subject reliability. [104]

1.5.6. Manifestation of Muscle Fatigue in the EMG signal

EMG measurements are the most common way to study muscle activity within the human body and as already discussed, has also been established as a non-invasive method to study muscle fatigue [155]. The first report of muscle fatigue discovered in the EMG signal was published at the beginning of the 20^{th} century by Piper, 1912, who described a 'slowing' of the signal during isometric contraction [60]. Since then, different methods have been proposed for the manifestation of fatigue in the myoelectric signal.

Time Domain Methods

The analysis of the number of zero-crossings was for example used by Hägg et al., 1991 [156] or Inbar et al., 1986 [157]. They defined the zero-crossing rate or zero-crossing frequency as half of the number of zero crossings per second. The main limitation of this method is a high dependency on the signal to noise ratio, which can be reduced by introducing a non-zero threshold to the signal [57]. Another limitation, however, is that the zero-crossings are linearly dependent on the force of the contraction during low intensity [158]. Furthermore, this method is very sensitive to the deviation of amplitude distribution. Due to these limitations, the method of zero-crossing analysis is not used frequently [155].
The method of spike analysis for fatigue manifestation has been proposed by Gabriel et al., 2000 [159]. Here a spike is defined as any pair of upward downward deflection. However, applying this method, contradictory results have been found on the reliability of EMG spike parameters and therefore, this method is also not used frequently when analysing fatigue.

The dominant changes of the EMG signal in time domain are changes of the amplitude caused by effort or fatigue. This was first reported by Inman et al., 1952 [136]. Basically two different variables can be calculated when investigating the signal amplitude. The first one is the mean absolute value or average rectified value, which is calculated as described by equation 1.14. The second and most common value is the RMS value which is described by equation 1.15.

$$MAV = \frac{1}{N}\sum_{i=1}^{N}|x_i| \tag{1.14}$$

$$RMS = \sqrt{\frac{1}{N}\sum_{i=1}^{N}x_i^2} \tag{1.15}$$

with N describing the number of samples and x_i is the i^{th} sample of the signal. Both variables are suitable to analyse the signal amplitude. However, the RMS may be more appropriate since it represents the signal power and has therefore a clearer physical meaning [160]. The changes of the signal amplitude are used as an indicator for fatigue.

Frequency Domain Methods

Additional to the time domain methods, several frequency domain methods have been proposed. The most frequently used method is the Fourier-based spectral estimation. Therein, the power spectral density and the periodigram of the signal are calculated.

Another method is the use of parametric based spectral estimators. Here the transfer functions of a finite number of parameters are calculated and an autoregressive model is used to approximate the original signal. In literature contradictory information for the order of the autoregressive model is proposed. Paiss and Inbar, 1987, for example found no significant changes of results testing autoregressive models with the orders 3-30 [161]. Compared to that, Merletti and Lo Conte, 1995 reported, that satisfactory results were only obtained by using orders of 4-6 [162].

Under the assumption of a stationary signal during isometric contraction a Fourier transform can be applied. This, however, is not possible when analysing dynamic

contraction. Therefore, a short-time Fourier transform and spectrogram can be calculated. This method has the advantage of allowing the analysis of dynamic contraction, since the stationary requirement can be fulfilled for short segments of the signal. Furthermore, it gives the possibility to analyse the spectrum as a function of time [155].
Since the EMG spectrum and the amplitude are both sensitive to muscle fatigue, a combined analysis is proposed and used in various studies. Luttmann et al., 2000 distinguished four different cases that are described in table 1.3 [163].

Table 1.3.: Four different cases of signal amplitude and signal spectogram progress and their interpretation by Luttmann et al., 2000 [163]

	Increasing EMG amplitude	**Decreasing EMG amplitude**
Increasing EMG spectrum	Muscle force increasing	Recovery from previous fatigue
Decreasing EMG spectrum	Muscle fatigue	Muscle force decreasing

2. Material and Methods

The main goal of this thesis was to develop and validate a novel fatigue algorithm and to implement it into the AMS allowing the simulation of long-term effects on the musculoskeletal system. In this chapter, the experimental studies which were conducted to develop the fatigue algorithms are described. Furthermore, the construction of the AMS model is explained. Therefore, the whole study was subdivided into four work packages shown in figure 2.1.

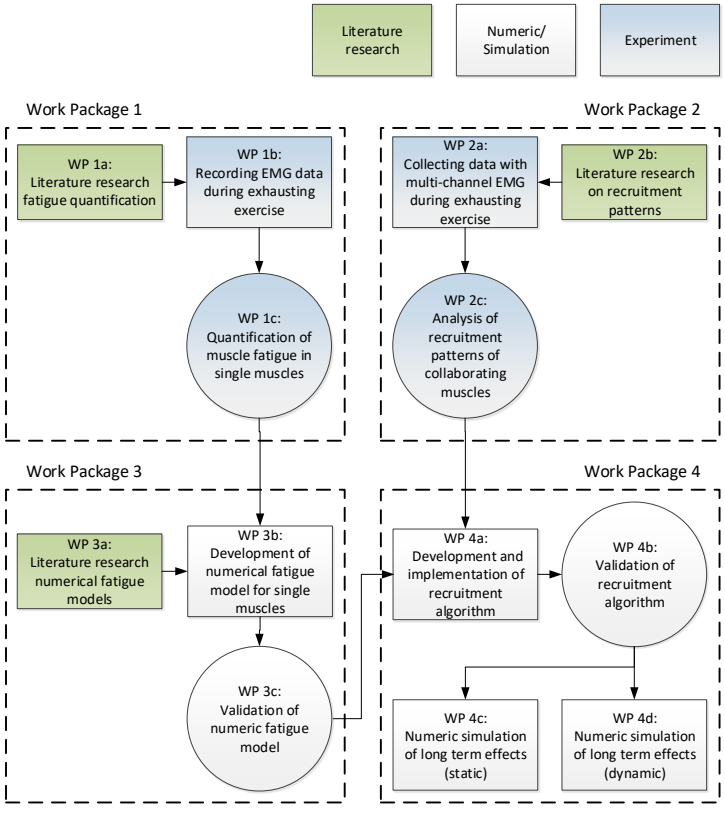

Figure 2.1.: Simplified workflow of the project

The first experimental study aimed to investigate the progress of muscle fatigue of single muscles. Furthermore, the data for the validation of the fatigue was recorded during this study. For the development of the novel algorithm, information about the progress of muscle fatigue in relation to relative muscle loading was required. The development of the novel fatigue algorithm based on electromyographic measurements as one of the main goals of this thesis is described in section 2.2.
The second experimental study was designed to analyse the global muscle recruitment pattern when experiencing fatigue. The design of the study is described in section 2.3.
The last section of this chapter describes the investigation of the muscle recruitment algorithm of the AMS with implemented muscle fatigue. The extension of the AMS model, the python script described in section 2.1 and the construction of the AMS model to analyse the behaviour of the muscle recruitment algorithm are described in the next sections.

2.1. Investigation of Fatigue Progress of m. Biceps Brachii and m. Triceps Brachii

In the following, the experimental study which was designed to collect information about the progress of muscle fatigue of single muscles in relation to relative muscle loading is described.

2.1.1. Experimental Set-up

Subject Description

In this study 20 healthy male subjects participated. Before including the subjects to the study, they were informed about the whole test protocol as well as potential risks and signed a written consent. The study was also approved by the local ethics committee. In order to minimize the risk of injuries, subjects with a medical history concerning the shoulder and arm of the dominant side were excluded from the start. The test subjects were asked to avoid exhausting physical activities one day prior to the measurements, to reduce the influence of initial exhaustion.

Study Protocol

During the study, the arm of the dominant side of each participant was measured. To record the muscle activity, four pre-amplified EMG Delsys Trigno^{TM} IM sensors (Delsys Inc., Wellesley MA, USA) were used. Two sensors were placed on the m. biceps brachii as shown in figure 2.2 (left). One of the sensors was placed following the recommendations by Criswell, 2010 [164]. The second sensor was placed proximal to this sensor to control the influence of muscle belly movement during dynamic contraction. The two sensors for the m. triceps brachii were placed alike. The EMG signal was collected with a sampling rate of 1111 Hz and was bandpass filtered between 20 Hz and 450 Hz following the recommendations by De Luca et al., 2010 [165], who proposed these filtering bounds to reduce the influence of high frequency noise and low frequency electrocardiographic artefacts. Before attaching the sensors with the Trigno^{TM} sensor skin interface, (SC-F03) (Delsys Inc., Wellesley MA, USA), the skin was prepared with alcohol to ensure a good signal quality.

All exercises were conducted using a dynamometer (CON-TREX® WS, Physiomed, Schneittach, Germany), which was utilized to measure the torque, angular position and angular velocity. The measurements were recorded using a HBM quantum X system (Hottinger Baldwin Messtechnik GmbH, Darmstadt, Germany) with a sampling rate of 300 Hz. The HBM system was also used to trigger the whole measurement to ensure a simultaneous start of the data recording from all used systems. To fixate the forearm at the dynamometer, an adapter was constructed which is shown in figure 2.3.

The centre of rotation of the elbow joint was aligned with the centre of rotation of the dynamometer. The forearm was then fixed with the two shells from above and below. To avoid discomfort during the exercises, the supporting areas of the elbow as well as the two shells were padded. The fixation of the forearm is shown in figure 2.2.

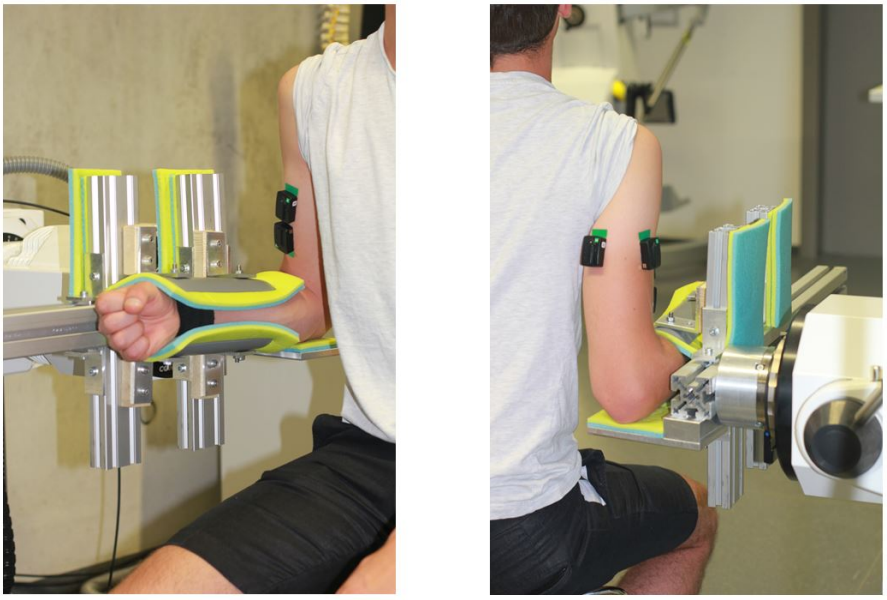

Figure 2.2.: Fixation of the forearm during isometric and dynamic fatigue exercises of the m. biceps brachii and m. triceps brachii

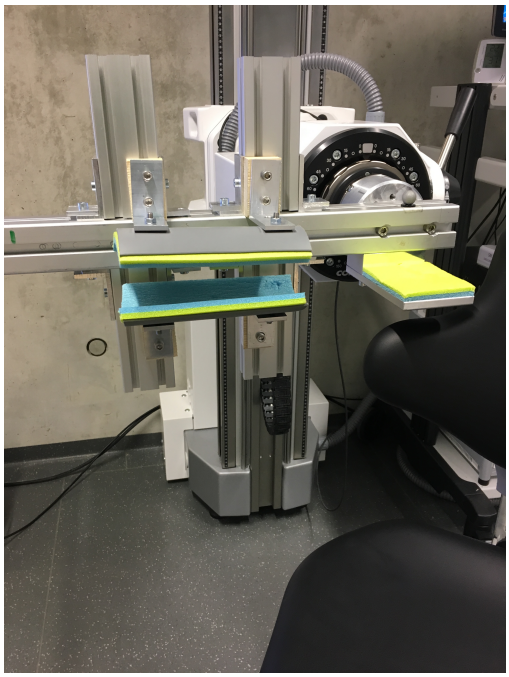

Figure 2.3.: Adjustable adapter used for the fixation of the forearm at the dynamometer during the exercises

Anthropometric Data

Various anthropometric data were measured from each participant. The length of the forearm was measured between the wrist and the elbow condyles with the elbow in a 90° flexion angle. The length of the upper arm was defined between the condyles of the elbow with a 90° flexion angle and the acromion. The width of the shoulder was measured between the left and right acromion. Furthermore, the length of the thorax was defined as the distance between C7 and the sacrum. The total height, weight and the age of each participant were also recorded. The landmarks used to measure the segment length are according to the AMS, so that the values can be used for scaling the model.

Reference Value for Normalization and Relative Muscle Loading

When comparing EMG recordings of different muscles or individuals, a normalization is required as described in section 1.5.5. The reference value for normalization in this study was estimated from a maximum voluntary isometric contraction measurement prior to the exhausting exercises. The test subject was placed and fixated at the dynamometer as described above with the arm in a 90° flexion angle of the elbow joint. Then the participants were advised to increase the force level to the maximum within 3 s and to sustain this force level for another 5 s. After a recovery phase of 60 s the exercise was repeated. This was done for the m. biceps brachii and the m. triceps brachii. The positioning and conduction of the exercise followed the recommendations of Konrad, 2005 [30]. The RMS of the recorded signal was calculated using a 0.1 s non-overlapping sliding window and the reference value was defined as the median of the five highest peaks of the RMS.
Furthermore, the joint torque during the MVC measurement was recorded. To determine the maximum torque, the two 5 s parts of maximum effort were separated from the signal and the mean value was taken as torque reference to calculate the relative muscle loadings during the exhausting exercises.

Isometric Fatigue Protocol

The isometric fatigue protocol was also conducted with the arm of the participants fixed in a 90° flexion angle of the elbow, while sitting in an upright position. Four

different load cases were recorded from each subject defined as 60 %, 50 %, 40 % and 30 % of maximum torque. An additional load case was recorded with alternating forces. The target force was changed every 20 s, starting from 60 % to 30 % to 50 % to 40 % of maximum force. Between two measurements of the same muscle, a recovery time of 5 minutes was ensured. The force level during the fatigue measurements was controlled by the test subject using a visual feedback system as shown in figure 2.4. The target force was marked with the green area ±2.5 %. The yellow areas defines the tolerated force area with another ±2.5 % window. During all exercises, the subjects were advised to sustain the required force as long as possible. The isometric fatigue protocol is shown on the left side of figure 2.5.

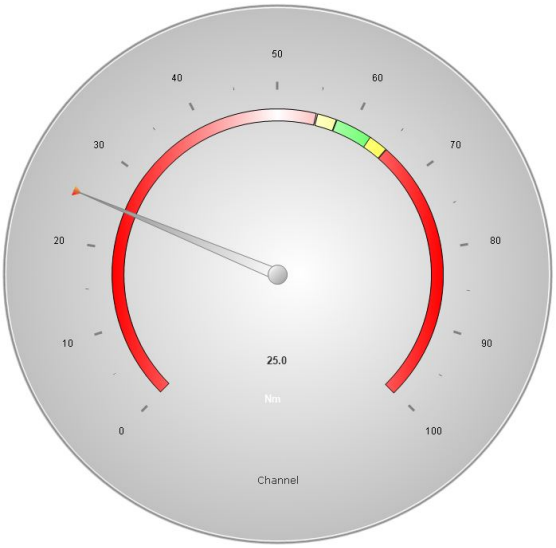

Figure 2.4.: Visual feedback system for subjects to control the force level during isometric exercises

Dynamic Fatigue Protocol

The dynamic fatigue protocol was also conducted in an upright seating position, with the forearm fixed to the dynamometer. The range of motion during dynamic exercises was restricted between 35° and 145° elbow flexion. Test subjects were advised to conduct the exercise with constant angular velocity. The force level during dynamic contraction was controlled by the dynamometer. Four different load cases were measured with 60 %, 50 %, 40 % and 30 % of the maximum force

as target force. Similar to the isometric exercise protocol, a recovery period of 5 minutes was assured between tasks. During all exercises, the participants were advised to conduct as many repetitions as possible.
The dynamic fatigue protocol is shown on the right side of figure 2.5.

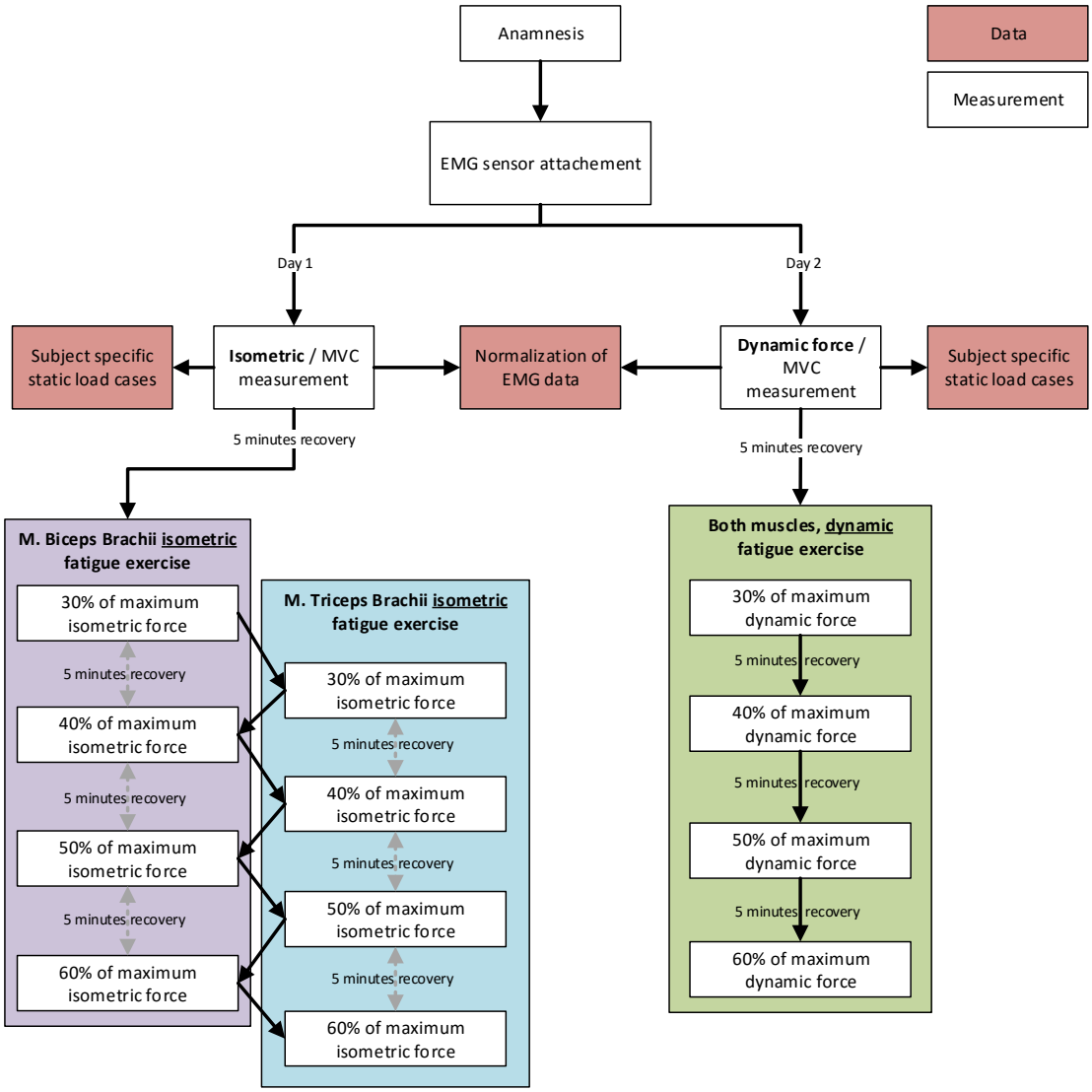

Figure 2.5.: Protocol of the m. biceps brachii and m. triceps brachii fatigue study

Data Processing of the EMG Signal

At first, the offset was corrected by subtracting the mean value of the whole signal from each sample. The second step was to remove the parts of the signal where the muscle was not loaded. Therefore, the torque signal was up-sampled to 1111 Hz and the point in time, where the torque first exceeds 80 % of maximum torque plus 0.5 s was detected. The second value was defined as the last peak of the torque curve that exceeded 80 % of maximum torque minus 0.5 s. These time values were taken to cut the EMG raw signal and to ensure, that the phases of force increase and relaxation at the beginning and the end of the exercise were excluded from analysis. The RMS and the MPF were calculated using a 0.1 s non-overlapping sliding window. The measurements from the exercises with alternating force targets were subdivided into segments with constant loads. The RMS and MPF were then calculated for these segments using a 0.1 s non-overlapping window.
A linear regression was applied to the calculated RMS and MPF. The slope of this fit was then taken to describe the progress of the muscle fatigue as introduced in various studies [166–169]. When assuming a linear force-EMG correlation, the signal can also be normalized to the measured output force to minimize the influence of force fluctuations. This was calculated additionally for the data from the isometric exercises.
An overview of the data processing steps is presented in the figures 2.6 - 2.8 with the calculation of the amplitude progress of the EMG raw signal as an example. The calculation of the MPF progress followed the same protocol.

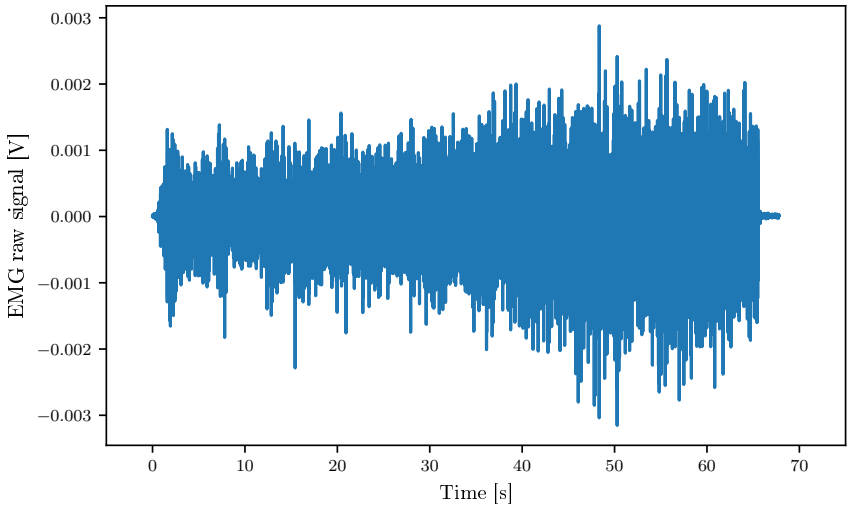

Figure 2.6.: EMG raw signal from isometric contraction

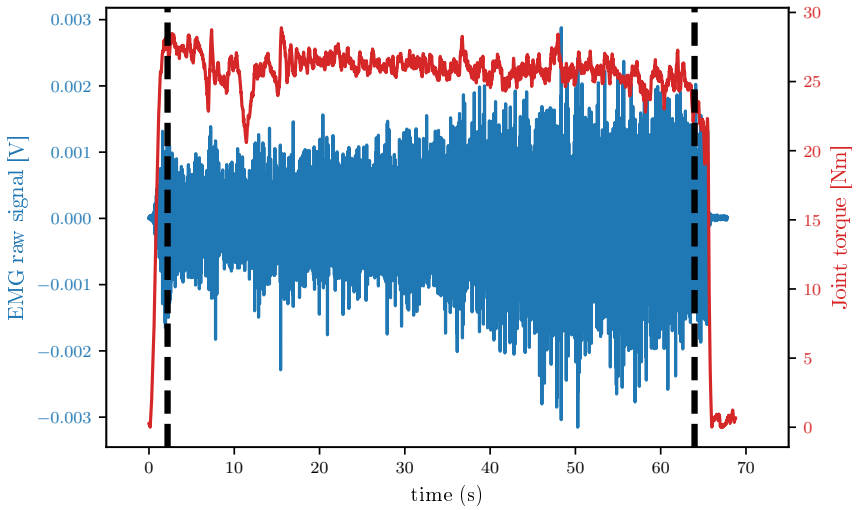

Figure 2.7.: Offset corrected EMG signal from isometric contraction with measured torque and cut times

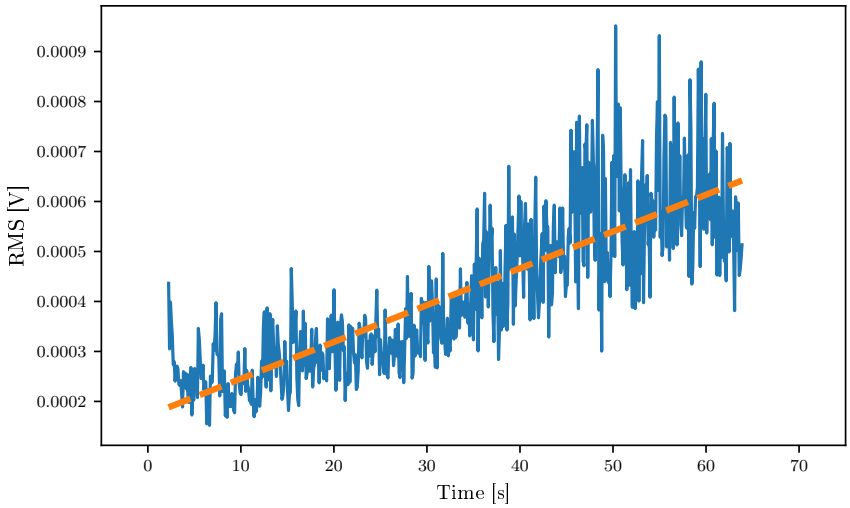

Figure 2.8.: RMS with linear fit to determine slope of RMS progression

For analysing the dynamic contraction, the collected signal was divided into loaded and non-loaded parts by using the measurement of the angular position. The RMS of each cycle was calculated using a 0.1 s non-overlapping window. The mean value of the RMS of each cycle was used to analyse the progress of the raw signal amplitude. Again a linear regression analysis was applied to calculate the slope of the progress. The processing of the data collected during dynamic contraction is shown in figures 2.9 and 2.10.

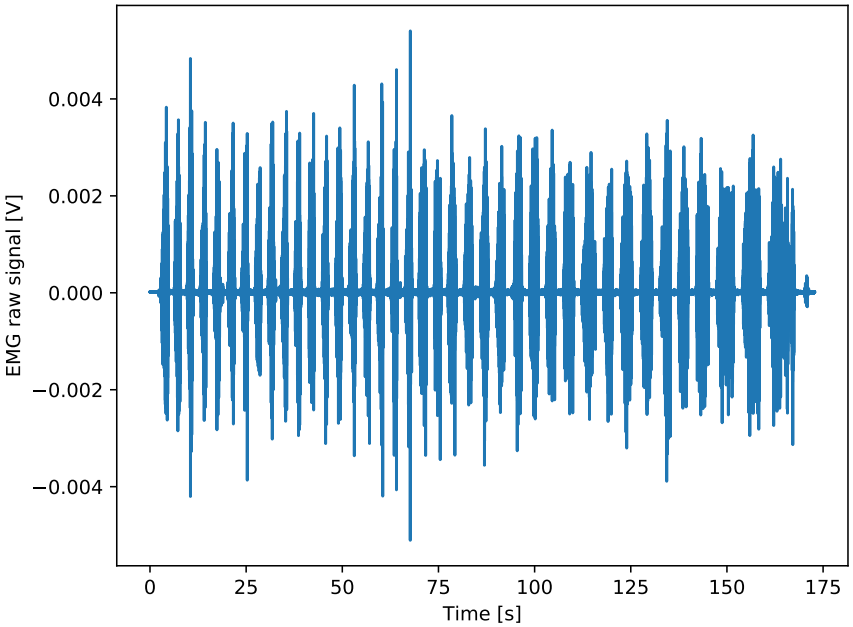

Figure 2.9.: EMG raw signal from dynamic contraction

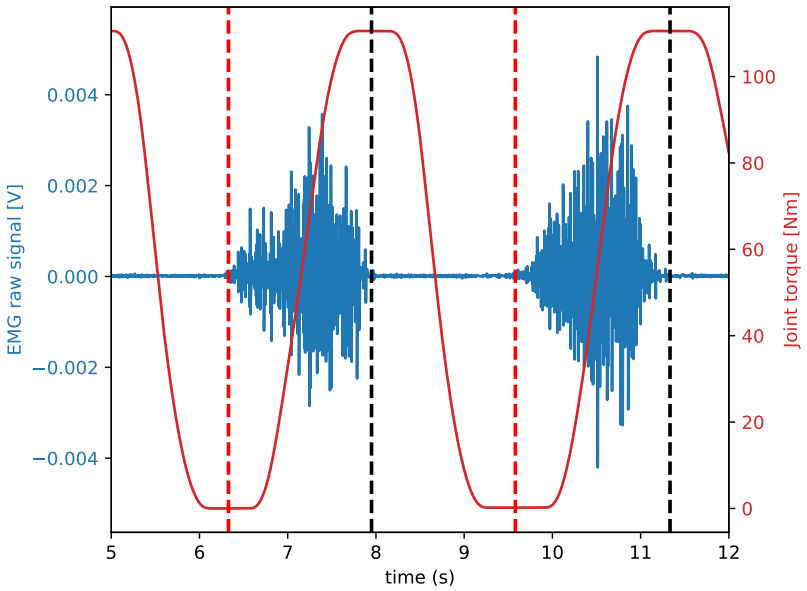

Figure 2.10.: Section of the EMG raw signal from dynamic contraction with cut lines

Statistical Analysis

The mean value ($\pm SD$) was calculated for all variables. Statistical significance of the relationship between the slope of the calculated variables and relative muscle loading was checked by one-way anova with post-hoc Tukey test. The statistical significance was defined for $p < 0.05$.

2.1.2. Summary Investigation of Fatigue Progress

The experimental study described above was designed to investigate the progress of muscle fatigue of single muscles. Therefore, the EMG signals of the m. biceps brachii and m. triceps brachii were collected during isometric and dynamic exercises with different relative muscle loadings. The MVC normalized RMS and the MPF of the signal were calculated and a linear regression analysis was applied to estimate the progress of fatigue. Furthermore, the absolute change of muscle activity during the exercises was calculated to compare the data to the results from the modified AMS model described in the following.

2.2. Development of Fatigue Algorithm, Implementation to AMS and Validation

The numerical model developed in course of this study is a framework of a script run in python from which an AMS model is controlled. In this section, the creation of the model as well as the structure are documented.
The python script requires the subject id, height, weight and force scaling factor. Furthermore, the path to the data file with recorded motion and force during the experimental study needs to be specified. Furthermore, a lowpass filter with a cut frequency of 10 Hz was applied to the motion and force data. This prevented fast muscle activation [170] with a simultaneous avoidance of acceleration peaks which would lead to non-physiological muscle forces.
To simulate the first time step, the force input file and motion input file for the AMS model are prepared. Therefore, a section of 10 values from the measured force data and the measured angular position data each are selected which contain

the time value of the current time step. These values are then written to the import files for the AMS model. This increases the performance of the model, since it needs to be reloaded for each time step and therefore, not the whole file of the measured data needs to be interpolated for every step. The provision of a single value is also not an option, since only one time step is calculated in the AMS and therefore, effects of inertia would not be considered. The main file for the AMS model is then prepared by setting tStart and tEnd to the first time value t_0 of the cut measured data. The variable nStep is set to 1. For the simulation of the first time step, the strength variables of all muscles are set to the initial strength as defined in the standard AMS StandingHuman model. With all files prepared, the AMS model is simulated. The model created in the AMS for this is described in detail in section 2.2.4.

The results from the simulation of the first time step is then imported to the python script. Based on this, the progress of muscle fatigue, muscle recovery and endurance time can be calculated for the next time step, resulting in the current maximum force capacity of each muscle for the next time step. With this calculated, the AMS model is prepared to simulate the next step. Therefore, the variables $tStart = tEnd = t_0 + x \cdot \Delta t$ are set (with x describing the number of the current time step), while nStep remains 1. The import files are rewritten so both files contain the current time step as described above. Furthermore, the strength variables are written according to the calculated $F_{cem}(t)$ for each muscle. Then the AMS model is simulated and the result files are stored. This process is looped until $tStart = tEnd >= t_{-1}$, with t_{-1} as the last time value of the cut measured data. The whole process of simulating the musculoskeletal model including muscle fatigue is shown in figure 2.11. The calculation of the fatigue progress, recovery progress and maximum endurance time is described in detail in the following.

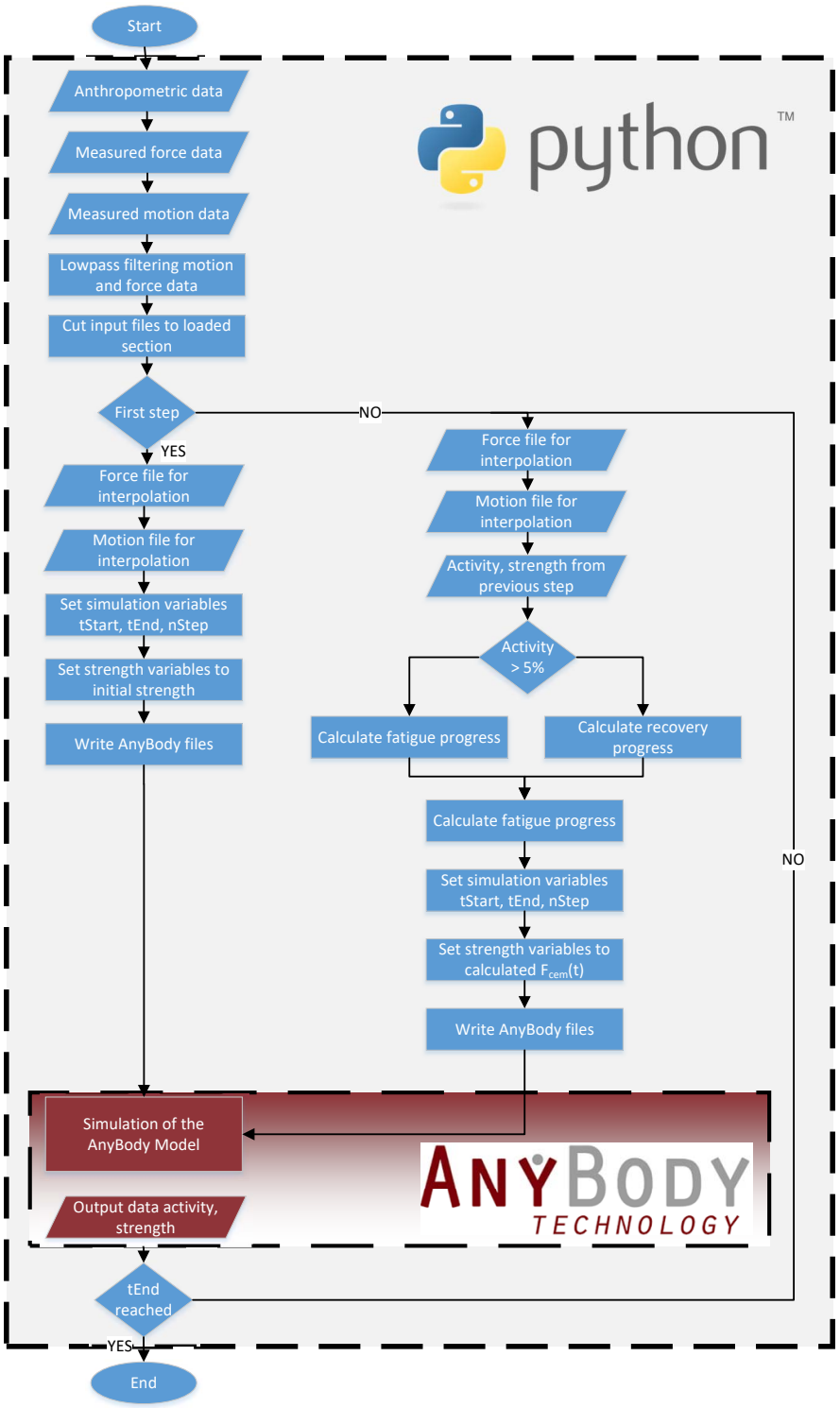

Figure 2.11.: Process of calculating the musculoskeletal model including muscle fatigue

2.2.1. Fatigue Algorithm

The muscle fatigue model is based on the results from the experimental study described in section 2.1. Basically, the activity in the AMS is defined as:

$$Act(t) = \frac{F_{out}(t)}{F_{max}} \tag{2.1}$$

where $Act(t)$ is the activity level of the muscle, F_{out} describes the current muscle force output and F_{max} is the maximum muscle force. Since the maximum force capacity of the muscle is reduced during fatigue, the equation 2.1 can be rewritten as:

$$Act(t) = \frac{F_{out}(t)}{F_{cem}(t)} \tag{2.2}$$

with F_{cem} describing the current maximum force capacity of the muscle.
The progress of the activity during measurements can be described by the equation:

$$Act_M(t + \Delta t) = m \cdot \Delta t \cdot Act_M(t) + Act_M(t) \tag{2.3}$$

where Act_M is the measured activity and m being the slope of the measured activity progress. Assuming a linear *muscle force - activity* correlation for the measured data Act_M is equal to Act and therefore, the progress of activity in the numerical model can be written as:

$$Act(t + \Delta t) = Act_M(t + \Delta t) = m \cdot \Delta t \cdot Act(t) + Act(t) \tag{2.4}$$

Combining the equations 2.2 and 2.4, the progress of the maximum force capacity is calculated as described by equation 2.5 under the assumption of $F_{out} = const.$ during small Δt.

$$F_{cem}(t + \Delta t) = \frac{F_{out}}{m \cdot \Delta t \cdot Act(t) + Act(t)} \tag{2.5}$$

With the equation 2.5 the current force capacity can be calculated for each muscle.

2.2.2. Recovery Model

The recovery model that is implemented was published by Ma et al., 2009a [171]. Similar to the fatigue algorithm, the force capacity of the muscle is altered to describe the muscle recovery. In equation 2.6, the differential equation of the muscle recovery model is shown.

$$\frac{dF_{cem}(t)}{dt} = R(F_{max} - F_{cem}(t)) \tag{2.6}$$

$F_{cem}(t)$ describes the current maximum force capacity at a given time and F_{max} represents the maximum force capacity of the non-fatigued muscle. The recovery rate $R\,[s^{-1}]$ describes the recovery speed of a certain muscle group and is a subject-specific parameter. The recovery level of a muscle is defined as the current strength of the muscle divided by its maximum force capacity in percent ($\frac{F_{cem}(t)}{F_{max}} \cdot 100\,\%$). Calculating the time integral of equation 2.6, the progress of the current force capacity of the muscle can be written as:

$$\begin{aligned} F_{cem}(t) &= F_{max} + (F_{cem}(0) - F_{max})e^{-Rt} \\ &= F_{cem}(0) + (F_{max} - F_{cem}(0))(1 - e^{-Rt}) \end{aligned} \tag{2.7}$$

$F_{cem}(0)$ describes the current force capacity of the muscle at the beginning of the recovery process. This recovery model is based on the physiological mechanism. As described in chapter 1.4.2, the muscle consists of MUs that are activated to contract and therefore to generate force. Different types of MUs react differently to continuous activation. Basically type I and type II fibres are distinguished. The type I fibres are more resistant to recovery, however the force generation is not as rapid as for the more prone to fatigue type II fibres. When a MU is fatigued it can no longer contribute to force generation. This force reduction is described by $(F_{max} - F_{cem}(0))$. The recovery factor is a subject and muscle specific parameter, depending on the physical condition of the subject and the composition of the muscle. However, it is very difficult to distinguish the proportion of type I and type II fibres that contribute to fatigued MUs in a muscle. Therefore, in this study, $R = 0.04s^{-1}$ is used, which fits best when simulating a population according to Liu et al., 2002 [172] or Wood et al., 1997 [173]. The described recovery model is

calculated for each muscle and each time step, provided that $Act(t) < 0.05$.

2.2.3. Endurance Time Model

The numerical model is fitted with a maximum endurance time (MET) model to predict the time how long a subject can sustain a certain load or perform an exercise. The algorithm used is published by Law and Avin, 2010 [174]. They suggest that a single generalized MET model does not describe individual joints appropriately. Furthermore, endurance is best represented by a power function. Therefore, since the m. biceps brachii and m. triceps brachii are of interest in the experimental study described above, an MET model of the elbow was implemented to the numerical simulation.

$$MET = 17.98 \cdot c \cdot F_{cem}(t)^{-2.21} \tag{2.8}$$

where MET is the maximum endurance time. Additionally, the scaling factor c was introduced to allow subject-specific METs. For the generic model used in this study, c is set to 0.95.

2.2.4. AnyBody Model^{TM} Set-up

The numerical model described in this section is based on the 'StandingModel' from the AMMR version 2.1.1 and on the data derived from the experimental study described in section 2.1. The basic model is shown in figure 2.12.

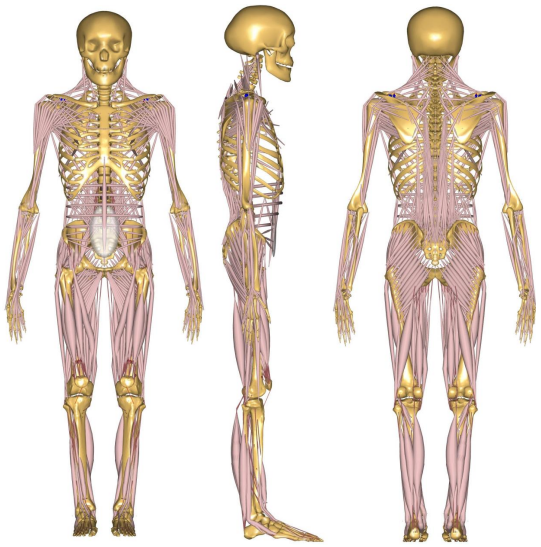

Figure 2.12.: Basic 'StandingHuman' model from the AnyBody AMMR version 2.1.1

Since the upper body with the upper extremities is simulated, the legs were excluded from the model. Furthermore, the muscles of the lower back and the abdomen were not considered. A detailed listing of the 24 segments and 142 muscles included in the model is shown in table C.1 and table C.2. To kinematically determinate the model, the pelvis was fixed at the global reference system in all six DoF and the reaction forces are absorbed (listing B.1). This steps resulted in a model with a total of 228 DoFs.
The angular position derived from the experimental study described in section 2.1 was used to specify the motion of the right arm. The data was lowpass filtered with a cut frequency of 10 Hz and the non - loaded parts of the signal were excluded to shorten the simulation time. The data was imported to the AMS model and interpolated using the 'PiecewiseLinear' interpolator.
The force from the measurements was also lowpass filtered with a cut frequency of 10 Hz, imported to the model and interpolated using the 'PiecewiseLinear' interpolator. As insertion a node was constructed on the segment of the radius in respect to the condyles of the elbow. The distance was adjusted subject - specifically. The force direction was defined as normal to the radius segment in the local coordinate system. The polynomial muscle recruitment solver with a power of 3.0 was used

for the simulations and the lower and upper bounds were turned off. The modified model used in this study is shown in figure 2.13.

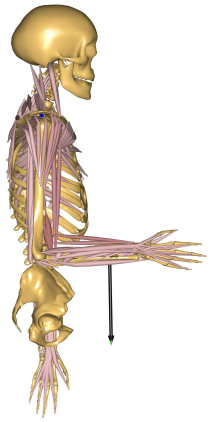

Figure 2.13.: Modified 'StandingHuman' model used to simulate m. biceps brachii and m. triceps brachii exercises; Force vector shows force insertion point exemplary for m. biceps brachii loading

2.2.5. Summary Modified AMS Model of Upper Extremities

To simulate the exhausting exercises, the 'StandingModel' from the AMMR was modified, so that the maximum force capacity of the shoulder and arm muscles could be adjusted. This model was controlled by a python script, where the developed fatigue algorithm, the MET model and the recovery algorithm were implemented to calculate the maximum force capacity of each single muscle for every time step. The calculated muscle activities were analysed and correlated with the results from the experimental study described in section 2.1.

2.3. Experimental Study to Investigate Muscle Recruitment Pattern of the Back Muscles

The progress of muscle fatigue of single muscles was the aim of the first experimental study described in section 2.1. In this section, the interaction of different muscles is examined under the influence of muscle fatigue. The experimental set-up, which was therefore constructed is described in the following. Furthermore,

an AMS model was created to simulate the collected data and to analyse the muscle recruitment solver of the AMS combined with the novel fatigue algorithm described in section 2.2.1.

2.3.1. Experimental Set-up

The experimental protocol was designed to study the interaction of muscles during exhausting exercises. The workflow of the study is shown in figure 2.14 and will be explained in detail in the following.

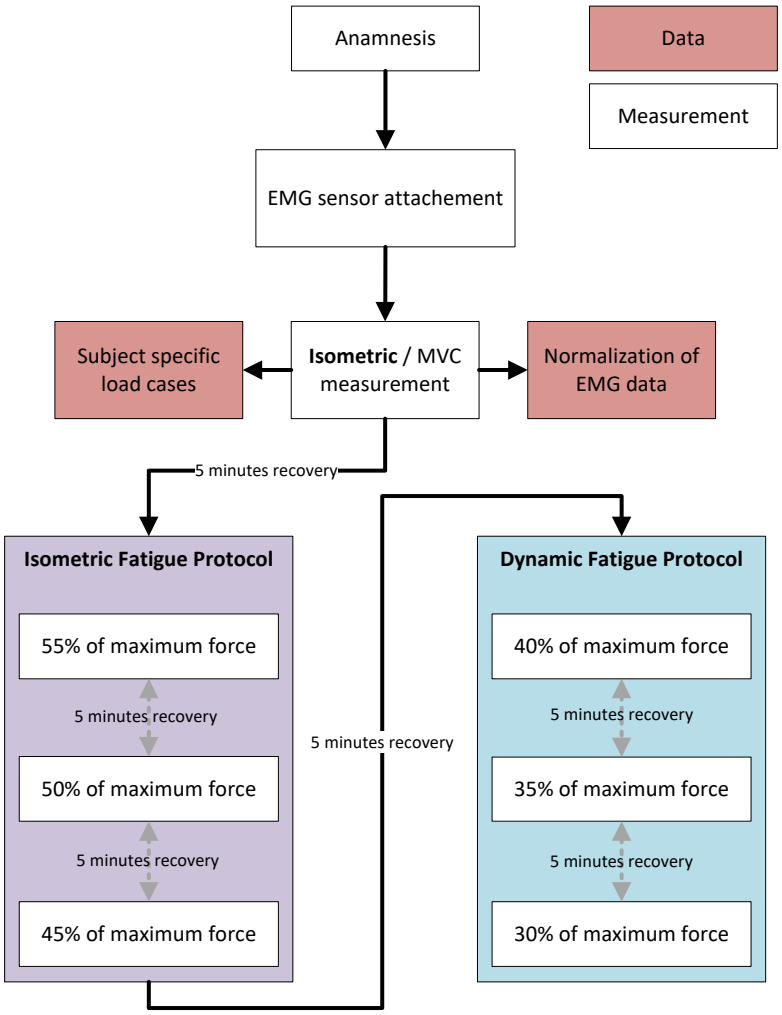

Figure 2.14.: Workflow of the experimental protocol to study muscle recruitment pattern during exhausting exercises

2.3.2. Subject Description

In this study a total of 41 (13 female, 28 male) subjects participated. Prior to the study, all subjects signed a written consent after being informed about the experimental protocol and potential risks. The study was also approved by the local ethics committee. Participants with a medical history of back pain or injuries were excluded from the study. Furthermore, all subjects were advised to avoid physical exercises one day prior to the measurements.

2.3.3. Study Protocol

In this study, the back and abdominal muscles were measured. In total, 16 pre-amplified EMG Delsys Trigno^{TM} sensors were used. Twelve sensors were placed on the back according to Criswell, 2010 [164] for the m. multifidi, m. erector spinae pars longissimus, m. erector spinae pars iliocostalis, m. trapezius ascendens, m. trapezius pars transversa and m. trapezius pars descendens. Furthermore, four sensors were used to measure the activity of rectus abdominis and obliquus externus abdominis. The sensor placement is shown in figure 2.15 with a detailed description in table 2.1.

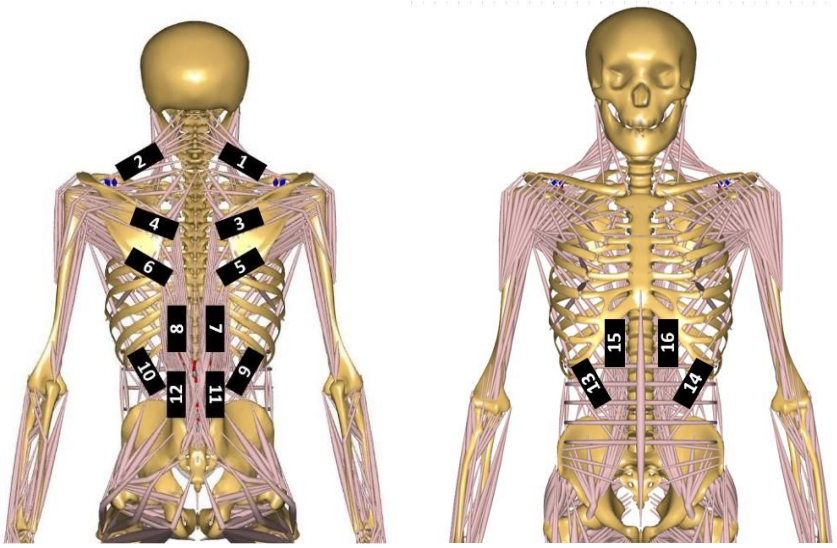

Figure 2.15.: Sensor placement on the back and abdominal muscles

Table 2.1.: Sensor assignment to the muscles used for the muscle recruitment pattern study

Sensor	**Back muscles**
1,2	m. trapezius pars descendens (right, left)
3,4	m. trapezius pars transversa (right, left)
5,6	m. trapezius pars ascendens (right, left)
7,8	m. erector spinae pars longissimus (right, left)
9,10	m. erector spinae pars iliocostalis (right, left)
11,12	m. multifidi (right, left)
Sensor	**Abdominal muscles**
13,14	m. obliquus externus (right, left)
15,16	m. rectus abdominis (right, left)

The signals were collected with a sampling rate of 1111 Hz and bandpass filtered between 20 Hz and 450 Hz following the recommendations by De Luca et al., 2010 [165]. All sensors were placed using the Trigno™ sensor skin interface (SC-F03) after cleaning the skin with alcohol.

To restrain the motion to a flexion and extension of the thorax, the CON-TREX® WS dynamometer combined with the CON-TREX® TP 500 adapter was used. The fixation of each test subject was made according to the manufacture specification above and below the knee as well as the pelvis. The rotational centre was adjusted for each participant and set between the L4 and L5 vertebrae. At the shoulders, the subjects were fixated with a belt, pressing the participant against two vertical cushions. It was ensured, that these cushions did not interfere with the EMG sensors. Additionally, the pelvis was also fixed with a belt, pressing it against another cushion. The settings of the CON-TREX® TP 500 adapter were adjusted for each participant individually. In figure 2.16 the positioning is shown exemplary.

Figure 2.16.: Subject placement in the CON-TREX® TP 500 adapter during the isometric and dynamic exercises

The measurements were recorded using a HBM quantum X system with a sampling rate of 300 Hz. To ensure a simultaneous start of all recording systems, the HBM quantum X was also used to trigger the EMG measurement with the Delsys Trigger Module (Delsys Inc., Wellesley MA, USA).

2.3.4. Anthropometric Data

The anthropometric data were collected for scaling the numerical model created in the AMS. This included:

- age
- height
- weight
- length of the forearm (between wrist and elbow condyles)
- length of the upper arm (between elbow condyles and acromion)

- length of the thorax (between C7 and sacrum)
- length of thigh (between trochanter major and knee condyles)
- length of the shank (between knee condyles and ankle joint)

Similar to the experimental study described in section 2.1, the anatomical landmarks to measure the anthropometric data were taken from the segment length definition of the AMS model.

2.3.5. Reference Values for Normalization and Relative Muscle Loading

As described in section 1.5.5, reference values for the EMG signal normalization are required. In this study, MVC measurements were used to determine these values. The measurement procedure was closely related to the recommendation by Konrad, 2005 [30]. For the m. trapezius pars descendens, the subject was seated in an upright position, and pressing the shoulder in a vertical direction against a static resistance. For the exercise to measure the reference value of the m. trapezius pars transversa, participants were also seated in an upright position with a 90° abduction angle of the humerus joint and a 90° flexion angle of the elbow. To activate the m. trapezius pars transversa in this position, the participants pulled backwards on a static handle. The exercise for maximum activation of the m. trapezius pars ascendens was conducted in an upright seating position with a 90° flexion angle in the humerus and the elbow. The exercises for the m. erector spinae pars longissimus, m. erector spinae pars iliocostalis, m. multifidi, m. rectus abdominis and m. obliquus externus were conducted in the CON-TREX® TP 500 adapter. Therefore, the subject was fixed in the adapter as described above in a 12.5° forward flexion angle.
During all MVC measurements, the subjects were advised to increase the force level to the maximum within 3 s and to preserve the maximum effort for another 5 s before relaxing slowly. Each exercise was repeated after a 60 s recovery break. The normalization value was determined from these measurements by calculating the RMS of each signal with a 0.1 s non-overlapping sliding window. The reference value was defined as the median of the five highest peak values.

To determine the reference value for the relative muscle loadings, the two time periods of maximum effort were taken from each MVC exercise. The mean value of the measured torque was defined as reference value for relative muscle loading.

2.3.6. Isometric Fatigue Protocol

The isometric fatigue protocol was recorded with the CON-TREX® TP 500 adapter set to a 12.5° forward flexion angle and therefore, in the same position as described for the MVC measurements of the abdominal muscles and the muscles of the lower back. Three different load cases were recorded defined as 55 %, 50 % and 45 % of maximum torque. Similar to the study described in section 2.1, the force level was controlled by the test subject using the visual feedback system shown in figure 2.4. Again the target force was in the middle of the green area ±2.5 %, surrounded by the yellow area marking ±2.5 % as tolerated force. During all exercises, the subjects were advised to sustain the required force level for as long as possible.

2.3.7. Dynamic Fatigue Protocol

During the dynamic fatigue protocol, the motion was defined as a flexion and extension of the thorax between 5° and 25° angle. The motion velocity was controlled by the participant, who were advised to keep the motion as constant as possible. The torque level was controlled by the CON-TREX® WS dynamometer. The dynamic fatigue protocol contains three different load cases defined as 40 %, 35 %, and 30 % of maximum force. The relative loading is lower compared to the isometric to ensure a certain amount of repetitions before the participant was exhausted. Furthermore, the resistant torque was only applied during the extension phases. During flexion, torque level is set to a minimum of 1 Nm. The ballistic setting of the dynamometer was used to subtract the influence of gravity so the pure muscle force of the subject was measured.

2.3.8. Data Processing

The data processing of signals collected from the isometric fatigue protocol was similar to the processing explained in section 2.1. At first, the raw data was cut

to the loaded part only and the offset was corrected. The RMS and MPF of the resulting signal was calculated using a 0.1 s non-overlapping window. The RMS was then normalized to the MVC value. A linear regression analysis was applied to evaluate the muscle fatigue. The resulting data were visually inspected to evaluate pattern changes in muscle activation. The processing of the data from isometric exercises is shown in the figures 2.6 - 2.8.

To analyse the recruitment pattern of during dynamic contractions, the onset points during each repetition of the muscles were determined. Yang et al., 2017 [175] proposes the Teager-Kaiser Energy (TKE) operator to do this. This method was originally developed to determine the energy of a sound signal [176] or the onset of a voice [177]. The TKE operator is defined as shown in equation 2.9 for a given $x(n)$.

$$\psi[x(n)] \equiv \psi(n) = x^2(n) - x(n+1) \cdot x(n-1) \tag{2.9}$$

Following this method, a threshold for $\psi(n)$ is defined based on the mean (μ_0) and standard deviation (δ_0) of the background noise (equation 2.10).

$$Th = \mu_0 + j \cdot \delta_0 \tag{2.10}$$

The variable j defines a scaling factor to control the sensitivity of the algorithm. Applying the threshold to the TKE as defined by equation 2.11 results in a binary signal describing the onset points of the EMG.

$$\hat{t} = \underset{n}{arg\,min}(n|index(n) = 1), index(n) = \begin{cases} 1 & \psi(n) > Th \\ 0 & \psi(n) < Th \end{cases} \tag{2.11}$$

This signal, however, contains many artefacts from tremor and spikes in the raw EMG signal. To eliminate these artefacts, a dilation on the binary signal is conducted, as defined by equation 2.12, where A is the binary signal and B is the structuring element, followed by an erosion of A by B as defined by equation 2.13. The signal processing is shown in figure 2.17.

$$A \oplus B = \{z|B_z \cap A \neq \phi\} \tag{2.12}$$

$$A \ominus B = \{z | B_z \subseteq A\} \tag{2.13}$$

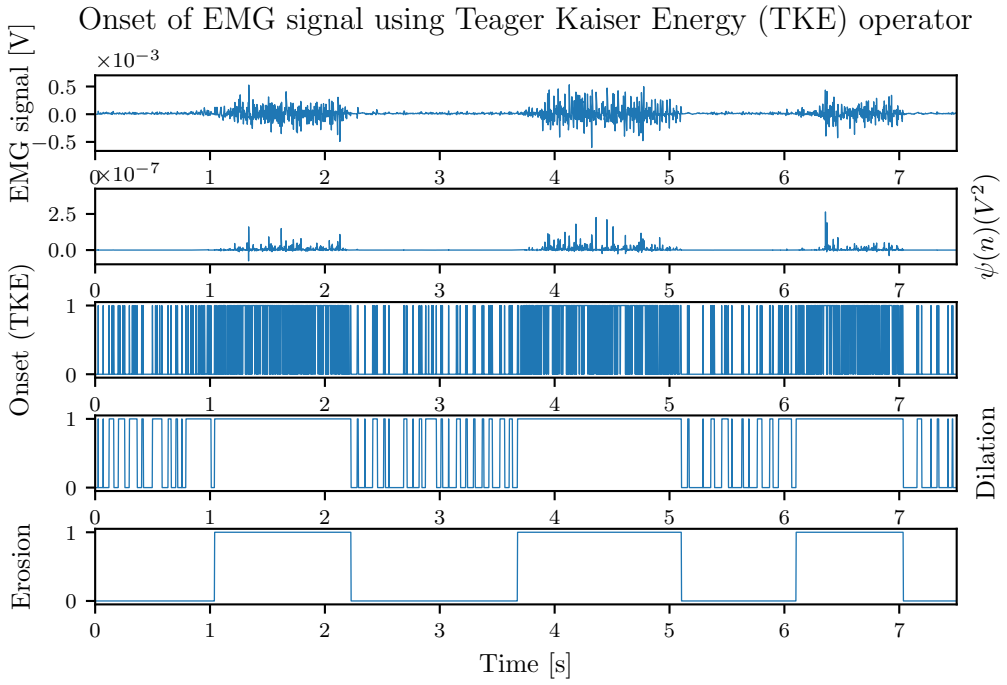

Figure 2.17.: Onset detection in the EMG signal using Teager-Kaier Energy operator

The scaling factor j in equation 2.10 depends on the signal quality of the raw signal and needs to be specified for each subject and each sensor individually. Therefore, the data from the MVC measurements were used. Since each MVC exercise consists of exactly two repetitions, the number of onset points is known. Therefore, an optimization algorithm was used to determine the minimum value for the scaling factor j, where exactly two onset points were detected. However, the EMG signal collected from dynamic exercises contains more motion artefacts than the data from MVC measurements. Therefore, the calculated values for j were multiplied by 2, to ensure a valid onset point detection.

The onset points were calculated for each sensor and each cycle during dynamic exercises. The time delay between the onset of the muscles and the onset of the motion were calculated. Furthermore, the standard deviation of onset points was calculated for each cycle. Changes of the standard deviation were taken as

an index of the synchrony of the muscle activation. Furthermore, the number of active muscles was investigated for each cycle to determine whether or not additional muscles were activated during the course of the exhausting exercises.

2.3.9. Summary Experimental Study Muscle Recruitment Pattern

The aim of the experimental study described above was to investigate the muscle recruitment pattern of back and abdominal muscles when experiencing fatigue. Therefore, the muscle activity of twelve back and four abdominal muscles was recorded during isometric and dynamic exercises with different relative muscle loadings. The MVC normalized RMS and the MPF were calculated from the signals of the isometric trials and analysed for additional activation of the muscles of the upper back or the abdomen.
The onset times of the muscles were analysed in the signals from the dynamic exercises and correlated with the onset time of the motion cycles. Furthermore, the synchrony of the muscle activation was investigated as a second indicator for changes in the muscle recruitment pattern.

2.4. Investigation of AMS Recruitment Algorithm with Implemented Fatigue

The numerical model was based on the model described in section 2.2. This model was extended by implementing the fatigue algorithm to the back and abdominal muscles following the same method as described above. The model consists of a python script to calculate the progress of muscle force capacity and a whole body model created in the AMS. The simulation follows the process shown in figure 2.11. The numerical fatigue model was created following the method described in section 2.2 and based on the data collected from the experimental study described in section 2.3.1. For the back and abdominal muscles, the MET model published by Law and Avin, 2010 [174] described in equation 2.14 was implemented.

$$MET_{trunk} = 22.69 \cdot (MVC)^{-2.27} \tag{2.14}$$

2.4.1. AnyBody^{TM} Model to Investigate Muscle Recruitment Pattern

The model was based on the 'StandingHuman' from the AMMR version 2.1.1. The fixation of the model was applied according to the fixation points in the dynamometer adapter during the experimental study. The motion of the model was specified by loading the data from the measurements and use them as input for the AnyKinEqInterPolDriver with the piecewise linear method used to interpolate the data. For the force input, a new node was constructed on the thorax segment. Furthermore, a variable was created to define the position of this node in vertical z - direction to allow subject - specific lever length. The force data was also imported from the measurements, interpolated with the piecewise linear method and implemented as an AnyForce3D in local x - direction. As described above, the subjects were fixed in the dynamometer at certain points. This needs to be addressed in the AMS model as well. Therefore, one node on each of the two thigh segments and the two shank segments were created above and below the knee. Reaction forces between each of the nodes and the global reference system were created to transmit the forces in the global x - direction.
The muscle fatigue was simulated by a reduction of the maximum force capacity. This required the construction of a new muscle model for each muscle. Furthermore, a strength variable was introduced defining the current maximum force capacity. These variables are stored in four different files:

- Strength parameters shoulder arm left
- Strength parameters shoulder arm right
- Strength parameters trunk left
- Strength parameters trunk right

An example of a muscle model in combination with the corresponding strength variable is shown in listing 2.1. For all muscles listed in D.2, a new muscle model was created this way.

Listing 2.1: Example of the muscle model for the m. multifidus between the L1 and L3 vertebrae; AnyVar MFdL1L3Par describing the current maximum muscle capacity which is used in the AnyMuscleModelUsr1 MFdL1L3Par to define the behaviour of the muscle.

```
AnyVar MFdL1L3Par = 51.9236025354;

AnyMuscleModelUsr1 MFdL1L3Par = {
     AnyVar PCSA = 0.38; //Physiological Cross Sectional Area in
        cm2
     F0 = ..StrengthScaleSpine*PCSA *...StrengthRef.
        SpecificMuscleTensionSpine; //Maximum force output at
        optimum fiber length
         S = .....BodyModel.Trunk.MuscleParametersSpineLeft.
            StrengthParameters.MFdL1L3Par;
   };
```

To allow an independent strength adjustment for the left and right shoulder and arm muscles, the 'ShoulderArmModel.root.any' file needed to be split into the 'ShoulderArmModelLeft.root.any' and 'ShoulderArmModelRight.root.any' files since these muscles use the same muscle model in the original model and would fatigue uniformly. The LowerBound setting was set to 0.0 and the UpperBound setting was turned off. All models were calculated using the polynomial solver with a power of three. The whole model consists of 65 segments listed in table D.1 and 396 DoFs. Each model was anthropometrically scaled by height and weight. Furthermore, the maximum force from the individual MVC measurement of the lower back muscles was used for a kinetic scaling. The model is represented as an example in figure 2.18.

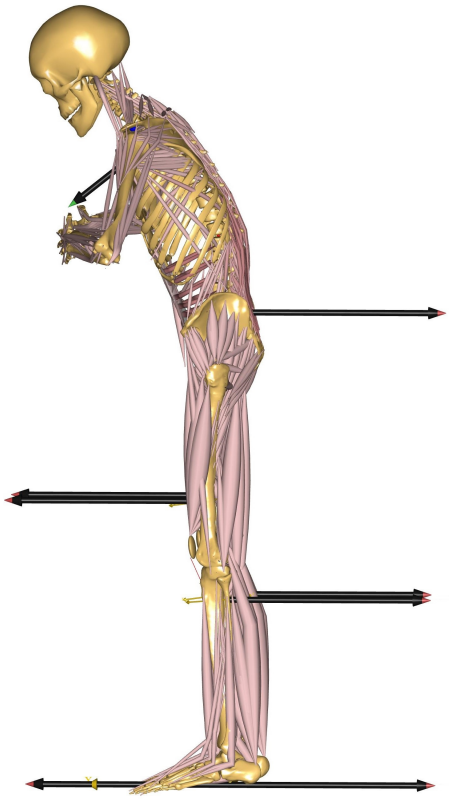

Figure 2.18.: Example of the AMS model developed to analyse muscle recruitment pattern; the black arrows indicate the input force at the thorax and the reaction forces at the pelvis, thighs and shanks

To analyse the recruitment pattern of the model, each dataset was simulated twice. The first simulation was conducted with the modified AMS model including the fatigue algorithm. The second simulation was the control model. Here the same boundary condition, anthropometric and kinetic scaling were used, but without any further modification of the generic AMS model. The force output of each muscle during the simulated exercises were recorded in both models. To analyse the recruitment pattern, the model was divided into the same three parts as for the analysis of the experimental data. The muscles from the AMS that were included in the different parts are presented in table 2.2.

Table 2.2.: Different regions of the body to analyse muscle recruitment pattern from AMS and considered muscles

Body region	**Included muscles**
Upper back	Trapezius clavicular 1-6 Trapezius scapular 1-6
Lower back	Multifidi (36 muscles) Erector spinae (58 muscles)
Abdomen	Rectus abdominis Obliquus externus (12 muscles)

The forces of the muscles of each region were added up and normalized to the added up forces from the control model. Then the ration between the forces of the upper back and the lower back as well as the abdominal muscles and the lower back were calculated to verify potential recruitment changes.

2.4.2. Summary Recruitment Pattern of modified AMS Model

The recruitment pattern of the AMS was investigated in this work package of the study. Therefore, the modified AMS model described in section 2.2.4 with the corresponding python script was extended to the back and abdominal muscles. To examine the behaviour of the recruitment pattern, the calculated muscle forces of the upper back and the abdomen were analysed in relation to the muscle forces of the lower back.

3. Results

In this chapter the outcome of the experimental studies to investigate the progress of muscle fatigue and its influence on muscle recruitment pattern are presented. Furthermore, the validation simulations of the fatigue algorithm are shown. Most graphs in this chapter show typical results as an example. Additional graphs are presented in the appendix E.

3.1. Experimental Study of Muscle Fatigue Progress

The aim of the first experimental study described in section 2.1 was to investigate the progress of muscle fatigue in respect to the relative muscle loading. Therefore, the electromyographic signals of the m. biceps brachii and m. triceps brachii were collected from 20 male subjects during isometric and dynamic contraction with different subject - specific relative muscle loadings. The RMS and MPF were calculated to verify fatigue and to determine the progress.
In table 3.1 the anthropometric data of the participants are shown. The MVC measurements resulted in a mean force of the m. biceps brachii of $430.75 \pm 102.32\,N$ and $301.85 \pm 80.95\,N$ for the m. triceps brachii.

Table 3.1.: Anthropometric data of all subjects measured for the experimental study to determine fatigue progress of the m. biceps brachii and m. triceps brachii

	Age	**Height [cm]**	**Weight [kg]**	**Upper arm length [cm]**	**Forearm length [cm]**	**Thorax length [cm]**
Mean	25.3	181.4	80.1	33.9	26.7	64.8
STD	2.6	6.6	12.0	1.9	2.2	4.6

3.1.1. Results from Isometric Fatigue Protocol

The mean values of the maximum endurance time for the biceps and triceps trials are presented in table 3.2.

Table 3.2.: Mean MET in [min] during isometric biceps and triceps trials

Load cases	**30 %**	**40 %**	**50 %**	**60 %**
m. biceps brachii	2.44 ± 1.56	1.86 ± 1.22	1.53 ± 0.90	1.28 ± 0.91
m. triceps brachii	3.27 ± 1.84	1.55 ± 0.59	1.21 ± 0.43	1.10 ± 0.38

As described in section 2.1, two sensors were used to record the EMG signal of each muscle. Since there are only minor differences between the results from the two sensors, only the results from one sensor each are presented here. Additional graphs are presented in appendix E. Furthermore, the results of the m. triceps brachii analysis are also presented in appendix E.

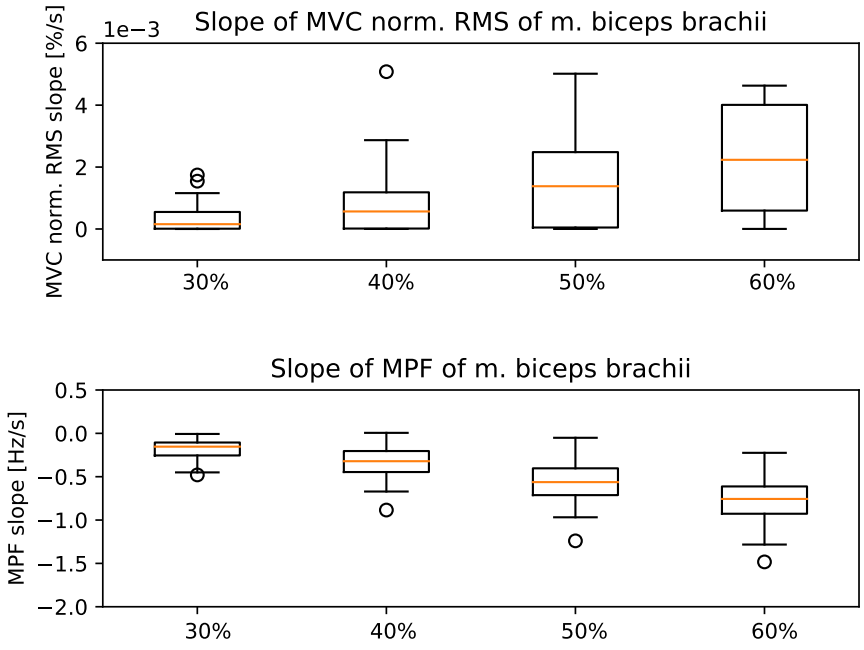

Figure 3.1.: Slope of MVC normalized RMS from m. biceps brachii from isometric fatigue protocol (top); Slope of the MPF from m. biceps brachii from isometric fatigue protocol (bottom)

In the top graph of figure 3.1 the results of the measured progress of m. biceps brachii are presented as an example. All slopes of the MVC normalized RMS signals are calculated in $[\% \, s^{-1}]$. The abscissa values of the plot show the four different load cases from 30 % to 60 % of subject - specific relative muscle loading. For each load case a box plot is presented combining the data from all measured subjects with the median value highlighted as an orange line.
It was found that the median of the slope increases from the 30 % load case to the 60 % load case. Similar results were found for the MVC normalized RMS calculated from the data collected with the additional biceps sensor (top graph figure E.1). However, the slope here only increases from the 30 % to the 50 % case and slightly drops from the 50 % to the 60 % case.
The bottom graph of figure 3.1 shows the slopes of the MPF in relation to the relative muscle loading, measured in $[Hz \, s^{-1}]$. It was found that the median of the MPF slopes decreases from the 30 % load case to the 60 % load case. This again also applies for the slopes calculated from the data collected with the second biceps sensor, which are presented in the bottom graph of figure E.1.
In figure 3.2, the force normalized data of the RMS collected from the m. biceps brachii are presented. Again the median of the slope increases from the 30 % to the 60 % load case. Analysing the force normalized RMS of the additional sensor (figure E.2), the drop of the slope from the 50 % and 60 % trial which was found in the MVC normalized data was also observed here.
The figure 3.3 shows the slope of the MVC normalized RMS and the MPF of m. biceps brachii derived from the data collected during the alternating fatigue protocol. It was found, that the median slope increases and decreases according to the relative muscle loadings during the alternating tests. However, for the 30 % and 50 % loadings, a negative median slope was calculated. This did not occur in the data from the additional biceps sensor which are presented in figure E.3.
The analysis of the MPF calculated from the data of the alternating trials revealed, that the slope of the MPF follows the changes of the relative muscle loading more precisely compared to the MVC normalized RMS. This can be seen in the bottom graph of figure 3.3. The additional sensor showed similar results, which are presented in figure E.3.

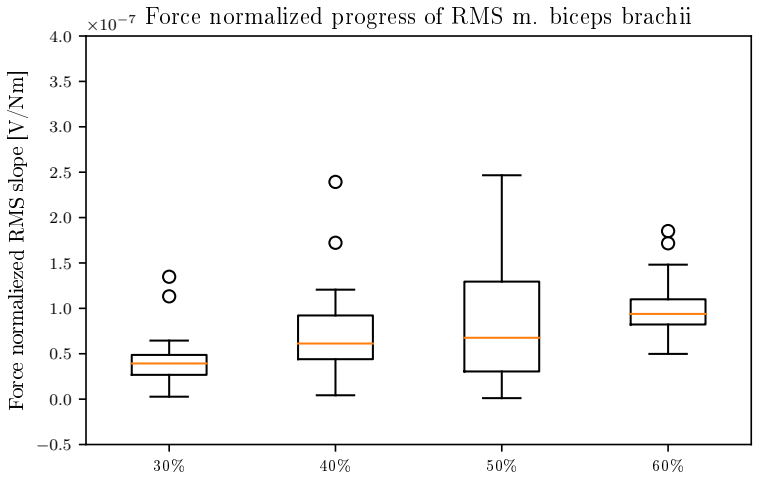

Figure 3.2.: Slope of force normalized RMS from m. biceps brachii from isometric fatigue protocol

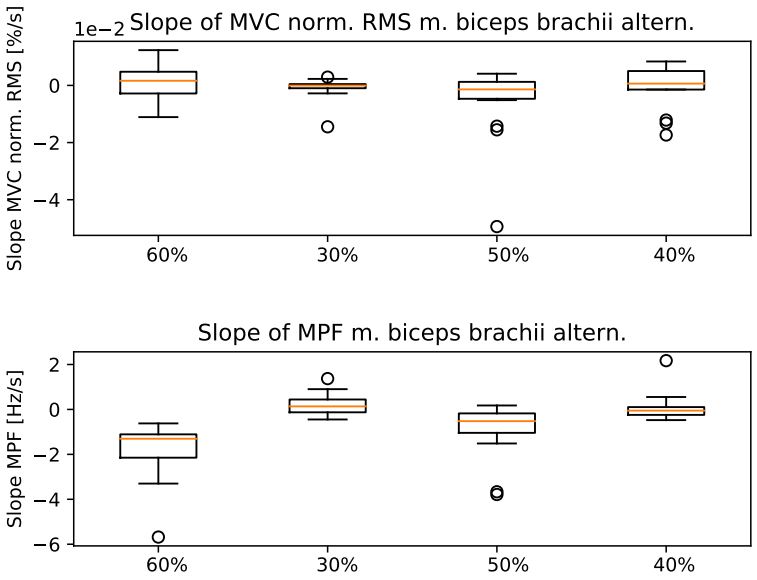

Figure 3.3.: Slope of MVC normalized RMS from m. biceps brachii from alternating fatigue protocol (top); Slope of the MPF from m. triceps brachii from alternating fatigue protocol (bottom)

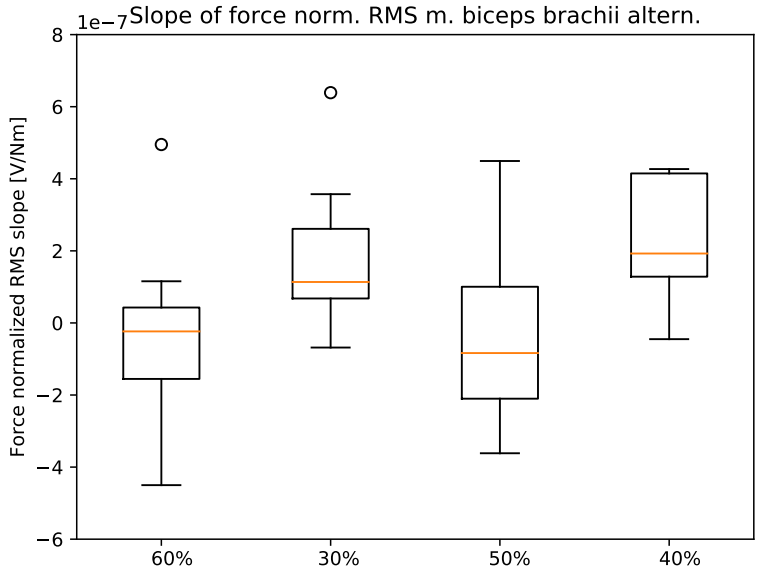

Figure 3.4.: Slope of force normalized RMS from m. biceps brachii from alternating fatigue protocol

The force normalized RMS was also calculated with the data collected during the alternating fatigue protocol. The results are presented in figure 3.4 and figure E.4. Similar to the MVC normalized data, the slopes follow the relative muscle loadings. A negative median slope was found for the 60 % and 50 % trials.

In figure E.5 the results from the recorded m. triceps brachii signal are presented. The slope of the MVC normalized RMS and of the MPF measurements are presented in the same way as for the m. biceps brachii results. It can be observed, that the slope increases from the 30 % to the 60 % load case. The results from the additional sensor that was placed on the m. triceps brachii are presented in figure E.6. The top graph again shows the MVC normalized RMS. The increasing slope from the 30 % to the 50 % can be observed here similar to the results from the additional m. biceps brachii sensor. Furthermore, a decreasing slope from the 50 % to the 60 % load case was found.
Investigating the changes of the MPF, an increasing decline with increasing external load was observed in the data collected with both triceps sensors (bottom graph in figure E.5 and figure E.6).

To minimize the influence of force fluctuations, the signals collected from the m. triceps brachii were also normalized to the measured forces. The results are presented in figure E.7. The slopes of the force normalized RMS show an increasing median from the lowest to the highest relative muscle loading. The results of the additional sensor are presented in figure E.8. Similar to the results from the m. biceps brachii data, the force normalized RMS of the second triceps sensor was found to be increasing from the 30 % to the 50 % load case and dropped again from the 50 % to the 60 % trials.

The results from the alternating fatigue protocol of the m. triceps brachii are similar to the results as for the biceps and are presented in figure E.9. The slope of the MVC normalized RMS, which is shown in the top graph, does not follow the changes of relative muscle loading throughout the trials. Other than the results from the first triceps sensor, the slope of the MVC normalized RMS of the additional sensor followed the alternation of the external load. This is presented in the top graph of figure E.10. However, the MPF slopes correlate well with the different load cases as shown in the bottom graph of figure E.9, which was also observed in the data collected with the second sensor shown in figure E.10.

Again the data was also force normalized as described above. The results from the alternating fatigue protocol with force normalized RMS are presented in figure E.11 and figure E.12 for the additional sensor. Similar to the results from the biceps sensors, the data showed that the slope of the force normalized RMS follows the alternating external loads. Here also one of the two equipped sensors measured a negative slope for the 60 % load case.

A detailed statistical analysis of the data collected during the isometric fatigue protocol is presented in table 3.3 and table 3.4.

Table 3.3.: Statistical analysis of the results from the isometric fatigue protocol of the m. biceps brachii; the first sensor on the muscle is marked with (1); the additional sensor is marked with (2); statistical significance was defined for $p < 0.05$ ($*$)

Load case combinations	**30-40**	**30-50**	**30-60**	**40-50**	**40-60**	**50-60**
	Single load trials m. biceps brachii					
MVC norm. RMS (1)		*	*			
MVC norm. RMS (2)		*	*		*	
MPF (1)		*	*	*	*	
MPF (2)		*	*	*	*	*
Force norm. RMS (1)	*					
Force norm. RMS (2)		*				
	Alternating load trials m. biceps brachii					
MVC norm. RMS (1)						
MVC norm. RMS (2)						
MPF (1)	*	*	*	*		
MPF (2)	*	*	*	*		
Force norm. RMS (1)						
Force norm. RMS (2)						

Table 3.4.: Statistical analysis of the results from the isometric fatigue protocol of the m. triceps brachii; the first sensor on the muscle is marked with (1); the additional sensor is marked with (2); statistical significance was defined for $p < 0.05$ ($*$)

Load case combinations	**30-40**	**30-50**	**30-60**	**40-50**	**40-60**	**50-60**
	Single load trials m. triceps brachii					
MVC norm. RMS (1)			*			
MVC norm. RMS (2)						
MPF (1)	*	*	*	*	*	
MPF (2)	*	*	*			
Force norm. RMS (1)		*	*	*	*	
Force norm. RMS (2)			*			
	Alternating load trials m. triceps brachii					
MVC norm. RMS (1)						
MVC norm. RMS (2)	*				*	
MPF (1)		*	*	*	*	
MPF (2)		*	*	*	*	
Force norm. RMS (1)						
Force norm. RMS (2)						

3.1.2. Results from Dynamic Fatigue Protocol

The analysis of the data gathered during the dynamic fatigue protocol showed no significant dependence on the external loading. Furthermore, similar results were found for the progress of the MPF calculated from the dynamic cycles of the m. biceps brachii signals. In figure 3.5 the results are presented for the four different load cases between 30 % and 60 % of relative muscle loading. Similar results were found for the analysis of the signals collected from the m. triceps brachii during dynamic contraction. The graphs in figure 3.6 show the calculated progress of MVC normalized RMS and the MPF of all tested subjects.

The results from the additional sensors are presented in E.13 for the m. biceps brachii and figure E.14 for the m. triceps brachii. In both cases, no significant effect on the progress of MVC normalized RMS and MPF from the relative muscle loading was found.

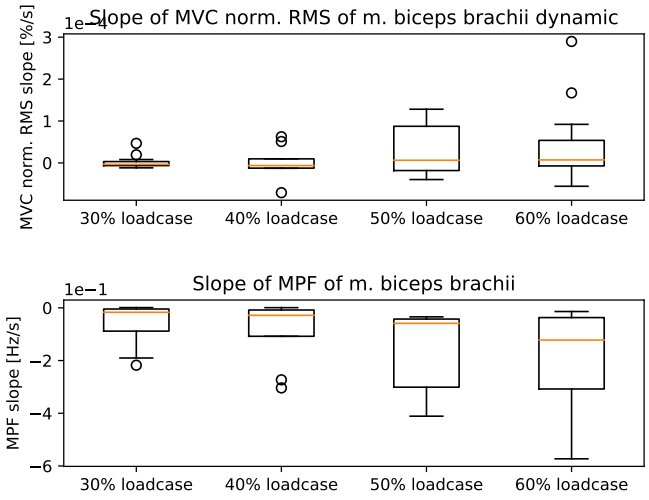

Figure 3.5.: Slope of MVC normalized RMS from m. biceps brachii from dynamic fatigue protocol (top); Slope of the MPF from m. biceps brachii from dynamic fatigue protocol (bottom)

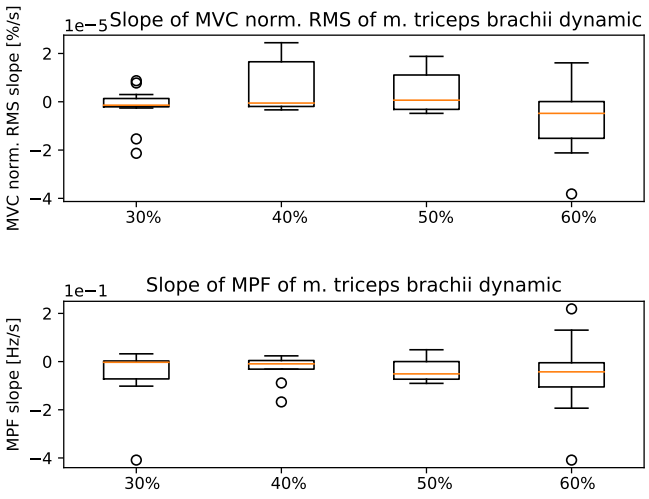

Figure 3.6.: Slope of MVC normalized RMS from m. triceps brachii from dynamic fatigue protocol (top); Slope of the MPF from m. triceps brachii from dynamic fatigue protocol (bottom)

3.2. Results of the Developed Novel Fatigue Algorithm and Its Validation

The aim was to develop a fatigue algorithm based on the data from the experimental study described above. Therefore, the measured slope of MVC normalized RMS was correlated with relative muscle loading to be able to calculate the progress of maximum force capacity in the AMS model which is described in section 2.2. In the following the variables for the fatigue model are presented which were used for the fatigue algorithm and the simulation of the exhausting exercises.

3.2.1. Model Parameters for the AMS Model and the Implemented Fatigue Algorithm

The model was scaled according to the anthropometric data presented in table 3.1. Furthermore, the generic model was kinetically scaled to suit the individual maximum muscle strength of each subject by a mean scaling factor of 2.34 $\pm$ 0.53 for the m. biceps brachii and 1.53 $\pm$ 0.42 for the m. triceps brachii.
The fatigue algorithm described in section 2.2.1 requires the variable m as input describing the slope of the activity progress in dependence of the relative muscle loading. This was derived from the data collected during the experimental study described above. The estimation of the variable m is shown in figure 3.7. The abscissa shows the relative muscle loading in [%] where the ordinate shows the slope of the MVC normalized activity. The points marked with the red 'x' represent the results from experimental study of the m. biceps brachii. A linear regression analysis was performed to fit the data points which is described by equation 3.1 with a determination coefficient of $R^2 = 0.92$.

$$m = 0.003182 \cdot load[\%] - 6.696e^{-13} \tag{3.1}$$

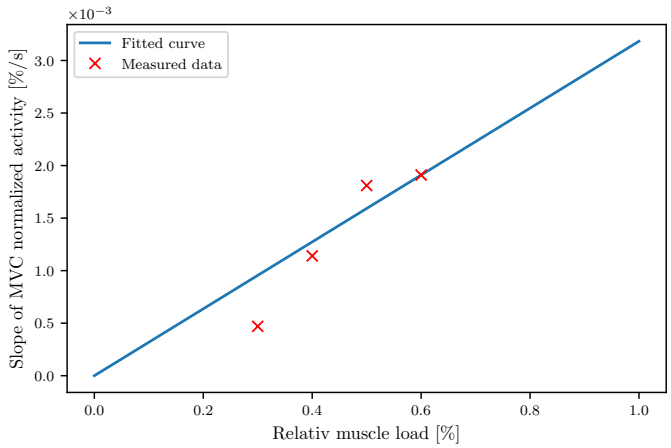

Figure 3.7.: Measured slope of activity ('x') from experimental study with linear regression analysis to estimate variable m for numerical fatigue algorithm

3.2.2. Validation of the Fatigue Algorithm in the AMS Model

For the validation, the algorithm was implemented to the AMS and all trials from the experimental study were simulated. The absolute changes of muscle activity were calculated from the data collected during the experimental study. The results are presented in figure 3.8 for the m. biceps brachii. Same calculations were made with the results from the modified AMS model which are shown in figure 3.9. Comparing these two results, it was found that the muscle activity increases about 10 % to 15 % during all different load cases. Similar results were found for the absolute changes of the simulated activity.

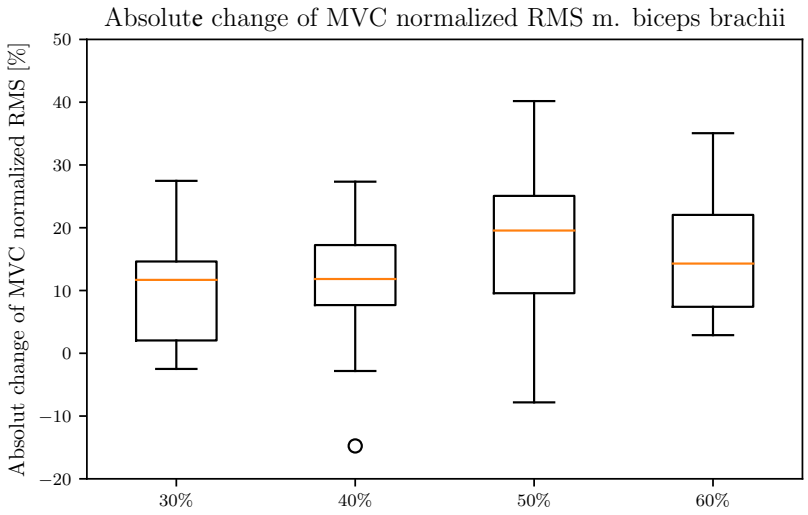

Figure 3.8.: Absolute changes of m. biceps brachii activity derived from experimental data

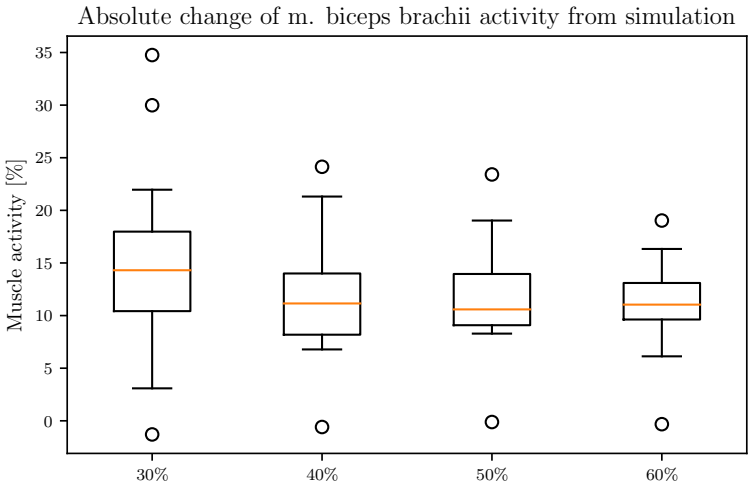

Figure 3.9.: Absolute changes of m. biceps brachii activity derived from simulation

The results from the m. triceps brachii measurement show an increasing muscle activity of about 5 % to 10 % which are presented in figure 3.10. These results

correlate well with the results from the simulated m. triceps brachii activity shown in figure 3.9, as the muscle activity also increases about 5 % to 10 %.

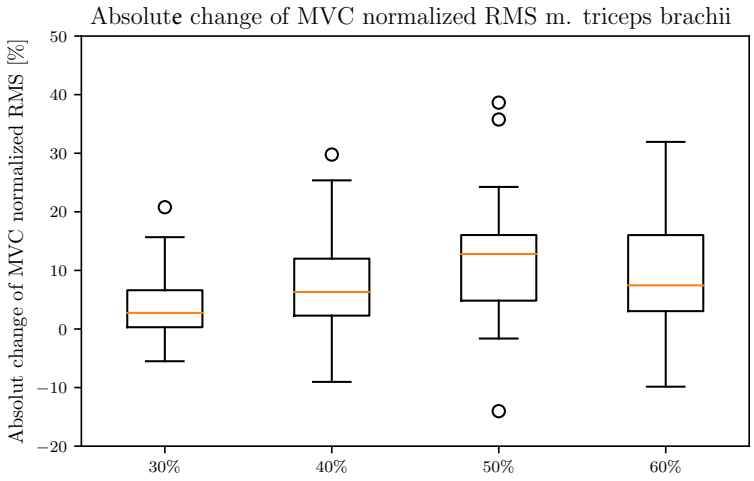

Figure 3.10.: Absolute changes of m. triceps brachii activity derived from experimental data

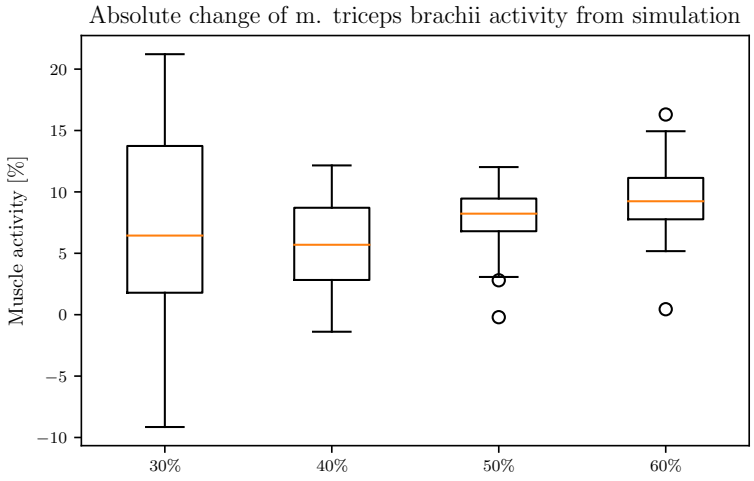

Figure 3.11.: Absolute changes of m. triceps brachii activity derived from simulation

Furthermore, the MET was calculated for each time step during the simulation and the state of fatigue was estimated which the subject experienced. The results are presented in table 3.5. For the whole population and load cases, a mean state of fatigue of 100.74 % was calculated for the m. biceps brachii. For the m. triceps brachii the level of fatigue calculation resulted in a mean value of 89.28 %.

Table 3.5.: Calculated state of fatigue from MET model in [%]

load cases	**30 %**	**40 %**	**50 %**	**60 %**
m. biceps brachii	93.17 ± 66.3	93.17 ± 56.5	96.4 ± 56.5	120.2 ± 31.2
m. triceps brachii	84.6 ± 82.6	74.3 ± 73.1	77.7 ± 25.5	120.5 ± 41.2

The analysis of the progress of maximum force capacity of the m. biceps brachii and m. triceps brachii showed a reduction of the strength of the muscle around 10% in the biceps and 10 % to 15 % in the triceps muscle. The results are presented in figure 3.12.

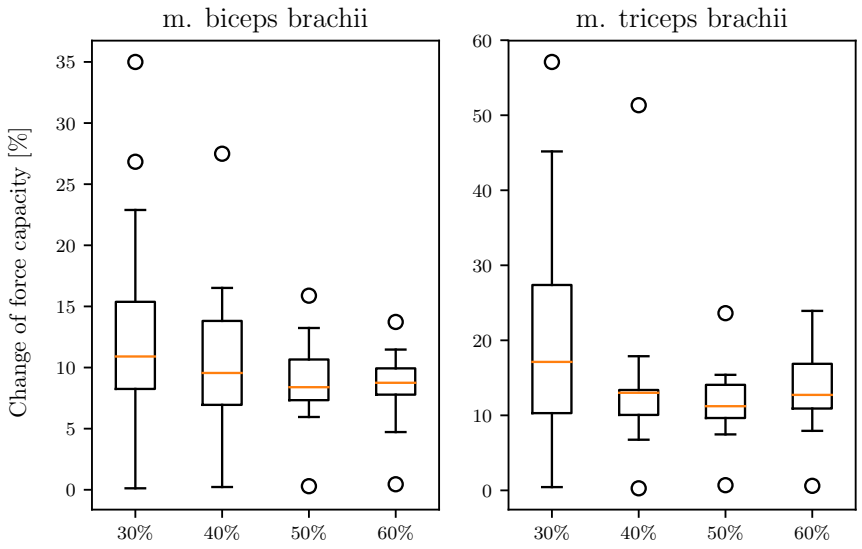

Figure 3.12.: Absolute changes of maximum force capacity of m. biceps brachii (left) and m. triceps brachii (right)

Analysing the data from the dynamic trials, it was found that the muscle activity did not change significantly during the trials. The results are presented in figure 3.13 for the m. biceps brachii and m. triceps brachii. These results were also

confirmed by the results from the AMS model simulation which also showed no significant change of muscle activity for all load cases.

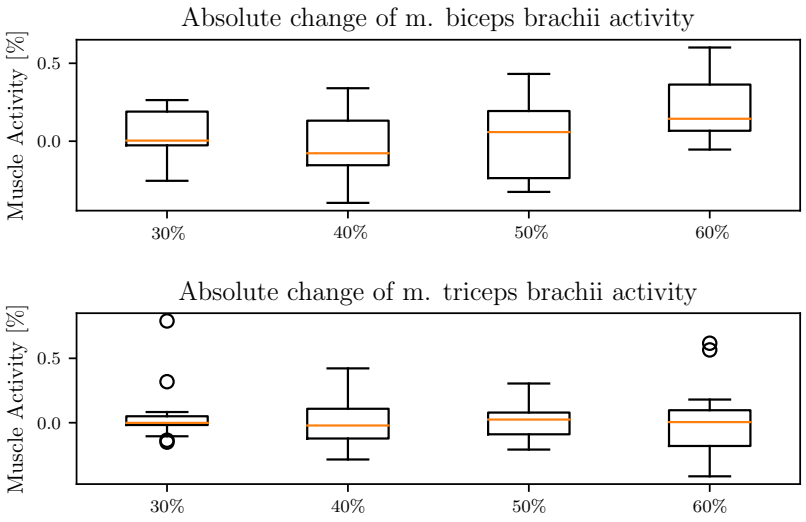

Figure 3.13.: Absolute changes of m. biceps brachii and m. triceps brachii activity derived from dynamic data

3.3. Experimental Study of Muscle Recruitment Pattern

The second experimental study described in section 2.3 aimed to analyse the recruitment pattern of the back and abdominal muscles when experiencing fatigue. The anthropometric data of all participants are presented in table 3.6. A total of seven subjects (five male, two female) had to be excluded from the analysis of the data due to incomplete data of the exercises or an incorrect execution.

Table 3.6.: Anthropometric data

	Age	**Height [cm]**	**Weight [kg]**	**Upper arm length [cm]**	**Forearm length [cm]**	**Thorax length [cm]**
Mean	23.7	177.8	75.1	33.7	28.1	66.0
STD	2.0	8.3	13.4	2.2	2.5	9.8

3.3.1. Results from Isometric Fatigue Protocol

Since the main load during the investigated exercise was carried by the muscles of the lower back (m. erector spinae, m. multifidi), the first step was to verify fatigue in these muscles. Therefore, the method of Luttmann et al., 2000 [163] was applied and the progress of MVC normalized RMS and MPF was analysed. In 84.9 % of all measurements, fatigue was detected regardless of gender. Subsequently, the progress of muscle activity of the abdominal muscles and the muscles of the upper back was analysed. It was found, that in 49.9 % of all measurements subjects additionally activated the abdominal muscles at some time during the exercise in order to support the muscles of the lower back. The m. trapezius was activated by a total of 55.9 % of all participants at some time during the trials. In 33.3 % of all measurements the subjects used both muscle regions to support the m. erector spinae and the m. multifidi during the exercises. In 28.0 % no additional muscles were activated. The results are presented in figure 3.14.

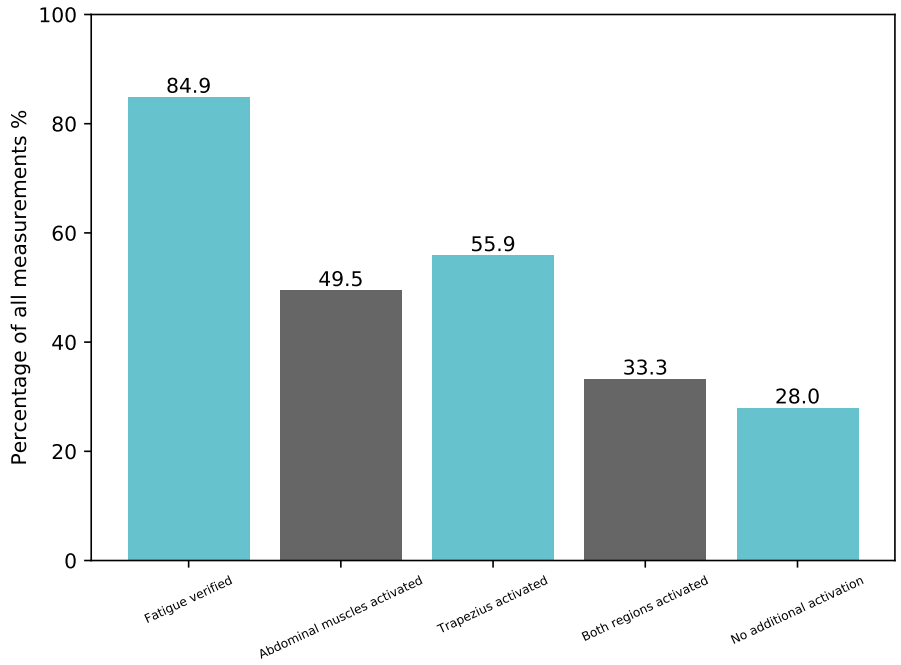

Figure 3.14.: Analysis of the recruitment pattern regardless of gender

When analysing the results from female subjects only, fatigue in the muscles of the lower back was verified in 87.9 % of all cases. The abdominal muscles were activated during 57.6 % of all load cases, while the m. trapezius was activated by 48.5 % of all female participants. Furthermore, both regions were activated by 33.3 % and no addition muscles by 27.7 %. The results are shown in figure 3.15.

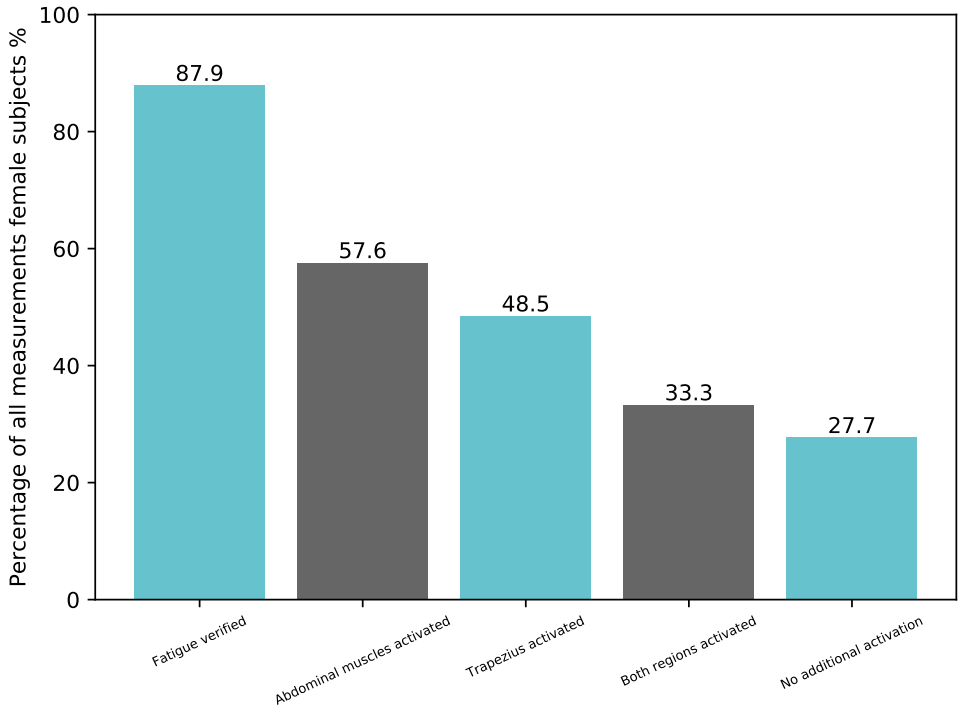

Figure 3.15.: Analysis of the recruitment pattern from female participants

The data from male participants showed that fatigue could be verified in 82.5 % of the participants. The abdominal muscles were activated by 43.9 % of the male subjects while the m. trapezius was used by 61.4 % to support the muscles of the lower back. Furthermore, 35.1 % of the male subjects activated muscles in both regions, while 29.8 % did not activate further muscles during the trials. The results from male participants are presented in figure 3.16.

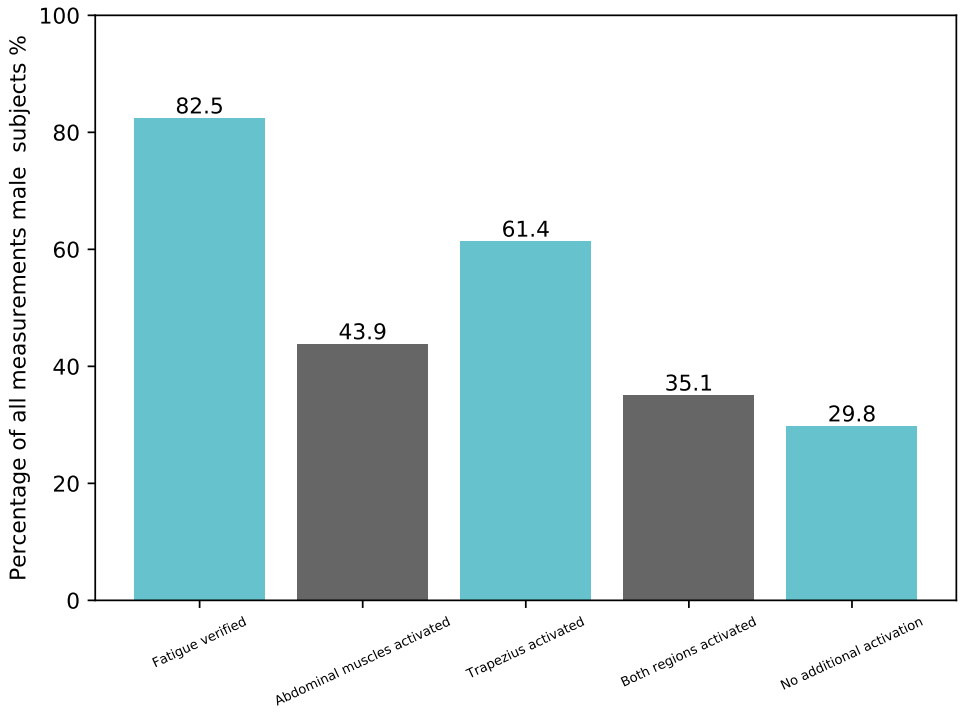

Figure 3.16.: Analysis of the recruitment pattern from male participants

3.3.2. Results from Dynamic Fatigue Protocol

In order to analyse the recruitment pattern during the dynamic trials, the muscle onset points were estimated using the method published by Yang et al., 2017 [175] as described in section 2.3. In this method a threshold is required which is described in section 2.3.8. This threshold was determined for each individual sensor and participant.

In the figures 3.17 to 3.19 the results from the onset point calculation for all 30 %, 35 % and 40 % load cases are presented. The abscissa shows the progress of the exercise in [%] divided into five sections. The ordinate of the respective plots shows the number of active muscles. Since six sensors have been used on the m. trapezius (top plot), the maximum number of active muscle is six. The same applies for the muscles of the lower back (four sensors for the m. erector spinae, two sensors

for the m. multifidus shown in the middle plot). The activity of the abdominal muscles was recorded with four sensors which makes the maximum number of active muscles in the lowest plot is equal to four.

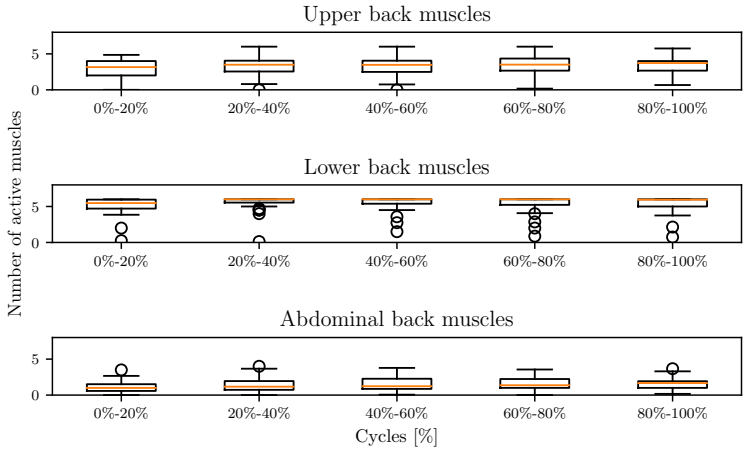

Figure 3.17.: Number of active muscles of the upper back (top), lower back (middle) and abdominal muscles (bottom) of all 30 % load case trials

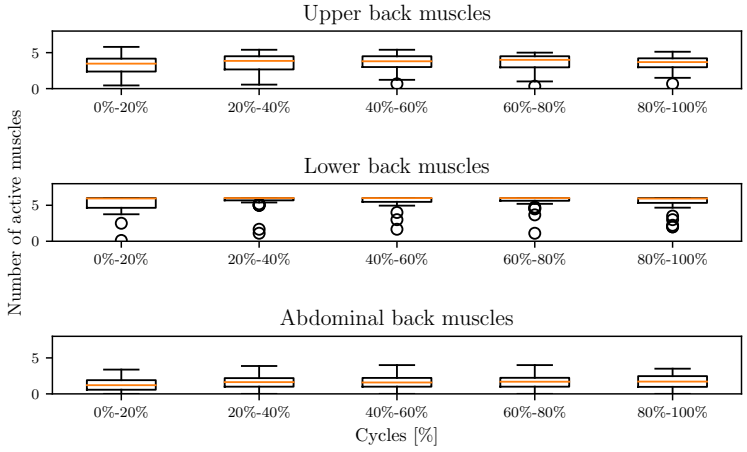

Figure 3.18.: Number of active muscles of the upper back (top), lower back (middle) and abdominal muscles (bottom) of all 35 % load case trials

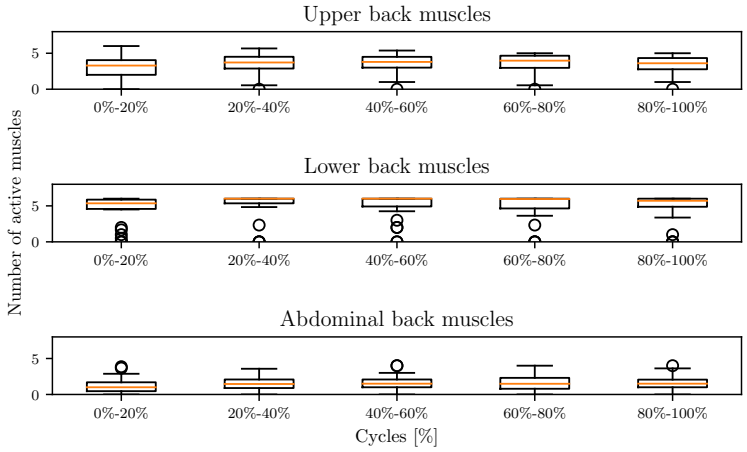

Figure 3.19.: Number of active muscles of the upper back (top), lower back (middle) and abdominal muscles (bottom) of all 40 % load case trials

The plots show that regardless of the relative muscle loading, the number of active muscles did not vary significantly. This was observed for the muscles of the upper back as well as the lower back and the abdominal region.
The sensors of the upper back indicated that the m. trapezius pars descendens and pars transversa were active during all trials. In the lower back, all six sensors indicated activity. The abdominal muscles only showed minor activity during the exercises.

3.4. Recruitment Pattern Modified AMS Model

The aim of this study was to investigate and validate the recruitment algorithm of the modified AMS model. Therefore, the model described in section 2.2.4 was extended and the back and abdominal muscles were included. In the following, the parameters for the modification of the back and abdominal muscles of the AMS model are described. Furthermore, the results of the isometric and dynamic simulations are presented. The measured motions and forces collected during the experimental study described in section 2.3 were used as boundary conditions.

3.4.1. Model Parameters for the Simulation and Validation of the Muscle Recruitment Pattern

The AMS model was subject-specifically adjusted with the anthropometric data presented in table 3.6. Furthermore, the whole model was kinetically scaled with a mean factor of 1.22 ± 0.36 to represent the individual strength of the test subjects. The fatigue algorithm for the back muscles was developed following the method described in section 2.2.1. The progress of muscle activity is described by equation 3.2.

$$m_{trunk} = 0.00272 \cdot load[\%] - 1.372e^{-19} \tag{3.2}$$

3.4.2. Results from Simulated Muscle Recruitment

As described in section 3.4, each dataset was simulated with the modified AMS model and a control model, where no fatigue is considered. The force output of the trapezius muscles from one isometric simulation is presented in figure 3.20 as an example.

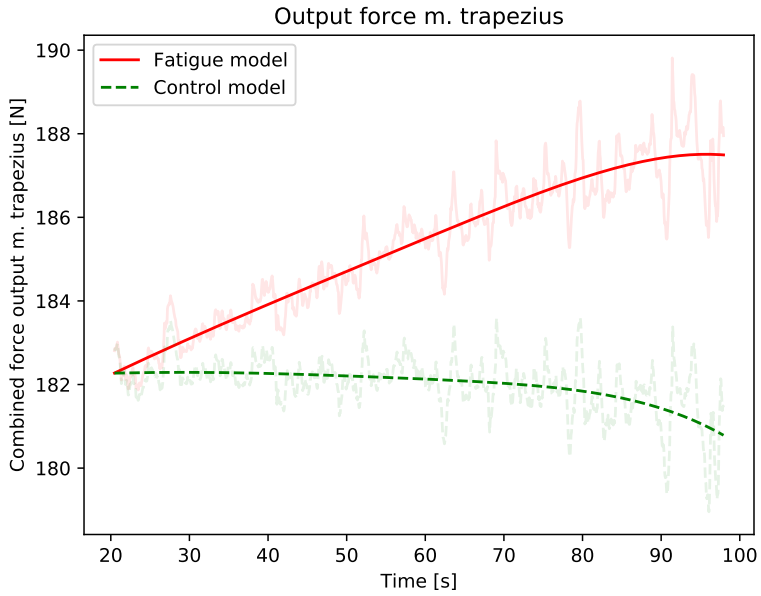

Figure 3.20.: Added up force output of trapezius muscles of the AMS control model (green-dashed) and the modified AMS model (red) in comparison

The figure shows the progress of the muscle force output of trapezius muscles from the AMS control model, represented by the green dashed line, and the progress from the modified AMS model, represented by the red line. The data, which is shown in the background respectively, was fitted with a third order fit. It can be observed that the force output simulated with the modified model increases compared to the force output of the control model.
The force output of the abdominal muscles of both models is presented in figure 3.21 from one subject as an example.

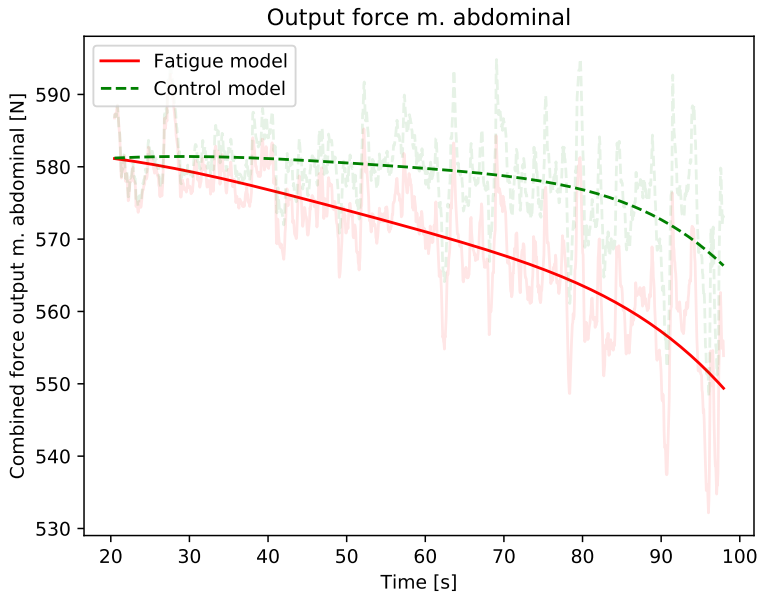

Figure 3.21.: Added up force output of abdominal muscles of the AMS control model (green-dashed) and the modified AMS model (red) in comparison

The results in figure 3.21 show that the muscles force output of the abdominal muscles decreases steeper in the modified AMS model than in the control model. As described in section 3.4, the ration between the muscle forces of the upper back and the forces of the lower back was calculated for each model. Again, the different load cases did not have an influence on the results. Therefore, the results of all isometric simulations are presented combined. The analysis showed a shift of the muscle force output towards the upper back in all isometric simulations. The result of the ratio between trapezius muscles before and after fatigue are presented

in figure 3.22.
Simultaneously the force output of the transversus muscles decreased, while the rectus abdominis muscle and the obliquus externus muscles were not activated. The results of the force output analysis of abdominal muscles are presented in figure 3.23.

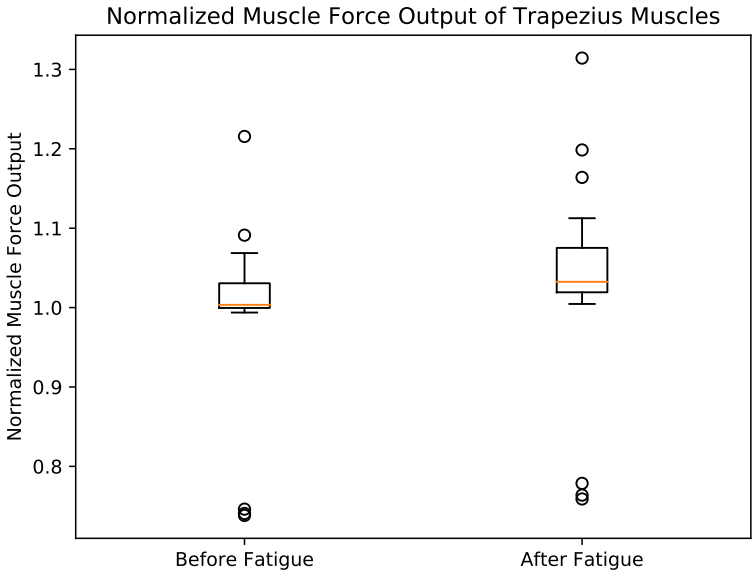

Figure 3.22.: Output forces of trapezius muscles normalized to output forces of control model at the beginning and at the end of exercise simulation

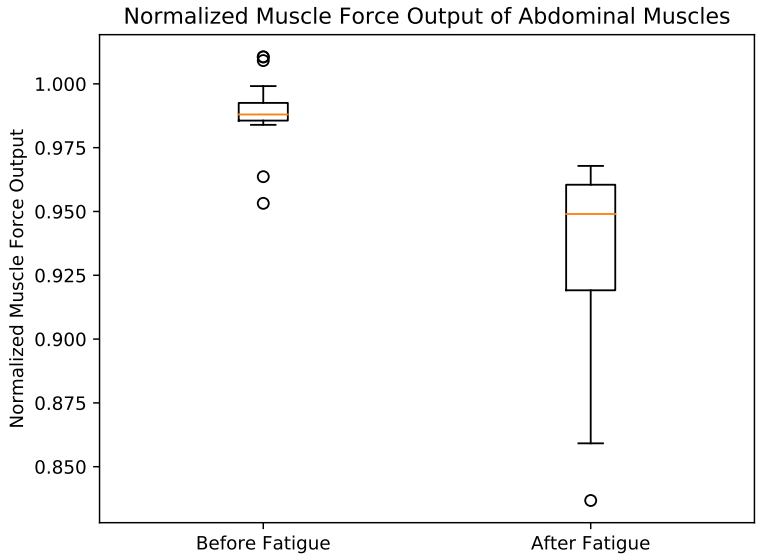

Figure 3.23.: Output forces of abdominal muscles normalized to output forces of control model at the beginning and at the end of exercise simulation

Similar to the experimental data, the simulation of the dynamic exercises did not show a change of muscle recruitment in the AMS model. The added up force output of the trapezius muscles from the modified AMS model and the control model are shown in figure 3.24. It can be observed that the progress of muscle force output simulated with the modified AMS model correlates with the calculated force output from the control model.
Similar results as for the trapezius forces were found for the abdominal forces which are exemplarily shown in figure 3.25.

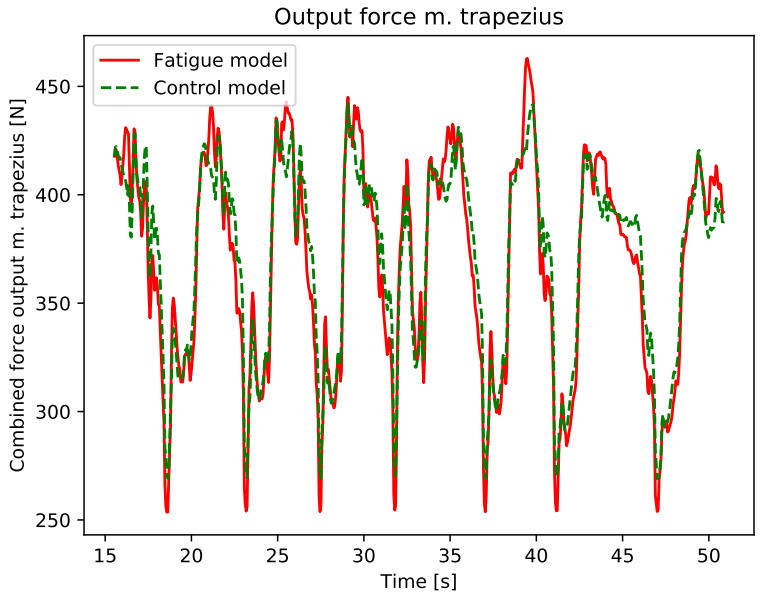

Figure 3.24.: Added up force output of trapezius muscles of the AMS control model (green-dashed) and the modified AMS model (red) with dynamic boundary conditions

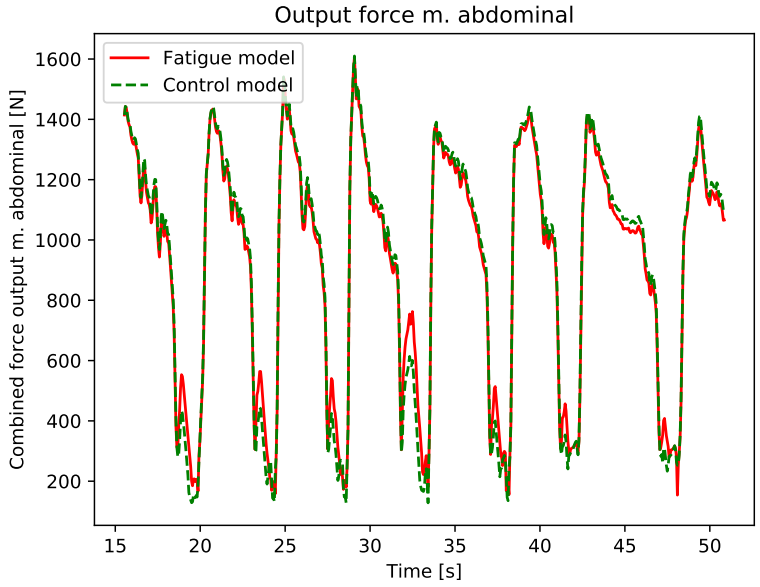

Figure 3.25.: Added up force output of abdominal muscles of the AMS control model (green-dashed) and the modified AMS model (red) with dynamic boundary conditions

In figure 3.26, the changes of the maximum force capacity of the erector muscles are presented exemplary. It can be observed, that there are only minor changes of the strength of the muscles throughout the exercise.

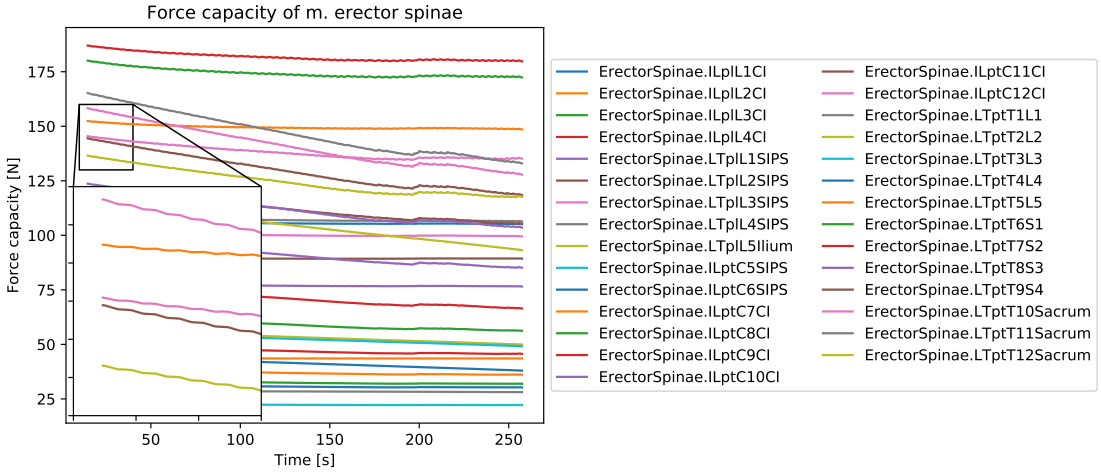

Figure 3.26.: Progress of maximum force capacity of erector muscles from modified AMS model during dynamic exercises simulation

4. Discussion

Today, MSDs are the most common reason for work-related absence. This is intensified by the demographic change as well. Marschall, 2017 [2] reports that the proportion of MSDs in this statistic increases with increasing age. This can be explained since MSDs are progressive disorders as a result of muscles and joints being loaded over a long period of time. Therefore, the study of the musculoskeletal system has become more and more important through the last decades. For a good understanding of the musculoskeletal system, numerical models like the AMS have been developed. In order to be able to study long-term effects with these models, muscle fatigue needs to be considered, since it is often involved in MSDs [3].

The first objective of this study was the experimental quantification of muscle fatigue. Therefore, the electromyographic signal of the m. biceps brachii and m. triceps brachii was collected during isometric and dynamic exercises with defined relative muscle loadings. The results showed a significant change of the slope of MVC normalized RMS between several load cases. It was found that the slope of the MPF significantly correlates with the relative muscle loading in almost all cases. This was also found for the analysis of the isometric fatigue protocol with alternating external load. However, the results from the data captured during dynamic exercises did not show a significant correlation between the relative muscle loadings and the slope of the MVC normalized RMS or the MPF.

The second main objective of this thesis was to develop a novel fatigue algorithm based on the electromyographic measurements recorded in the first experimental study. The validation of the algorithm in the modified AMS model showed a good correlation between the simulated muscle activity and the experimental data. Furthermore, the implemented MET model delivered realistic calculation of the level of fatigue. The results also revealed a minor reduction of maximum muscle force

capacity compared to muscle fatigue algorithm from literature.
The third objective was to investigate the influence of fatigue on the global muscle recruitment of back and abdominal muscles. The results from the second experimental study (section 2.3) showed that recruitment pattern of the measured test subjects reacted differently to the exhausting isometric exercises. The additional activation of trapezius muscles or abdominal muscles was observed here. Furthermore, a potential difference between genders was found. During the dynamic exercises no change of the muscle recruitment pattern was observed in the second experimental study.
The last objective of this thesis was the analysis of the AMS muscle recruitment with the implemented fatigue algorithm. Therefore, the isometric and dynamic exercises of the second experimental study were modelled with the modified AMS. The simulated muscle forces were analysed regarding muscle recruitment changes. The results showed a shift of the muscle force output towards the trapezius muscles in the upper back. The additional activation of the abdominal muscles could not be simulated.
In the following, all findings of this study are discussed in detail.

4.1. Fatigue Progress of Single Muscles

The first experimental study was designed to investigate the progress of muscle fatigue of a single muscle dependent on the relative muscle loading. In this study only healthy male subjects with a similar level of fitness were included in order to have a group as homogeneous as possible. As target muscles the m. biceps brachii and the m. triceps brachii were selected. These two muscles allow the minimization of the influence of cross-talk from neighbouring muscles. Furthermore, the flexion and extension exercise of the elbow as well as the isometric loading in the 90° elbow flexion position was chosen since it is common scenario in daily living. The MVC normalization method was chosen for this study. As described in section 1.5.5, this is the most reliable for comparing the EMG data of healthy subjects. Furthermore, the maximum force was recorded during these measurements to determine the subject-specific relative muscle loadings for the different load cases. During isometric and dynamic trails four different load cases between

30 % and 60 % of maximum effort were selected. These load cases have been determined in a preceding test with the aim of balancing the endurance time of the exercises and to exhaust the test subjects. The upright seating position during the isometric and dynamic trials was chosen to minimize the influence of upper body movement on the joint angle of the elbow joint during the exercises. Muscle fatigue was verified in the data following the method published by Luttmann et al., 2000 [163]. Therefore, fatigue is verified by an increasing amplitude of the EMG signal and a decreasing MPF. The RMS of the signal was calculated with a window size of 100 ms to analyse the progress of the signal amplitude. Konrad, 2005 [30] recommends a window size between 50 ms and 500 ms depending on the motion speed. Since the angular velocity during the dynamic contraction was relatively low, the window size was defined as 100 ms and also used for analysing the data from the isometric protocol. Same window size was used to calculate the MPF of the collected signals.

The data recorded during the isometric fatigue protocol show a negative slope of the MPF while the MVC normalized RMS show a positive slope in all cases. Therefore, muscle fatigue can be verified in the datasets for both recorded muscles. When analysing the slope of the MVC normalized RMS in respect to the load case, an increasing median with increasing load was found. However, this effect was only significant comparing the 30 % and 50 % load case as well as the 30 % and 60 % load case of the m. biceps brachii data. The m. triceps brachii data showed a significant dependence of the MVC normalized RMS on relative muscle loading. Similar results were found by Chang et al., 2016 [178], who described a large effect of muscle force on the instantaneous RMS value and therefore, also on the MVC normalized RMS value. It was reported that the force level dropped over time during isometric maximum voluntary contraction. During such a contraction, the RMS value was supposed to increase since the subject was experiencing fatigue. However, the RMS was found to be decreasing since the force level was dropping during a sustained maximum voluntary contraction. This means that the influence of the force level is overlaying the influence of fatigue on the progress of the EMG signal amplitude. However, since the force level was kept constant during the isometric load cases, the influence of load variation was minimized and the changes of the signal amplitude can be attributed to muscle fatigue.

When analysing the MVC normalized RMS slope from the data collected during the alternating fatigue protocol, it was found that the slope is relatively constant. It was also observed that the slope even reached negative values which would indicate a recovery phase. The alternating fatigue protocol started with the highest force level of 60 % relative muscle loading. Therefore, a high level of fatigue at the beginning of the test might have an influence on the measurements of lower force levels afterwards. Nevertheless, the sequence of the load cases was defined as described in section 2.1.1, since it was very challenging for the participants to sustain the four different load cases during this protocol.
Nargol et al., 1999 [179] described the progress of the EMG amplitude as a reliable fatigue indicator, but more sensitive to external load as the MPF progress. In this study, the MPF was also found to be a more reliable indicator than the MVC normalized RMS. Similar observations were made by Larivire et al., 2002 [167], who described the slope of the median frequency as the most reliable fatigue index. When investigating the slope of the MPF derived from the isometric fatigue protocol, a significant influence of relative muscle loading was found for all load cases except between the 30 % and 40 % load case. This could be explained by the types of muscle fibres that are in action. Higher forces result in a higher number of type II muscle fibres being activated. These fibres fatigue faster than type I fibres which results in a steeper slope [180]. Since the muscle loading at 30 % of maximum force is relatively low, mostly type I fibres are recruited. This could explain the relatively small increase of the slope between the 30 % and 40 % load case.

The results from the dynamic fatigue protocol showed no significant dependency of the slope of MVC normalized RMS on the relative muscle loading. There is a slight increase of the median value with increasing loading observed in the data, however, the standard deviation is very high. This could be explained by the high variation of cycles performed by each test subject. Since the speed of motion was at participant's preference, especially for the 30 % and 40 % load cases the number of cycles was very high and duration of the tests were very long. This indicates that the fatigue level during these load cases might not have been high enough. Since the angular velocity was chosen by the participant, the recovery

time during loading of the antagonist might have been too high. Different studies show, that the reliability of SEMG to detect muscle fatigue is challenging for low exhaustion intensity levels [181]. Ament et al., 1993 [182] described the analysis of the MPF derived from data collected during an exhausting uphill run with an average duration of 1.5 min. The results showed a decline of the MPF of more than 10 % during the exercise. In a subsequent study, the MPF was analysed from data collected during a dynamic exercise at medium exercise intensity [181]. It was concluded, that two types of exhaustion can be distinguished when analysing dynamic exhausting exercises: At a low level of exercise intensity, no decline of the MPF occurs, while exercises with a high level of intensity are accompanied by a decline of the MPF.

These results can be confirmed by the results from this study. The median slope of the 30 % and 40 % load cases is almost zero, followed by a steeper decline in the 50 % and 60 % load cases. However, the effect was not significant in this study. This could also be a result of high variance of the number of cycles performed by each subject. Furthermore, compared to the results published by Ament et al., 1993 [182], the intensity of the exercise was still relatively low. This can be seen in the duration time of the dynamic exercises with a mean duration between 1182.9 s and 152.8 s from the 30 % to the 60 % load case compared to the 90 s described by Ament et al., 1993 [182]. Furthermore, the dynamic trials have been terminated after 1800 s, which some of the subjects reached during the 30 % and 40 % load cases. Here the effort of the participant during the maximum force measurements had a huge influence, since the relative muscle loadings were calculated based on this value.

The analysis of the progress of MVC normalized RMS also did not show a significant dependence on the relative muscle loading. Here again, the level of exercise intensity can explain this results.

4.2. Fatigue Algorithm and Implementation to AMS Model

The fatigue algorithm was developed based on the results of the isometric fatigue protocol described in section 2.1.1. The slope of the MVC normalized RMS was used since this parameter can be correlated with the calculated muscle activity

from the AMS under the assumption of a linear muscle force - muscle activity correlation in the EMG measurements. This assumption is a topic of controversy in literature. Various studies investigated the EMG signal - muscle force correlation with different results. For the m. biceps brachii for example, the description of a linear relation [183, 184] as well as a non - linear relation [185] exists. Since in this study, one fatigue algorithm was used for all muscles in the shoulder and arm part of the AMS model, a linear relation was assumed as a first approach. As described in section 1.5.4 reasonable results can be achieved with this assumption.
The fatigue algorithm was based on the definition of muscle activity in the AMS. Starting from this, the muscle activity of the subsequent time step during simulation was estimated following the results from the measured muscle activity progress. This estimated activity was then used to calculate the associated strength of the muscle for this time step. The applied method ensures that the calculated muscle activity follows the progress of the measured activity. For the estimation of the variable m, which is shown in figure 3.7, a linear fit was used in order to include 0.0 to the fit.
The MET model which was implemented together with the fatigue algorithm was published by Law and Avin, 2010 [174], who described different endurance time models for different joints and recommend the use of power function models. Since the MET model that was used in this study was calculated for each time step of the simulation using the current maximum force capacity of the muscle, a scaling factor was required. This scaling factor was determined empirically and set to a value of $c = 0.95$ in this study.
The recovery model was published by Ma et al., 2009a [171] and is based on two recovery models published by Carnahan at al., 2001 [186] and Wood et al., 1997 [173]. It was implemented without modifications using the recovery ratio of $R = 0.04\,s^{-1}$ which was also adopted from literature. This model was chosen since it is a simple recovery model based on the current maximum force capacity, and the non-fatigued maximum force capacity of a muscle and can therefore be calculated easily. Furthermore, the model was proven to be capable of simulating the empirical exponential recovery relationship [187].

The generic AMS model was configured without the lower extremities. Further-

more, the back and abdominal muscles have been removed to save computation time. For each muscle in the shoulder arm region of the AMS, a new muscle model was defined. This was necessary for adjusting the strength of the muscles during simulation.

As described in section 2.2.4, the model was scaled according to subject-specific height and weight. Furthermore, the individual strength was adjusted by scaling the whole model with a single strength scaling factor. These scaling factors of 2.34 ± 0.53 for the loading of the m. biceps brachii and 1.53 ± 0.42 for the m. triceps brachii can be explained by the generic AMS model representing the 50^{th} percentile model and therefore, the mean strength of the population. Since the sample that was measured during the experimental study consisted of healthy, young male subjects only, the AMS model needs to be strengthened to represent the individual muscle force. As output, the muscle activity of the m. biceps brachii and the m. triceps brachii as well as the strength of these muscles were recorded. The data of the simulated muscle activity and the data from the experimental study showed good correlation. In both, the activity of the measured muscle changed about 10 % to 15 % during the exhausting exercises. This resulted in a reduction of the maximum force capacity of about 10 % to 15 %. Compared to fatigue models from literature, this is a relatively low value. The model published by Ma et al., 2009a [171], for example calculates the current muscle loading according to the equation $F_{cem}(t) = MVC \cdot e^{-kCt}$ which results in a significantly higher loss of maximum force capacity. However, this model was validated against different endurance time models from literature and therefore, equates the calculated muscle fatigue with peripheral fatigue. As described in section 1.4.3, fatigue of the central nervous system as well as fatigue of the neuromuscular junction also needs to be considered when investigating muscle fatigue. In the proposed model, the change of force capacity of the muscles is dependent on the current force capacity and the current relative loading of each single muscle.

The MET model was utilized to calculate the current state of fatigue of the AMS model when simulating the different subjects. The model was not used as a termination criterion and therefore, the values can exceed 100 %. The calculation of the state of fatigue showed a good correlation for all models compared to the population data.

4.3. Muscle Recruitment Pattern - Experimental Study

The second experimental study aimed to investigate potential changes of the muscle recruitment pattern when experiencing fatigue. Therefore, a study protocol was designed consisting of isometric and dynamic exercises for the back muscles. As target muscles, twelve muscles on the back and four muscles on the abdomen were recorded. Although the influence of cross-talk can be up to 15 % [30] and is certainly an issue when recording EMG data from back and abdominal muscles, the number of muscles involved in the thorax motion offer a good opportunity to study recruitment pattern and were therefore chosen for this study. The measurement of the test subjects using the CON-TREX TP 500 adapter offered the possibility to limit the range of motion to an exclusive thorax flexion and extension. In this study a total of 40 healthy young subjects, male and female, were included. Participants with a medical history of back injuries or low back pain were excluded from the beginning.

As in the first experimental study, the MVC normalization method described in section 1.5.5 was used to compare the recorded EMG data between trials and subjects. Therefore, a total of five MVC measurements were conducted with each participant prior to the exercises. During the MVC measurement for the m. erector spinae and the m. multifidus, the maximum forces were recorded as well. Based on this value the subject-specific loadings were determined. In this study, three isometric load cases with 55 %, 50 % and 45 % of maximum force, as well as three dynamic trials with 40 %, 35 % and 30 % of maximum force were measured. These load cases were defined in a preliminary study to balance the experienced fatigue with the endurance time of the participants. Aforementioned the maximum individual force was determined from the isometric MVC measurement of the muscles of the lower back. However, the maximum dynamic forces of the muscles tend to be lower than the isometric maximum force, which is why the dynamic trials were measured with lower relative muscle loadings.

The positioning of the subjects during isometric trials and the range of motion during the dynamic trials were also defined in a preliminary study. The criteria that had to be met were a comfortable position and motion for the participants, and the possibility to produce maximum forces with a minimum risk of injuries.

Following the method by Luttmann et al., 2000 [163], the muscle fatigue was verified by calculating the MVC normalized RMS and the MPF of the collected signals. For both, a window size of 100 ms was used which is sufficient for the analysis of data collected with the angular velocity during the dynamic exercises as well as during the isometric measurements [30].
The analysis of the isometric exercises showed that fatigue could be verified in 84.9 % of the data. This means that the protocol was suitable for the exhaustion of the participants. One possible explanation for the 15.1 % of trials where no fatigue could be verified could be a lack of motivation of the participant during the exercise or an underestimated maximum force. The results showed, that in most trials additional muscles were activated at some point throughout the exercise by the participants in order to support the muscles of the lower back. During more than 55 % of all exercises the trapezius muscle showed an increasing activity. Furthermore, in almost half of the measured cases, the abdominal muscles were activated. These muscles are proven to support the lumbar spine by increasing the intra-abdominal pressure [188]. The results indicate, that the participating subjects can be subdivided into three different groups:

1. Additional activation of the trapezius muscle
2. Additional activation of abdominal muscles
3. Additional activation of both muscle regions

In some measurements, no additional activation was found. However, these trials mostly correlate with the trials where no fatigue of the lower back muscles could be verified.
The analysis of the data grouped by gender showed similar results for the verification of fatigue in the m. erector spinae and m. multifidi. However, the data showed that the female participants tended to activate the abdominal muscles preferably compared to the trapezius muscles, where the male subjects primarily activated muscles of the upper back as support.
The different load cases which were recorded with each subject did not show significant variations in the results. Possibly, the minor difference between the loadings can be the cause of this.

The onset points of muscle activation adapted for the dynamic measurements were used to study muscle recruitment pattern during dynamic contraction. The method of onset point estimation was published by Li et al., 2007 [189] and modified by Yang et al., 2017 [175]. It requires a threshold value that is calculated from the signal to noise ratio of the EMG signal combined with a scaling factor as described in equation 2.10. Li et al., 2007 recommend a scaling factor between 6-8, where Yang et al., 2007 used a factor of 17-20. To ensure a consistent estimation of the threshold, the MVC measurements of each subjects were used to optimize the threshold value for each sensor individually. The doubling of the estimated value was done since the MVC measurements were isometric measurements without motion artefacts. Using these threshold values, the estimation of muscle activation onset points during the dynamic contractions worked well. The calculated onset points of the muscles were correlated with the onset point of the motion. Therefore, a window of 500 ms around the motion onset was defined, and the number of muscle onset points were counted within this window. The window size was chosen, since various studies show that there is an offset between the EMG onset and the actual onset of the motion. Begovic et al., 2014 [190], for example, described delay of $49.73 \pm 6.99\,ms$ between the onset of the EMG and the measured force output of m. rectus femoris.

Due to the electrode placement, the maximum number of active muscles in the upper back and the lower back is six respectively. Four sensors were placed on the abdomen which makes the maximum number of active muscles four. Obviously, the actual number of active muscles is higher but it is not possible to differentiate this with surface EMG sensors due to cross-talk effects. Therefore, the three different simplified regions 'upper back', 'lower back' and 'abdomen' were analysed. The results showed no significant change of recruitment pattern during the dynamic trials for all different load cases. Furthermore, a gender-specific analysis did not reveal changes in recruitment pattern. The analysis of the synchrony of muscle activation also did not show significant changes throughout the dynamic trials. Since the angular velocity during the dynamic exercises was chosen by the test subject, the muscle loading might have been too low so central fatigue effects may have predominated the muscle fatigue effects.

4.4. Muscle Recruitment Pattern - AMS

The aim of this study was to analyse the AMS recruitment algorithm with the implemented fatigue algorithm. The fatigue algorithm for the back and abdominal muscles was developed following the same method as described above for the shoulder and arm muscles of the AMS. Again, a joint specific MET model for the thorax published by Law and Avin, 2010 [174] was implemented to calculate the level of fatigue during the simulated exercises. While the MET model for the shoulder and arm muscles correlated well with the data from the m. biceps brachii and m. triceps brachii exercises, the MET model implemented for the thorax muscles overestimated the level of fatigue in both, the simulated isometric and dynamic exercises. The MET model described in equation 2.14 was used for all back and abdominal muscles of the AMS model. Law and Avin, 2010 [174] described, that endurance time models are highly dependent on the joint and therefore, on the muscles which the model is developed for. Compared to the first study, where the implemented MET model was designed specifically for the elbow joint, in this case, different MET models might be necessary for the back and abdominal muscles. The recovery model for the back and abdominal muscles is equal to the model described for the shoulder and arm muscles and implemented with the same recovery ratio of $R = 0.04s^{-1}$.

The reaction forces were modelled according to the fixation of the test subjects. As described for the implementation of the fatigue algorithm for the shoulder and arm muscles, a new muscle model was required for each back and abdominal muscle to be able to adjust the current strength capacity. For detailed subject-specific models the anthropometric scaling and the kinetic scaling was conducted. The mean kinetic scaling factor was lower compared to the scaling factors used for the simulation of the data from the biceps-triceps exercises. In this study also some scaling factors < 1 were used, mainly for the subject-specific modelling of the female participants. The generic AMS model represents the 50^{th} percentile model and therefore, possibly needs to be scaled down kinetically.
The analysis of the recruitment pattern was conducted by analysing the force output of the muscles in the three different regions upper back, lower back and abdomen. The force was analysed rather than the calculated muscle activity, since

the muscle activity is directly influenced by the fatigue algorithm. The force output, however, provided a good possibility to analyse the interaction of the muscles. The results of the simulated isometric models showed a shift of muscle recruitment towards the upper back during the exercises. Since the position of the upper body and arms was stable throughout the whole simulation of the different models, the recruitment change can only be explained by the altered muscle activity of the muscles in the lower back. The rectus abdominis and obliquus externus muscle of the model however showed no activity during the whole exercise. In the abdominal region only the transversus muscles were active. This does not correlate with the results from the experimental study where m. obliquus externus and m. rectus abdominis were activated additionally by about 49.5 % of all subjects. In the AMS, the transversus muscle is linked to the simulation of intra-abdominal pressure, which also stabilizes the lumbar spine. Therefore, the activity of the muscle is relatively high during all simulations. This leads to the fatigue algorithm applying to the transversus muscles and therefore, an increase of its activity. Since the recruitment algorithm in the AMS is basically a 'minimum fatigue' algorithm as described in section 1.3.3, the recruitment does not shift towards the abdominal muscles.

In the data captured during the dynamic exercises no change of muscle recruitment pattern of the back and abdominal muscles was observed. Similar results were found for the simulated exercises with the modified AMS model. When analysing the progress of maximum force capacity of single muscles which is shown in figure 3.26 it can be observed, that the force capacity only decreased slightly during the simulated exercises and is partly annulled by the recover algorithm. Therefore, the muscle recruitment algorithm is not forced to change the recruitment pattern. The overestimation of the level of fatigue during dynamic contraction simulation is enhanced by the fact, that the level of fatigue is calculated during each time step but does not consider recovery phases.

The limitations of the model are that the motion was only measured by the dynamometer and therefore, possible slight changes of the position of the test subjects were not surveyed. Furthermore, only two different fatigue models were used for the muscles of the shoulder and arm region of the AMS and the thorax muscles.

5. Conclusion

Due to demographic changes and the increasing significance of MSDs, the study of the musculoskeletal system, in particular the biomechanics of the human body, has gained in importance in the last decades. However, the experimental measurement of joint and muscle forces within the human body is hardly possible. In literature, only few studies describe the analysis of joint reaction forces with, for example, instrumented implants. To enhance the knowledge of the musculoskeletal system, numerical models have been developed in recent years. These models allow the calculation of muscle and joint forces within the human body during specific motions using subject-specific data.

The aim of this thesis was to develop and introduce an EMG base fatigue algorithm to the AMS. Therefore, an experimental study was designed to quantify the progress of muscle fatigue of single muscles in relation to the relative muscle loading. This novel approach first conducted in this study revealed a significant difference of MPF progresses for the different muscle loadings, as well as for some of the MVC normalized RMS progresses. No significant dependence of the progress of fatigue indicating variables was found for the dynamic exercises.

Based on these results, the fatigue algorithm was developed. Since the shape and progress of the EMG signal is influenced not only by muscle fatigue but also by central and peripheral fatigue, this novel approach considers the different systems contributing to the fatigue of a human being. The model including fatigue, recovery and MET algorithms was validated against the data from the experimental study and showed a good correlation. Especially the prediction of the level of fatigue delivers good results when calculating the isometric exercises. Furthermore, the simulation showed that the reduction of the maximum force capacity is distinctly lower compared to the results from models from literature, which did not consider peripheral or central fatigue.

The second experimental study conducted in the course of this thesis aimed to investigate the global muscle recruitment of back and abdominal muscles under the influence of muscle fatigue and was first reported here. The results indicate, that there are different reactions of the muscle recruitment pattern to muscle fatigue, distinguishing three major groups. The first group supported the muscles of the lower back by additionally activating muscles of the upper back. The second group used the abdominal muscles in order to delay the exhaustion. The third group showed an additional activation of both muscle regions during the exercises. Furthermore, the data indicated a gender-specific difference in the recruitment pattern of back and abdominal muscles when experiencing fatigue. However, further research is required to verify this hypothesis.
The analysis of the muscle recruitment of the AMS model with implemented fatigue algorithm showed, that the muscle activation shifts towards the muscles of the upper back, which correlated with the outcome of the experimental study. However, an additional activation of the abdominal muscles could not be reproduced.

The proposed method of developing an EMG based fatigue algorithm has been proven to simulate realistic fatigue behaviour. For a further improvement of the fatigue algorithm, more fatigue studies should be conducted for different muscles following the methods proposed in this thesis. Especially, the muscles of the lower extremities have not yet been considered in the described modified AMS. Furthermore, fatigue is muscle-specific and therefore needs to be analysed more in detail. Since the first experimental study was conducted with only male subjects, it is also required to analyse the behaviour of muscle fatigue progress of female subjects.
Although further research is required, the proposed modified AMS model serves as the foundation for simulating long-term effects on the musculoskeletal system and therefore, is capable of enhancing a better understanding of the effects of MSDs of the human body.

Bibliography

[1] Michael Damsgaard, John Rasmussen, Søren Tørholm Christensen, Egidijus Surma, and Mark de Zee. Analysis of musculoskeletal systems in the AnyBody Modeling System. *Simulation Modelling Practice and Theory*, 14(8): 1100–1111, 2006.

[2] Jörg Marschall, Susanne Hildebrandt, Hanna Sydow, Hans-Dieter Nolting, Elena Burgart, and Tobias Woköck. *Gesundheitsreport 2017. Analysen der Arbeitsunfähigkeitsdaten.* Number Band 16. 2017. ISBN 9783862163458.

[3] Amedeo Troiano, Francesco Naddeo, Erik Sosso, Gianfranco Camarota, Roberto Merletti, and Luca Mesin. Assessment of force and fatigue in isometric contractions of the upper trapezius muscle by surface EMG signal and perceived exertion scale. *Gait & Posture*, 28(2):179–186, 2008.

[4] Work – related musculoskeletal disorders : Back to work. Technical report, Office for Official Publications of the European Communities: European Agency for Safety and Health at Work., 2007.

[5] Liang Ma, Damien Chablat, Fouad Bennis, and Wei Zhang. A new simple dynamic muscle fatigue model and its validation. *International Journal of Industrial Ergonomics*, 39(1):211–220, 2009.

[6] R Merletti and A. Rainoldi. Myoelectric Manifestations of Muscle Fatigue. *Electromyography: Physiology, Engineering, and Non-Invasive Applications*, pages 233–258, 2004.

[7] S. Boyas and A. Guével. Neuromuscular fatigue in healthy muscles: Underlying factors and adaptation mechanisms. *Annals of Physical and Rehabilitation Medicine*, 54(2):88–108, 2011.

[8] Miguel T. Silva, André F. Pereira, and Jorge M. Martins. An efficient muscle fatigue model for forward and inverse dynamic analysis of human movements. *Procedia IUTAM*, 2:262–274, 2011.

[9] A/S AnyBody Technology. 2018.

[10] B. Amevo, D. Worth, and N. Bogduk. Instantaneous axes of rotation of the typical cervical motion segments: a study in normal volunteers. *Clinical Biomechanics*, 6(2):111–117, 1991.

[11] M. D. Klein Horsman, H. F.J.M. Koopman, F. C.T. van der Helm, L. Poliacu Prosé, and H. E.J. Veeger. Morphological muscle and joint parameters for musculoskeletal modelling of the lower extremity. *Clinical Biomechanics*, 22 (2):239–247, 2007.

[12] V. Carbone, R. Fluit, P. Pellikaan, M. M. van der Krogt, D. Janssen, M. Damsgaard, L. Vigneron, T. Feilkas, H. F J M Koopman, and N. Verdonschot. TLEM 2.0 - A comprehensive musculoskeletal geometry dataset for subject-specific modeling of lower extremity. *Journal of Biomechanics*, 48(5):734–741, 2015.

[13] Mark de Zee, Michel Dalstra, Paolo M. Cattaneo, John Rasmussen, Peter Svensson, and Birte Melsen. Validation of a musculo-skeletal model of the mandible and its application to mandibular distraction osteogenesis. *Journal of Biomechanics*, 40(6):1192–1201, 2007.

[14] Michael Skipper Andersen, Mark de Zee, Michael Damsgaard, Daniel Nolte, and John Rasmussen. Introduction to Force-Dependent Kinematics: Theory and Application to Mandible Modeling. *Journal of Biomechanical Engineering*, 139(9):91001–91014, jul 2017.

[15] John Rasmussen, Mark De Zee, Michael Damsgaard, Søren T Christensen, Clemens Marek, and Karl Siebertz. A GENERAL METHOD FOR SCALING MUSCULO-SKELETAL MODELS. In *2005 International Symposium on Computer Simulation in Biomechanics*, Cleveland, Ohio, USA, 2005.

[16] David C Frankenfield, William A Rowe, Robert N Cooney, J.Stanley Smith, and Dolores Becker. Limits of body mass index to detect obesity and predict body composition. *Nutrition*, 17(1):26–30, 2001.

[17] John Rasmussen, Michael Damsgaard, and Michael Voigt. Muscle recruitment by the min/max criterion - A comparative numerical study. *Journal of Biomechanics*, 34(3):409–415, 2001.

[18] A. V. Hill. The Heat of Shortening and the Dynamic Constants of Muscle. *Proceedings of the Royal Society B: Biological Sciences*, 126(843):136–195, 1938.

[19] Andrew Fielding Huxley. Muscle structure and theories of contraction. *Progress in biophysics and biophysical chemistry*, 7:255–318, 1957.

[20] B. M. Moss, P. E. Refsnes, A. Abildgaard, K. Nicolaysen, and J. Jensen. Effects of maximal effort strength training with different loads on dynamic strength, cross-sectional area, load-power and load-velocity relationships. *European Journal of Applied Physiology and Occupational Physiology*, 75 (3):193–199, 1997.

[21] T. Fukunaga, M. Miyatani, M. Tachi, M. Kouzaki, Y. Kawakami, and H. Kanehisa. Muscle volume is a major determinant of joint torque in humans. *Acta Physiologica Scandinavica*, 172(4):249–255, 2001.

[22] Michio Ikai and Tetsuo Fukunaga. Calculation of muscle strength per unit cross-sectional area of human muscle by means of ultrasonic measurement. *Internationale Zeitschrift für Angewandte Physiologie Einschließlich Arbeitsphysiologie*, 26(1):26–32, 1968.

[23] E J Jones, P a Bishop, a K Woods, and J M Green. Cross-sectional area and muscular strength: a brief review. *Sports Med*, 38(12):987–994, 2008.

[24] F E Zajac. Muscle and tendon: properties, models, scaling, and application to biomechanics and motor control. *Critical reviews in biomedical engineering*, 17 4:359–411, 1989.

[25] Robert F Schmidt, editor. *Neuro- und Sinnesphysiologie*. Springer Berlin Heidelberg, Berlin, Heidelberg; s.l., 1993. ISBN 978-3-540-56238-2.

[26] W. Bloom and D. W. Fawcett. *A textbook of histology*. Saunders, Philadelphia, 11th edition, 1986.

[27] Jacques Duchateau and Roger M. Enoka. Human motor unit recordings: Origins and insight into the integrated motor system. *Brain Research*, 1409: 42–61, 2011.

[28] R M Enoka and J Duchateau. Physiology of Muscle Activation and Force Generation, apr 2016.

[29] C J Heckman and Roger M Enoka. Motor Unit, oct 2012.

[30] Peter Konrad. The abc of emg. *A practical introduction to kinesiological ...*, (April):1–60, 2005.

[31] Allan Fletcher. Action potential: Generation and propagation. *Anaesthesia and Intensive Care Medicine*, 17(4):204–208, 2016.

[32] David a D.a. David a. Winter. *BIOMECHANICS AND MOTOR CONTROL OF Fourth Edition*, volume 2nd. 2009. ISBN 0470398183.

[33] Roberto Merletti and Dario Farina. *Surface electromyography: physiology, engineering and applications*. Wiley-IEEE Press, Hoboken, NJ, 2016.

[34] R H Edwards. Human muscle function and fatigue. *Ciba Foundation symposium*, 82:1–18, 1981.

[35] S. Heimer. Fatigue. In R. Medved, editor, *Sports Medicine*, pages 147–151. Croatian, second ed. edition, 1987.

[36] Nina K. Vøllestad. Measurement of human muscle fatigue. *Journal of Neuroscience Methods*, 74(2):219–227, 1997.

[37] J. Swart, R. P. Lamberts, M. I. Lambert, E. V. Lambert, R. W. Woolrich, S. Johnston, and T. D. Noakes. Exercising with reserve: Exercise regulation

by perceived exertion in relation to duration of exercise and knowledge of endpoint. *British Journal of Sports Medicine*, 43(10):775–781, 2009.

[38] Roger M. Enoka and Andrew J. Fuglevand. Motor unit physiology: Some unresolved issues. *Muscle and Nerve*, 24(1):4–17, 2001.

[39] Jing Jing Wan, Zhen Qin, Peng Yuan Wang, Yang Sun, and Xia Liu. Muscle fatigue: General understanding and treatment. *Experimental and Molecular Medicine*, 49(10):e384–11, 2017.

[40] Janet L. Taylor, Markus Amann, Jacques Duchateau, Romain Meeusen, and Charles L. Rice. *Neural contributions to muscle fatigue: From the brain to the muscle and back again*, volume 48. 2016. ISBN 0000000000000.

[41] Jean Luc Darques, Patrick Decherchi, and Yves Jammes. Mechanisms of fatigue-induced activation of group IV muscle afferents: The roles played by lactic acid and inflammatory mediators. *Neuroscience Letters*, 257(2): 109–112, 1998.

[42] J. L. Darques and Y. Jammes. Fatigue-induced changes in group IV muscle afferent activity: Differences between high- and low-frequency electrically induced fatigues. *Brain Research*, 750(1-2):147–154, 1997.

[43] Bruno Vie, Nicolas Gomez, Christelle Brerro-Saby, Jean Paul Weber, and Yves Jammes. Changes in stationary upright standing and proprioceptive reflex control of foot muscles after fatiguing static foot inversion. *Journal of Biomechanics*, 46(10):1676–1682, 2013.

[44] Christelle Brerro-Saby, Stéphane Delliaux, Jean Guillaume Steinberg, and Yves Jammes. Fatigue-induced changes in tonic vibration response (TVR) in humans: Relationships between electromyographic and biochemical events. *Muscle and Nerve*, 38(5):1481–1489, 2008.

[45] J R Wright, D I McCloskey, and R C Fitzpatrick. Effects of muscle perfusion pressure on fatigue and systemic arterial pressure in human subjects. *Journal of applied physiology (Bethesda, Md. : 1985)*, 86(3):845–51, 1999.

[46] H. Degens, S. Salmons, and J. C. Jarvis. Intramuscular pressure, force and blood flow in rabbit tibialis anterior muscles during single and repetitive contractions. *European Journal of Applied Physiology and Occupational Physiology*, 78(1):13–19, 1998.

[47] Julia B Pitcher and Timothy S Miles. Influence of muscle blood flow on fatigue during intermittent human hand-grip exercise and recovery. *Clin Exp Pharmacol Physiol*, 24:471–476, 1997.

[48] Masanobu Tachi, Motoki Kouzaki, Hiroaki Kanehisa, and Tetsuo Fukunaga. The influence of circulatory difference on muscle oxygenation and fatigue during intermittent static dorsiflexion. *European Journal of Applied Physiology*, 91:682–688, 2004.

[49] Hans Degens, J Manuel Sanchez Horneros, and Maria T E Hopman. Acute hypoxia limits endurance but does not affect muscle contractile properties. *Muscle & Nerve*, 33(April):532–537, 2006.

[50] M D Cole and M A Brown. Response of the human triceps surae muscle to electrical stimulation during varying levels of blood fow restriction. *European Journal of Applied Physiology*, 82:39–44, 2000.

[51] Ian R. Lanza, Danielle M. Wigmore, Douglas E. Befroy, and Jane A. Kent-Braun. In vivo ATP production during free-flow and ischaemic muscle contractions in humans. *Journal of Physiology*, 577(1):353–367, 2006.

[52] Markus Amann, Lee M. Romer, Andrew W. Subudhi, David F. Pegelow, and Jerome A. Dempsey. Severity of arterial hypoxaemia affects the relative contributions of peripheral muscle fatigue to exercise performance in healthy humans. *Journal of Physiology*, 581(1):389–403, 2007.

[53] Bruno Grassi, Harry B. Rossiter, Michael C. Hogan, Richard A. Howlett, James E. Harris, Matthew L. Goodwin, John L. Dobson, and L. Bruce Gladden. Faster O2uptake kinetics in canine skeletal muscle in situ after acute creatine kinase inhibition. *Journal of Physiology*, 589(1):221–233, 2011.

[54] Jane A. Kent, Niels Ørtenblad, Michael C. Hogan, David C. Poole, and Timothy I. Musch. No muscle is an Island: Integrative perspectives on muscle fatigue. *Medicine and Science in Sports and Exercise*, 48(11):2281–2293, 2016.

[55] Roger M. Enoka. Mechanisms of muscle fatigue: Central factors and task dependency. *Journal of Electromyography and Kinesiology*, 5(3):141–149, 1995.

[56] Roger M. Enoka and Jacques Duchateau. Muscle fatigue: what, why and how it influences muscle function. *The Journal of Physiology*, 586(1):11–23, 2008.

[57] C J De Luca. Myoelectrical manifestations of localized muscular fatigue in humans. *Critical reviews in biomedical engineering*, 11(4):251–279, 1984.

[58] John V. Basmajianm and Carlo J. De Luca. *Muscles alive: Their functions revealed by electromyography*. Williams & Wilkins, Boltimore, 1953.

[59] Emil Heinrich Du Bois-Reymond. *Gesammelte Abhandlungen zur allgemeinen Muskel- und Nervenphysik /*, volume 1. Veit„ Leipzig :, 1875.

[60] H. Piper. *Elektrophysiologie menschlicher Muskeln*. Springer Berlin Heidelberg, Berlin, Heidelberg, 1912. ISBN 978-3-642-50634-5.

[61] Mohamed Kazamel and Paula Province Warren. History of electromyography and nerve conduction studies: A tribute to the founding fathers. *Journal of Clinical Neuroscience*, 43:54–60, 2017.

[62] Shrawan Kumar and Anil Mital. *Electromyography In Ergonomics*. CRC Press, London, 1st ed. edition, 1996. ISBN 9780748401307.

[63] Carlo J. De Luca and Roberto Merletti. Surface myoelectric signal cross-talk among muscles of the leg. *Electroencephalography and Clinical Neurophysiology*, 69(6):568–575, 1988.

[64] MS S. Redfern, RE E. Hughes, and DB B. Chaffin. High-pass filtering to remove electrocardiographic interference from torso EMG recordings. *Clinical Biomechanics*, 8(1):44–48, 1993.

[65] Luca Mesin, Stuart Smith, Suzanne Hugo, Suretha Viljoen, and Tania Hanekom. Effect of spatial filtering on crosstalk reduction in surface EMG recordings. *Medical Engineering and Physics*, 31(3):374–383, 2009.

[66] Hermie J. Hermens, Bart Freriks, Catherine Disselhorst-Klug, and Günter Rau. Development of recommendations for SEMG sensors and sensor placement procedures. *Journal of Electromyography and Kinesiology*, 10(5):361–374, 2000.

[67] Seniam. 2018.

[68] NIOSH. Selected topics in surface electromyography for use in the occupational setting: expert perspectives. *National Institute for Occupational Safety and Health*, Publication No. 91-100:1–189, 1992.

[69] Jeffrey R. Cram, Glenn S. Kasman, and Jonathan Holtz. *Introduction to surface electromyography*. Aspen Publishers, Gaithersburg, Md., 1998. ISBN 0-8342-0751-6.

[70] John V. Basmajian, editor. *Biofeedback: Principles and practice for clinicians*. Williams & Wilkins, Baltimore, 3rd ed. edition, 1989. ISBN 0-683-00357-7.

[71] T. Finni, P. V. Komi, and J. Lukkariniemi. Achilles tendon loading during walking: Application of a novel optic fiber technique. *European Journal of Applied Physiology and Occupational Physiology*, 77(3):289–291, 1998.

[72] Jack Tigh Dennerlein, Edward Diao, C. D. Mote, and David M. Rempel. Tensions of the flexor digitorum superficialis are higher than a current model predicts. *Journal of Biomechanics*, 31(4):295–301, 1998.

[73] H S Milner-Brown and R B Stein. With 7 text-ftgure8 THE RELATION BETWEEN THE SURFACE ELECTROMYOGRAM AND MUSCULAR FORCE. *J. Phy.iol*, 246:549–569, 1975.

[74] J. H. Blok, J. P. Van Dijk, G. Drost, M. J. Zwarts, and D. F. Stegeman. A high-density multichannel surface electromyography system for the characterization of single motor units. *Review of Scientific Instruments*, 73(4): 1887, 2002.

[75] Gea Drost, Dick F. Stegeman, Baziel G M van Engelen, and Machiel J. Zwarts. Clinical applications of high-density surface EMG: A systematic review. *Journal of Electromyography and Kinesiology*, 16(6):586–602, 2006.

[76] Dario Farina, Luca Mesin, Simone Martina, and Roberto Merletti. A Surface EMG Generation Model with Multilayer Cylindrical Description of the Volume Conductor. *IEEE Transactions on Biomedical Engineering*, 51(3): 415–426, 2004.

[77] Gonzalo A. García, Ryuhei Okuno, and Kenzo Akazawa. A decomposition algorithm for surface electrode-array electromyogram. *IEEE ENGINEERING IN MEDICINE AND BIOLOGY MAGAZINE*, 24(4):63–72, 2005.

[78] Andreas Holtermann, Karin Roeleveld, and J. Stefan Karlsson. Inhomogeneities in muscle activation reveal motor unit recruitment. *Journal of Electromyography and Kinesiology*, 15(2):131–137, 2005.

[79] Didier Staudenmann, Idsart Kingma, Dick F. Stegeman, and Jaap H. Van Dieën. Towards optimal multi-channel EMG electrode configurations in muscle force estimation: A high density EMG study. *Journal of Electromyography and Kinesiology*, 15(1):1–11, 2005.

[80] C J De Luca, CJ De Luca, and C J De Luca. The use of surface electromyography in biomechanics. *Journal of applied biomechanics*, 13(July 1993):1–38, 1997.

[81] A. L. Hof. The relationship between electromyogram and muscle force. *Sportverletz Sportschaden*, 11(3):79–86, 1997.

[82] T G Welter and M F Bobbert. During slow wrist movements, distance covered affects EMG at a given external force. *Motor control*, 5(1):50–60, 2001.

[83] E. A. Clancy, E. L. Morin, and R. Merletti. Sampling, noise-reduction and amplitude estimation issues in surface electromyography. *Journal of Electromyography and Kinesiology*, 12(1):1–16, 2002.

[84] D T Godin, P A Parker, and R N Scott. Noise characteristics of stainless-steel surface electrodes. *Medical biological engineering computing*, 29(6):585–590, 1991.

[85] E. Huigen, Abraham Peper, and C. A. Grimbergen. Investigation into the origin of the noise of surface electrodes. *Medical and Biological Engineering and Computing*, 40(3):332–338, 2002.

[86] A. C. Metting van Rijn, A. Peper, and C. A. Grimbergen. High-quality recording of bioelectric events - Part 1 Interference reduction, theory and practice, 1990.

[87] Suzushi Nishimura, Yutaka Tomita, and Toshio Horiuchi. Clinical application of an active electrode using an operational amplifier. *IEEE Trans. Biomed. Eng.*, 39(10):1096–1099, 1992.

[88] John G. Webster. Reducing Motion Artifacts and Interference in Biopotential Recording. *IEEE Transactions on Biomedical Engineering*, BME-31(12): 823–826, 1984.

[89] Brenda Bigland and O. C. J. Lippold. The Relation Between Force, Velocity and Integrated Electrical Activity in Human Muscles. *Journal of Physiology*, 123(1):214–224, 1953.

[90] R. H. De Jong and F. G. Freud. Relationship between electromyogram and isometric twitch tension in human muscle. *Archives of Physical Medicine and Rehabilitation*, 48(10):539–42, 1967.

[91] Herber A. DeVries. Efficiency of electrical activity as a physiological measure of the functional state of muscle tissue. *American Journal of Physical Medicine*, 47(1):10–22, 1968.

[92] L Korner, P Parker, C Almstrom, P Herberts, and R Kadefors. The relation between spectral changes of the myoelectric signal and the intramuscular pressure of human skeletal muscle. *European Journal of Applied Physiology*, 52:202–206, 1984.

[93] B A Alkner, P A Tesch, and H E Berg. Quadriceps EMG/force relationship in knee extension and leg press. *Medicine & Science in Sports & Exercise*, 32(2):459–63, 2000.

[94] P. V. Komi. Reproductibility of electromyographic measurements with inserted wire electrodes and surface electrodes. *Electromyography*, 10(4):357–67, 1970.

[95] J. R. Potvin, R. W. Norman, and S. M. McGill. Mechanically corrected EMG for the continuous estimation of erector spinae muscle loading during repetitive lifting. *European Journal of Applied Physiology and Occupational Physiology*, 74(1-2):119–132, 1996.

[96] M. Solomonow, A. Guzzi, R. Baratta, H. Shoji, and R. D'Ambrosia. EMG-force model of the elbows antagonistic muscle pair. The effect of joint position, gravity and recruitment. *American Journal of Physical Medicine*, 65 (5):223–44, 1986.

[97] P. Vink, E. A. van der Velde, and A. J. Verbout. A functional subdivision of the lumbar extensor musculature. Recruitment patterns and force-RA-EMG relationships under isometric conditions. *Electromyography and clinical neurophysiology*, 27(8):517–25, 1987.

[98] E N Zuniga and E G Simons. Nonlinear relationship between averaged electromyogram potential and muscle tension in normal subjects. *Archives of Physical Medicine and Rehabilitation*, 50(11):613–620, 1969.

[99] a C Guimaraes, W Herzog, T L Allinger, and Y T Zhang. The EMG-force relationship of the cat soleus muscle and its association with contractile conditions during locomotion. *The Journal of experimental biology*, 198(Pt 4):975–987, 1995.

[100] Moshe Solomonow, Richard Baratta, Bing He Zhou, Hiromu Shoji, and Robert D. D'Ambrosia. The EMG-Force Model of Electrically Stimulated Muscle: Dependence on Control Strategy and Predominant Fiber Composition. *IEEE Transactions on Biomedical Engineering*, BME-34(9):692–703, 1987.

[101] J J Woods and B Bigland-Ritchie. Linear and non-linear surface EMG/force relationships in human muscles. An anatomical/functional argument for the existence of both. *American journal of physical medicine*, 62(6):287–299, 1983.

[102] Didier Staudenmann, Karin Roeleveld, Dick F. Stegeman, and Jaap H. van Dieen. Methodological aspects of SEMG recordings for force estimation - A tutorial and review. *Journal of Electromyography and Kinesiology*, 20(3): 375–387, 2010.

[103] Jacquelin Perry and Judith M Burnfield. *Gait Analysis: Normal and Pathological Function*. SLACK, Thorofare, NJ, 2. ed. edition, 2010. ISBN 978-1556427664.

[104] Mark Halaki and Karen Ginn. Normalization of EMG Signals: To Normalize or Not to Normalize and What to Normalize to? In Ganesh R. Naik, editor, *Computational Intelligence in Electromyography Analysis - A Perspective on Current Applications and Future Challenges*, chapter 7. InTech, 2012. ISBN 978-953-51-0805-4, 448.

[105] P W Hodges and C A Richardson. Inefficient muscular stabilization of the lumbar spine associated with low back pain. A motor control evaluation of transversus abdominis. *Spine*, 21(22):2640–2650, 1996.

[106] R Di Fabio. Reliability of computerized surface electromyography for determining the onsent of muscle activity. *Physical Therapy*, 67(1):43–48, 1987.

[107] H. D. Eberhart, V. T. Inman, and B. Bresler. The principal elements in human locomotion. In Paul. E. Klopsteg, editor, *Human Limbs and their substitutes*, pages 437–71. McGraw-Hill, New York, 1954.

[108] Adrian Burden. How should we normalize electromyograms obtained from healthy participants? What we have learned from over 25years of research. *Journal of Electromyography and Kinesiology*, 20(6):1023–1035, 2010.

[109] A B Arsenault, D A Winter, R G Marteniuk, and K C Hayes. How many strides are required for the analysis of electromyographic data in gait? *Scandinavian journal of rehabilitation medicine*, 18(3):133–135, 1986.

[110] D A Neumann and T M Cook. Effect of load and carrying position on the electromyographic activity of the gluteus medius muscle during walking. *Physical therapy*, 65(3):305–311, 1985.

[111] G L Soderberg, T M Cook, S C Rider, and B L Stephenitch. Electromyographic activity of selected leg musculature in subjects with normal and chronically sprained ankles performing on a BAPS board. *Physical therapy*, 71(7):514–522, 1991.

[112] S. E. Mathiassen, J. Winkel, and G. M. Hägg. Normalization of surface EMG amplitude from the upper trapezius muscle in ergonomic studies - A review. *Journal of Electromyography and Kinesiology*, 5(4):197–226, 1995.

[113] G. T. Allison, R. N. Marshall, and K. P. Singer. EMG signal amplitude normalization technique in stretch-shortening cycle movements. *Journal of Electromyography and Kinesiology*, 3(4):236–244, 1993.

[114] J F Yang and D A Winter. Electromyographic amplitude normalization methods: improving their sensitivity as diagnostic tools in gait analysis. *Archives of Physical Medicine and Rehabilitation*, 65(9):517–521, 1984.

[115] G. T. Allison, P. Godfrey, and G. Robinson. EMG signal amplitude assessment during abdominal bracing and hollowing. *Journal of Electromyography and Kinesiology*, 8(1):51–57, 1998.

[116] D. A. Winter. EMG interpretation. In Shrawan Kumar and Anil Mital, editors, *Electromyography in ergonomics*, pages 109–25. Taylor & Francis, London, 1996.

[117] Frank W. Jobe, James E. Tibone, Jacquelin Perry, and Diane Moynes. An EMG analysis of the shoulder in throwing and pitching: A preliminary report. *The American Journal of Sports Medicine*, 11(1):3–5, 1983.

[118] Karin Harms-Ringdahl, J. Ekholm, K. Schüldt, J. Linder, and M. O. Ericson. Assessment of jet pilots' upper trapezius load calibrated to maximal voluntary contraction and a standardized load. *Journal of Electromyography and Kinesiology*, 6(1):67–72, 1996.

[119] Jaclyn N. Chopp, Steven L. Fischer, and Clark R. Dickerson. On the feasibility of obtaining multiple muscular maximal voluntary excitation levels from test exertions: A shoulder example. *Journal of Electromyography and Kinesiology*, 20(5):896–902, 2010.

[120] Richard A. Ekstrom, Gary L. Soderberg, and Robert A. Donatelli. Normalization procedures using maximum voluntary isometric contractions for the serratus anterior and trapezius muscles during surface EMG analysis. *Journal of Electromyography and Kinesiology*, 15(4):418–428, 2005.

[121] Craig E. Boettcher, Karen A. Ginn, and Ian Cathers. Standard maximum isometric voluntary contraction tests for normalizing shoulder muscle EMG. *Journal of Orthopaedic Research*, 26(12):1591–1597, 2008.

[122] B. T. Kelly, W. R. Kadrmas, D. T. Kirkendall, and K. P. Speer. Optimal normalization tests for shoulder muscle activation: An electromyographic study. *Journal of Orthopaedic Research*, 14(4):647–653, 1996.

[123] Nicolas J. O'Dwyer, Peter T. Quinn, B. E. Guitar, G. Andrews, and Peter D. Neilson. Procedures for verification of electrode placement in EMG studies of orofacial and mandibular muscles. *Journal of Speech Language and Hearing Research*, 24(2):273–88, 1981.

[124] K. A. Ginn, M. Halaki, and I. Cathers. Revision of the Shoulder Normalization tests is required to include rhomboid major and teres major. *Journal of Orthopaedic Research*, 29(12):1846–1849, 2011.

[125] Derek J. Rutherford, Cheryl L. Hubley-Kozey, and William D. Stanish. Maximal voluntary isometric contraction exercises: A methodological investigation in moderate knee osteoarthritis. *Journal of Electromyography and Kinesiology*, 21(1):154–160, 2011.

[126] Stuart M. McGill. Electromyographic activity of the abdominal and low back musculature during the generation of isometric and dynamic axial trunk torque: Implications for lumbar mechanics. *Journal of Orthopaedic Research*, 9(1):91–103, 1991.

[127] Jay Smith, Denny J. Padgett, Kenton R. Kaufman, Shawn P. Harrington, Kai Nan An, and Steven E. Irby. Rhomboid muscle electromyography activity during 3 different manual muscle tests. *Archives of Physical Medicine and Rehabilitation*, 85(6):987–992, 2004.

[128] H Nieminen, E P Takala, and E Viikari-Juntura. Normalization of electromyogram in the neck-shoulder region. *European journal of applied physiology and occupational physiology*, 67:199–207, 1993.

[129] Kim Hébert-Losier, Anthony G. Schneiders, José A. García, S. John Sullivan, and Guy G. Simoneau. Peak triceps surae muscle activity is not specific to knee flexion angles during MVIC. *Journal of Electromyography and Kinesiology*, 21(5):819–826, 2011.

[130] Richard A Ekstrom, Roy W Osborn, Heather M Goehner, Adam C Moen, Brian M Ommen, Michael J Mefferd, Thomas R Bergman, Timothy B Molencamp, and Steven A Kelsey. Electromyographic normalization procedures for determining exercise intensity of closed chain exercises for strengthening the quadriceps femoris muscles. *Journal of strength and conditioning research*, 26(3):766–771, 2012.

[131] Yumna Albertus-Kajee, Ross Tucker, Wayne Derman, Robert P. Lamberts, and Michael I. Lambert. Alternative methods of normalising EMG during running. *Journal of Electromyography and Kinesiology*, 21(4):579–586, 2011.

[132] Eneko Fernández-Peña, Francesco Lucertini, and Massimiliano Ditroilo. A maximal isokinetic pedalling exercise for EMG normalization in cycling. *Journal of Electromyography and Kinesiology*, 19(3):162–170, 2009.

[133] David M. Rouffet and Christophe A. Hautier. EMG normalization to study muscle activation in cycling. *Journal of Electromyography and Kinesiology*, 18(5):866–878, 2008.

[134] W. T. Liberson, M. Dondey, and M. M. Asa. Brief repeated isometric maximal exercises. An evaluation by integrative electromyography. *American journal of physical medicine*, 41:3–14, 1962.

[135] J D Lunnen, J Yack, and B F LeVeau. Relationship between muscle length, muscle activity, and torque of the hamstring muscles. *Physical therapy*, 61 (2):190–195, 1981.

[136] Verne T. Inman, H. J. Ralston, J. B. De, M. B. Bertram Feinstein, and Elwood W. Wright. Relation of human electromyogram to muscular tension. *Electroencephalography and Clinical Neurophysiology*, 4(2):187–194, 1952.

[137] Danny M. Pincivero, Yuliya Salfetnikov, Robert M. Campy, and Alan J. Coelho. Angle- and gender-specific quadriceps femoris muscle recruitment and knee extensor torque. *Journal of Biomechanics*, 37(11):1689–1697, 2004.

[138] J. E. Kasprisin and M. D. Grabiner. EMG variability during maximum voluntary isometric and anisometric contractions is reduced using spatial averaging. *Journal of Electromyography and Kinesiology*, 8(1):45–50, 1998.

[139] J. S. Leedham and J. J. Dowling. Force-length, torque-angle and EMG-joint angle relationships of the human in vivo biceps brachii. *European Journal of Applied Physiology and Occupational Physiology*, 70(5):421–426, 1995.

[140] Ann E. Barr, David Goldsheyder, Nihat Özkaya, and Margareta Nordin. Testing apparatus and experimental procedure for position specific normalization of electromyographic measurements of distal upper extremity musculature. *Clinical Biomechanics*, 16(7):576–585, 2001.

[141] Gary A. Mirka. The quantification of EMG normalization error. *Ergonomics*, 34(3):343–352, 1991.

[142] A. M. Burden, M. Trew, and V. Baltzopoulos. Normalisation of gait EMGs: A re-examination. *Journal of Electromyography and Kinesiology*, 13(6):519–532, 2003.

[143] C W Heckathorne and D S Childress. Relationships of the surface electromyogram to the force, length, velocity, and contraction rate of the cineplastic human biceps. *American journal of physical medicine*, 60(1):1–19, 1981.

[144] K B Veiersted. The reproducibility of test contractions for calibration of electromyographic measurements. *European Journal of Applied Physiology*, 62(2):91–98, 1991.

[145] Wim Dankaerts, Peter Bruce O'sullivan, Angus Firth Burnett, Leon Melville Straker, and Lieven Andre Danneels. Reliability of EMG measurements for trunk muscles during maximal and sub-maximal voluntary isometric contractions in healthy controls and CLBP patients. *Journal of Electromyography and Kinesiology*, 14(3):333–342, 2004.

[146] Andrew R. Chapman, Bill Vicenzino, Peter Blanch, Joanna J. Knox, and Paul W. Hodges. Intramuscular fine-wire electromyography during cycling: Repeatability, normalisation and a comparison to surface electromyography. *Journal of Electromyography and Kinesiology*, 20(1):108–117, 2010.

[147] Shihan Bao, Svend Erik Mathiassen, and Jorgen Winkel. Normalizing upper trapezius EMG amplitude: Comparison of ramp and constant force procedures. *Journal of Electromyography and Kinesiology*, 5(4):245–250, 1995.

[148] D. A. Winter and H. J. Yack. EMG profiles during normal human walking: stride-to-stride and inter-subject variability. *Electroencephalography and Clinical Neurophysiology*, 67(5):402–411, 1987.

[149] Beverley A. Trevithick, Karen A. Ginn, Mark Halaki, and Ronald Balnave. Shoulder muscle recruitment patterns during a kayak stroke performed on

a paddling ergometer. *Journal of Electromyography and Kinesiology*, 17(1): 74–79, 2007.

[150] Loretta M. Knutson, Gary L. Soderberg, Bryon T. Ballantyne, and William R. Clarke. A study of various normalization procedures for within day electromyographic data. *Journal of Electromyography and Kinesiology*, 4(1):47–59, 1994.

[151] A. R. Pucci, L. Griffin, and E. Cafarelli. Maximal motor unit firing rates during isometric resistance training in men. *Experimental Physiology*, 91(1): 171–178, 2006.

[152] Nicola A. Maffiuletti and Romuald Lepers. Quadriceps femoris torque and EMG activity in seated versus supine position. *Medicine and Science in Sports and Exercise*, 35(9):1511–1516, 2003.

[153] A G Cresswell, W N Löscher, and A Thorstensson. Influence of gastrocnemius muscle length on triceps surae torque development and electromyographic activity in man. *Experimental Brain Research*, 105(2):283–290, 1995.

[154] Kylie J. Tucker, Meltem Tuncer, and Kemal S. Türker. A review of the H-reflex and M-wave in the human triceps surae. *Human Movement Science*, 24(5-6):667–688, 2005.

[155] Mario Cifrek, Vladimir Medved, Stanko Tonković, and Saša Ostojić. Surface EMG based muscle fatigue evaluation in biomechanics. *Clinical Biomechanics*, 24(4):327–340, 2009.

[156] G M Hägg. Electromyographic fatigue analysis based on the number of zero crossings. *Pflügers Archiv*, 391(1):78–80, 1981.

[157] G F Inbar, O Paiss, J Allin, and H Kranz. Monitoring surface EMG spectral changes by the zero crossing rate. *Medical and Biological Engineering and Computing*, 24(1):10–18, 1986.

[158] L. Lindstrom and I. Petersen. *Power spectra of myoelectric signals: Motor-unit activity and muscle fatigue*, volume 66. Butterworth, London, 1981.

[159] D A Gabriel. Reliability of SEMG spike parameters during concentric contractions. *Electromyography and clinical neurophysiology*, 40(7):423–430, 2000.

[160] Carlo J De Luca. the Use of Surface Electromyography in Biomechanics. *Journal of Applied Biomechanics*, 13(2):135–163, 1993.

[161] Omry Paiss and Gideon F. Inbar. Autoregressive modeling of surface EMG and its spectrum with application to fatigue. *Mathematical and Computer Modelling*, 10(10):793–794, 1988.

[162] R. Merletti and L. R. Lo Conte. Advances in processing of surface myoelectric signals: Part 1. *Medical and Biological Engineering and Computing*, 33(3 SPEC. ISSUE):373–384, 1995.

[163] Alwin Luttmann, Matthias Jäger, and Wolfgang Laurig. Electromyographical indication of muscular fatigue in occupational field studies. *International Journal of Industrial Ergonomics*, 25(6):645–660, 2000.

[164] Eleanor Criswell. *Cram's Introduction to Surface Electromyography, Second Edition*. Jones and Bartlett Publishers, Sudbury, MA, 2 edition, 2010. ISBN 9780763732745.

[165] Carlo J. De Luca, L. Donald Gilmore, Mikhail Kuznetsov, and Serge H. Roy. Filtering the surface EMG signal: Movement artifact and baseline noise contamination. *Journal of Biomechanics*, 43(8):1573–1579, 2010.

[166] Thomas Kienbacher, Richard Habenicht, Christian Starek, Patrick Mair, Markus Wolf, Birgit Paul, Sara Riegler, Josef Kollmitzer, and Gerold Ebenbichler. The potential use of spectral electromyographic fatigue as a screening and outcome monitoring tool of sarcopenic back muscle alterations. *Journal of NeuroEngineering and Rehabilitation*, 11(1):106, 2014.

[167] C. Larivière, A. B. Arsenault, D. Gravel, D. Gagnon, and P. Loisel. Evaluation of measurement strategies to increase the reliability of EMG indices to assess back muscle fatigue and recovery. *Journal of Electromyography and Kinesiology*, 12(2):91–102, 2002.

[168] Christian Larivière, Rubens A. Da Silva, A. Bertrand Arsenault, Sylvie Nadeau, Andri Plamondon, and Roger Vadeboncoeur. Specificity of a back muscle roman chair exercise in healthy and back pain subjects. *Medicine and Science in Sports and Exercise*, 43(1):157–164, 2011.

[169] R A da Silva, C Larivière, A B Arsenault, S Nadeau, and A Plamondon. The comparison of wavelet- and Fourier-based electromyographic indices of back muscle fatigue during dynamic contractions: validity and reliability results. *Electromyography and clinical neurophysiology*, 48(3-4):147–162, 2008.

[170] R J Elble and J E Randall. Motor-unit activity responsible for 8- to 12-Hz component of human physiological finger tremor. *Journal of neurophysiology*, 39:370–383, 1976.

[171] Liang Ma, Damien Chablat, Fouad Bennis, Wei Zhang, and François Guillaume. A new muscle fatigue and recovery model and its ergonomics application in human simulation. In *Proceedings of IDMME - Virtual Concept 2008*, Beijing, China, 2009. ISBN 1745-2759.

[172] Jing Z Liu, Robert W Brown, and Guang H Yue. A dynamical model of muscle activation, fatigue, and recovery. *Biophysical journal*, 82(5):2344–2359, 2002.

[173] D D Wood, D L Fisher, and R O Andres. Minimizing fatigue during repetitive jobs: optimal work-rest schedules. *Human factors*, 39(1):83–101, 1997.

[174] Laura A Frey Law and Keith G. Avin. Endurance time is joint-specific: A modelling and meta-analysis investigation. *Ergonomics*, 53(1):109–129, 2010.

[175] Dapeng Yang, Huajie Zhang, Yikun Gu, and Hong Liu. Accurate EMG onset detection in pathological, weak and noisy myoelectric signals. *Biomedical Signal Processing and Control*, 33:306–315, 2017.

[176] J.F. Kaiser. On a simple algorithm to calculate the 'energy' of a signal. *International Conference on Acoustics, Speech, and Signal Processing*, 2(10): 381–384, 1990.

[177] C Lemyre, M Jelinek, and R Lefebvre. New approach to voiced onset detection in speech signal and its application for frame error concealment. In *2008 IEEE International Conference on Acoustics, Speech and Signal Processing*, pages 4757–4760, 2008. ISBN 1520-6149 VO -.

[178] Jing Chang, Damien Chablat, Fouad Bennis, and Liang Ma. Estimating the EMG response exclusively to fatigue during sustained static maximum voluntary contraction. *Advances in Intelligent Systems and Computing*, 489 (Cv):29–39, 2016.

[179] Antoni V F Nargol, Anthony P C Jones, Peter J Kelly, and Charles G Greenough. Factors in the Reproducibility of Electromyographic Power Spectrum Analysis of Lumbar Paraspinal Muscle Fatigue. *Spine*, 24(9), 1999.

[180] B. Gerdle, M. Edström, and M. Rahm. Fatigue in the shoulder muscles during static work at two different torque levels. *Clinical Physiology*, 13(5): 469–482, sep 1993.

[181] W Ament, G J Bonga, a L Hof, and G J Verkerke. Electromyogram median power frequency in dynamic exercise at medium exercise intensities. *European journal of applied physiology and occupational physiology*, 74(1-2): 180–6, 1996.

[182] W. Ament, G. J. J. Bonga, A. L. Hof, and G. J. Verkerke. EMG median power frequency in an exhausting exercise. *Journal of Electromyography and Kinesiology*, 3(4):214–220, 1993.

[183] O. C. J. Lippold. The Relation Between Integrated Action Potentials in a Human Muscle and its Isometric Tension. *Journal of Physiology*, 117: 492–499, 1952.

[184] Toshio Moritani and Herbert A DeVries. REEXAMINATION OF THE RELATIONSHIP BETWEEN THE SURFACE INTEGRATED ELECTROMYOGRAM (IEMG) AND FORCE OF ISOMETRIC CONTRACTION. *American Journal of Physical Medicine & Rehabilitation*, 57(6):263–277, 1978.

[185] J H Lawrence and C J De Luca. Myoelectric signal versus force relationship in different human muscles. *Journal of applied physiology (Bethesda, Md. : 1985)*, 54(6):1653–1659, 1983.

[186] Brian J Carnahan, Bryan A Norman, and Mark S Redfern. Incorporating physical demand criteria into assembly line balancing. *IIE Transactio*, 33: 875–887, 2001.

[187] Liang Ma, Wei Zhang, Su Wu, and Zhanwu Zhang. A new simple local muscle recovery model and its theoretical and experimental validation. *International Journal of Occupational Safety and Ergonomics*, 21(1):86–93, 2015.

[188] Paul W. Hodges, A. E.Martin Eriksson, Debra Shirley, and Simon C. Gandevia. Intra-abdominal pressure increases stiffness of the lumbar spine. *Journal of Biomechanics*, 38(9):1873–1880, 2005.

[189] Xiaoyan Li, Ping Zhou, and Alexander S. Aruin. Teager-kaiser energy operation of surface EMG improves muscle activity onset detection. *Annals of Biomedical Engineering*, 35(9):1532–1538, 2007.

[190] Haris Begovic, Guang Quan Zhou, Tianjie Li, Yi Wang, and Yong Ping Zheng. Detection of the electromechanical delay and its components during voluntary isometric contraction of the quadriceps femoris muscle. *Frontiers in Physiology*, 5(DEC):1–8, 2014.

A. Work Packages of the Thesis

Table A.1.: Work packages 1: Experimental quantification of muscle fatigue

Work Package 1	
Description	In this work package the behaviour of a single muscle during static and dynamic muscle prolonged loading is analysed. Therefore, the myoelectric signal from m. biceps brachii and m. triceps brachii are collected under different relative muscle loadings using two sEMG sensors for each muscle. In total 20 healthy subjects participate in this research. The study is divided into five static and four dynamic trials. The forces and motions in both trials are measured by a dynamometer (CON-TREX®WS, Physiomed Elektromedizin AG, Schneittach, Germany). Prior to the exhausting exercises, a maximum force measurement is performed with each subject. The collected data from this measurement is used to calculate the required relative loading individually, as well as the normalization value for the sEMG data. The five different static exercises are performed with the arm fixed in a 90° flexion angle. The subjects are advised to sustain the required force as long as possible. During the static trials the dominant arm of each participant is loaded with 60 %, 50 %, 40 %, and 30 % of predetermined maximum force. As a fifth exercise an alternating trial is conducted, where the required force level changes from 60 % to 30 % to 50 % to 40 % with a duration of 20 s. The m. biceps brachii and m. triceps brachii are measured alternately with 5 min recovery time between two measurements of the same muscle. During the dynamic protocol each subject performs four trials with 60 %, 50 %, 40 %, and 30 % relative muscle loading. The motion for the dynamic tests is defined between 45° and 135° elbow flexion with an angular velocity of $60\,^{\circ}s^{-1}$. For the dynamic tasks, each subject is advised to perform as many repetitions as possible. All collected data is processed by calculating the maximum voluntary contraction (MVC) normalized root mean square (RMS) of the signals with a window length of 100 ms as well as the median power frequency (MPF) with the same window length. The progress of these two parameters is assessed by performing a linear regression analysis and estimating the slope of the calculated fit.
Outcome	The outcome of this study is the progression of fatigue parameters in sEMG signals depending on relative muscle loading.

Table A.2.: Work packages 2: Experimental study of muscle recruitment pattern under the influence of fatigue

Work Package 2	
Description	In the second study the collaboration of different muscles during exhausting exercises is investigated. Therefore, an experiment is designed to measure the recruitment pattern of back and abdominal muscles when experiencing fatigue. The myoelectric signals of 16 different muscles is collected during static and dynamic tasks with various relative muscle loadings. In both scenarios forces and motion are measured utilizing the CON-TREX®WS dynamometer with the connected CON-TREX®TP 500 isokinetic back module for trunk flexor and extensor muscles (CON-TREX®WS, Physiomed Elektromedizin AG, Schneittach, Germany). The maximum force of each participant is determined prior to the experiment. During the isometric tasks each subject is loaded with 55 %, 45 %, and 35 % of maximum force. Each subject is advised to sustain the required force as long as possible. The isokinetic tasks are performed in a 15° flexion position of the thorax. During the dynamic tasks the subjects are loaded with 40 %, 35 %, and 30 % of maximum force. The range of motion is defined as a flexion and extension motion between 5° and 25°. The angular velocity is chosen by the subject. All collected data is processed by calculating the MVC normalized RMS and MPF with a window length of 100 ms. Afterwards, the fatigue of the main muscles in the lower back is analysed since these muscles carry the main load during the performed exercises. For the upper back as well as the abdominal muscles, the main focus is set to changes in activity. This is also analysed by studying the progresses of RMS and MPF curves from these muscles.
Outcome	The outcome of this study is the influence of fatigue on recruitment pattern of back and abdominal muscles.

Table A.3.: Work packages 3: Development of novel fatigue algorithm and implementation to the AMS

Work Package 3	
Description	In this work package the gathered results from the first two work packages and information from literature are combined to develop a numerical fatigue model that is capable of simulating the progress of fatigue for a single muscle. Therefore, the results from the former studies are described by mathematical algorithms as a function of current muscle loading, maximum force capacity and time. Subsequently, these algorithms are included to a simple model created in the AnyBody^{TM}modelling system (AMS) (AnyBody Technology, Aarhus, Denmark). As a second step, the findings from the simplified model are then transferred to the standing model from the AnyBody Managed Model Repository (AMMR). Therefore, a new muscle model is created for all muscles in the shoulder arm complex. As a third step, the novel model is validated against the measured data from the first study.
Outcome	The outcome of this work package is a validated numeric fatigue model in the AMS that is capable of simulating the fatigue of single muscles.

Table A.4.: Work packages 4: Validation of the AMS muscle recruitment with included muscle fatigue

Work Package 4	
Description	This work package is about the inclusion of the analysed recruitment pattern to the AMS. As a first step, the results from the third work package are transferred to the thoracic part of the model using the measured data from the second study. The next step is to test the behaviour of the current recruitment solver that is implemented to the AMS when the muscles are experiencing fatigue. Therefore, the exercises from the second experimental study are modelled and the findings are compared to the results from the measurements described in work package 2. Based on this comparison the recruitment algorithm in the AMS is modified to suit the recruitment patterns found in the experimental data. This new model is again validated against the measured data.
Outcome	The outcome of this work package is a validated numeric model of the upper body that is capable of simulating long-term effects and supporting the prevention of MSDs.

B. Additional AnyBody^{TM} Source Code of Upper Limb Model

Listing B.1: Linear and rotational measures and driver to fix the pelvis to the global reference system

```
AnyKinLinear PelvisFixLin = {
  AnyRefFrame &ref1 = Main.Model.EnvironmentModel.GlobalRef;
  AnyRefFrame &ref2 = Main.HumanModel.BodyModel.Trunk.SegmentsLumbar.
      PelvisSeg;
};

AnyKinRotational PelvisFixRot = {
  Type = RotAxesAngles;
  AnyRefFrame &ref1 = Main.Model.EnvironmentModel.GlobalRef;
  AnyRefFrame &ref2 = Main.HumanModel.BodyModel.Trunk.SegmentsLumbar.
      PelvisSeg;
};

AnyKinEqSimpleDriver PelvisFix = {
  DriverPos = {0,0,0,0,0,0};
  DriverVel = {0,0,0,0,0,0};
  AnyKinMeasure &lin = .PelvisFixLin;
  AnyKinMeasure &rot = .PelvisFixRot;
  Reaction.Type = {On,On,On,On,On,On};
};
```

Listing B.2: Modelling of external load in the forearm; switch for isometric and dynamic models; switch for constant force and measured force data

```
Main.HumanModel.BodyModel.Right.ShoulderArm.Seg.Radius = {

  AnyRefNode ForceNode ={
    sRel = {-0.15, 0.0, 0.0};
    //ARel = {{1.0, 0.0, 0.0}, {0.0, 1.0, 0.0}, {0.0, 0.0, 1.0}};
    AnyDrawRefFrame drw = {};
  };//ForceNode
};//Radius Seg

AnyString force_input_path = "..\Input\1712_torque_input.txt";
AnyFloat Force = -320;

#define StatDynSwitch 0
//0 for isometric models; 1 for dynamic models
#define MeasuredData 0
//0 constant force; 1 simulation with measured data



  #if StatDynSwitch == 0
#if MeasuredData == 0
AnyForce3D RightHandConst ={
  //RefFrames = ;
  //Surfaces = ;
  //KinMeasureArr = {..Linear, ..Linear, ..Linear};
  //KinMeasureIndexArr = {0, 1, 2};
  Flocal = {0.0 ,...Force, 0.0};
  //Flocal = {0.0, 0.0, 0.0};
  AnyRefNode &ref1 = ...HumanModel.BodyModel.Right.ShoulderArm.Seg.
      Radius.ForceNode;
  AnyDrawForce drw = {};
};
#endif
```

```
#if MeasuredData == 1
AnyInputFile force_inp ={
  // dynamic data
  FileName = Main.force_input_path;
};

AnyFloat T = force_inp.T;
AnyFloat force_x = force_inp.Data[0]*0;
AnyFloat force_y = force_inp.Data[0]*50/0.15;
AnyFloat force_z = force_inp.Data[0]*0; //converte [V] to [Nm] to [N]
AnyFloat inp = {force_x,-force_y, force_z};

AnyForce3D RightHand ={
  AnyFunInterpol FL_interp ={
    Type=PiecewiseLinear;
    T= ..force_inp.T;
    Data=..inp;
  };
  AnyRefNode &ref1 = ...HumanModel.BodyModel.Right.ShoulderArm.Seg.
      Radius.ForceNode;

  Flocal= FL_interp(t);
  AnyDrawForce drw = {};
};//End Force 3D

#endif//MotionData
#endif//StatDynSwitch

#if StatDynSwitch == 1
#if MeasuredData == 0
AnyForce3D RightHandConst =
{
  Flocal = {0.0, 0.0, ...Force};
  AnyRefNode &ref1 = ...HumanModel.BodyModel.Right.ShoulderArm.Seg.
      Radius.ForceNode;
```

```
  AnyDrawForce drw = {};
};
#endif

#if MeasuredData == 1
AnyInputFile force_inp ={
  // dynamic data
  FileName = Main.force_input_path;
};

AnyFloat T = force_inp.T;
AnyFloat force_x = force_inp.Data[0]*0;
AnyFloat force_y = force_inp.Data[0]*50/0.15;
AnyFloat force_z = force_inp.Data[0]*0; //converte [V] to [Nm] to [N]
AnyFloat inp = {force_x,-force_y, force_z};

AnyForce3D RightHand ={
  AnyFunInterpol FL_interp ={
    Type=PiecewiseLinear;
    T= ..force_inp.T;
    Data=..inp;
  };
  AnyRefNode &ref1 = ...HumanModel.BodyModel.Right.ShoulderArm.Seg.
      Radius.ForceNode;

  Flocal= FL_interp(t);
  AnyDrawForce drw = {};
};//End Force 3D

#endif//MotionData
#endif//StatDynSwitch
```

C. Segments and Muscles of the AMS Model to Simulate Fatigue of Shoulder and Arm Muscles

Table C.1.: Segments of the AMS model created for the simulation of fatigue of the shoulder and arm muscles

Shoulder arm segments (left and right)	
Clavicular	Radius
Scapular	WristJointSeg
Humerus	Hand
Ulna	Glove
Segments of the Trunk	
Segments Lumbar:	Segments Cervical Spine:
PelvisSeg	C1Seg
SacrumSeg	C2Seg
L5Seg	C3Seg
L4Seg	C4Seg
L3Seg	C5Seg
L2Seg	C6Seg
L1Seg	C7Seg
Segments Thorax:	
SkullSeg	
ThoraxSeg	

Table C.2.: Muscles of the AMS model created for the simulation of fatigue of the shoulder and arm muscles

Muscles of the shoulder arm region of the model	
levator_scapulae_1	subscapularis_6
levator_scapulae_2	supraspinatus_1
levator_scapulae_3	supraspinatus_2
levator_scapulae_4	supraspinatus_3
trapezius_clavicular_part_1	supraspinatus_4
trapezius_clavicular_part_2	supraspinatus_5
trapezius_clavicular_part_3	supraspinatus_6
trapezius_clavicular_part_4	teres_major_1
trapezius_clavicular_part_5	teres_major_2
trapezius_clavicular_part_6	teres_major_3
Sternocleidomastoid	teres_major_4
biceps_brachii_caput_breve	teres_major_5
biceps_brachii_caput_longum	teres_major_6
coracobrachialis_1	teres_minor_1
coracobrachialis_2	teres_minor_2
coracobrachialis_3	teres_minor_3
coracobrachialis_4	teres_minor_4
coracobrachialis_5	teres_minor_5
coracobrachialis_6	teres_minor_6
deltoideus_scapular_part_1	trapezius_scapular_part_1
deltoideus_scapular_part_2	trapezius_scapular_part_2
deltoideus_scapular_part_3	trapezius_scapular_part_3
deltoideus_scapular_part_4	trapezius_scapular_part_4
deltoideus_scapular_part_5	trapezius_scapular_part_5
deltoideus_scapular_part_6	trapezius_scapular_part_6
deltoideus_clavicular_part_1	Brachialis_1
deltoideus_clavicular_part_2	Brachialis_2
deltoideus_clavicular_part_3	Triceps_LH_1

Table C.2.: Muscles of the AMS model created for the simulation of fatigue of the shoulder and arm muscles

Muscles of the shoulder arm region of the model	
deltoideus_clavicular_part_4	Triceps_LH_2
deltoideus_clavicular_part_5	Triceps_ME_1
deltoideus_clavicular_part_6	Triceps_ME_2
infraspinatus_1	Triceps_LA_1
infraspinatus_2	Triceps_LA_2
infraspinatus_3	Brach_rad_1
infraspinatus_4	Brach_rad_2
infraspinatus_5	Anconeus_1
infraspinatus_6	Anconeus_2
latissimus_dorsi_1	Pronator_teres_caput_humeral_1
latissimus_dorsi_2	Pronator_teres_caput_humeral_2
latissimus_dorsi_3	Pronator_teres_caput_ulnare_1
latissimus_dorsi_4	Supinator_humerus_part_1
latissimus_dorsi_5	Supinator_humerus_part_2
pectoralis_major_thoracic_part_1	Pron_quadr_1
pectoralis_major_thoracic_part_2	Pron_quadr_2
pectoralis_major_thoracic_part_3	Extensor_Indicis
pectoralis_major_thoracic_part_4	Abductor_Pollicis_Longus
pectoralis_major_thoracic_part_5	Extensor_Pollicis_Brevis
pectoralis_major_clavicular_part_1	Extensor_Pollicis_Longus
pectoralis_major_clavicular_part_2	Extensor_Carpi_Radialis_Longus
pectoralis_major_clavicular_part_3	Extensor_Carpi_Radialis_Brevis
pectoralis_major_clavicular_part_4	Extensor_Carpi_Ulnaris
pectoralis_major_clavicular_part_5	Flexor_Carpi_Ulnaris
pectoralis_minor_1	Flexor_Carpi_Radialis
pectoralis_minor_2	Palmaris_Longus
Pectoralis_minor1_cyl	Flexor_Carpi_Ulnaris
pectoralis_minor_3	Flexor_Carpi_Radialis

Table C.2.: Muscles of the AMS model created for the simulation of fatigue of the shoulder and arm muscles

Muscles of the shoulder arm region of the model	
pectoralis_minor_4	Palmaris_Longus
rhomboideus_1	Flexor_Digitorum_Superficialis_Digit5
rhomboideus_2	Flexor_Digitorum_Superficialis_Digit4
rhomboideus_3	Flexor_Digitorum_Superficialis_Digit3
serratus_anterior_1	Flexor_Digitorum_Superficialis_Digit2
serratus_anterior_2	Flexor_Digitorum_Profundus_Digit5
serratus_anterior_3	Flexor_Digitorum_Profundus_Digit4
serratus_anterior_4	Flexor_Digitorum_Profundus_Digit3
serratus_anterior_5	Flexor_Digitorum_Profundus_Digit2
serratus_anterior_6	Extensor_Digitorum_Digit5
subscapularis_1	Extensor_Digitorum_Digit4
subscapularis_2	Extensor_Digitorum_Digit3
subscapularis_3	Extensor_Digitorum_Digit2
subscapularis_4	Extensor_Digitorum_Minimi
subscapularis_5	Flexor_Pollicis_Longus

D. Segments and Muscles of the AMS Model to Study Muscle Recruitment Pattern

Table D.1.: Segments of the AMS model created for investigating recruitment pattern of the back muscles during exhausting exercises

Shoulder arm segments (left and right)	
Clavicular	Radius
Scapular	WristJointSeg
Humerus	Hand
Ulna	Glove
Segments of the Trunk	
Segments Lumbar:	Segments Cervical Spine:
PelvisSeg	C1Seg
SacrumSeg	C2Seg
L1Seg	C3Seg
L2Seg	C4Seg
L3Seg	C5Seg
L4Seg	C6Seg
L5Seg	C7Seg
Segments Thorax:	
PelvisSeg	
SacrumSeg	
Segments Buckle:	
Buckle Slider2 Seg	Disc3 Disc DiscSeg
Buckle Slider3 Seg	Disc3 Disc VirtuelSeg
Buckle Slider4 Seg	Disc4 Disc DiscSeg
Buckle Slider5 Seg	Disc4 Disc VirtuelSeg
Disc1 Disc DiscSeg	Disc5 Disc DiscSeg
Disc1 Disc VirtuelSeg	Disc5 Disc VirtuelSeg
Disc2 Disc DiscSeg	
Disc2 Disc VirtuelSeg	
Segments of the Legs (left and right)	
Talus	
Foot	
Shank	
Patella	
Thigh	

Table D.2.: Muscles of the AMS model created for the investigation of recruitment pattern of the back and abdominal muscles

Muscles of the upper body of the model	
RotMuscleZPos	Extensor_PolliciBrevis
RotMuscleZNeg	Extensor_PolliciLongus
RotMuscleYPos	Extensor_Carpi_RadialiLongus
RotMuscleYNeg	Extensor_Carpi_RadialiBrevis
RotMuscleXPos	Extensor_Carpi_Ulnaris
RotMuscleXNeg	Flexor_Carpi_Ulnaris
levator_scapulae_1	Flexor_Carpi_Radialis
levator_scapulae_2	PalmariLongus
levator_scapulae_3	Flexor_Digitorum_SuperficialiDigit5
levator_scapulae_4	Flexor_Digitorum_SuperficialiDigit4
trapeziuclavicular_part_1	Flexor_Digitorum_SuperficialiDigit3
trapeziuclavicular_part_2	Flexor_Digitorum_SuperficialiDigit2
trapeziuclavicular_part_3	Flexor_Digitorum_ProfunduDigit5
trapeziuclavicular_part_4	Flexor_Digitorum_ProfunduDigit4
trapeziuclavicular_part_5	Flexor_Digitorum_ProfunduDigit3
trapeziuclavicular_part_6	Flexor_Digitorum_ProfunduDigit2
SternocleidomastoidPar	Extensor_Digitorum_Digit5
bicepbrachii_caput_breve	Extensor_Digitorum_Digit4
bicepbrachii_caput_longum	Extensor_Digitorum_Digit3
coracobrachiali1	Extensor_Digitorum_Digit2
coracobrachiali2	Extensor_Digiti_Minimi
coracobrachiali3	Flexor_PolliciLongus
coracobrachiali4	MFdL1L3Par
coracobrachiali5	MFdL3L5Par
coracobrachiali6	MFdL4S1Par
deltoideuscapular_part_1	MFdL5S1Par
deltoideuscapular_part_2	MFmL1L4Par
deltoideuscapular_part_3	MFdL2L4Par

Table D.2.: Muscles of the AMS model created for the investigation of recruitment pattern of the back and abdominal muscles

Muscles of the upper body of the model	
deltoideuscapular_part_4	MFmL2L5Par
deltoideuscapular_part_5	MFmL3S1Par
deltoideuscapular_part_6	MFmL4SacrumPar
deltoideuclavicular_part_1	MFmL5SacrumPar
deltoideuclavicular_part_2	MFtsL1L5Par
deltoideuclavicular_part_3	MFtsL1S1Par
deltoideuclavicular_part_4	MFtsL2L5Par
deltoideuclavicular_part_5	MFtsL2S1Par
deltoideuclavicular_part_6	MFtsL3LigamentPar
infraspinatu1	MFtsL4SacrumPar
infraspinatu2	MFtsL5SacrumPar
infraspinatu3	MFtstL1SIPSPar
infraspinatu4	MFtstL2SIPSPar
infraspinatu5	ILplL1CIPar
infraspinatu6	ILplL2CIPar
latissimudorsi_1	ILplL3CIPar
latissimudorsi_2	ILplL4CIPar
latissimudorsi_3	LTplL1SIPSPar
latissimudorsi_4	LTplL2SIPSPar
latissimudorsi_5	LTplL3SIPSPar
pectoralimajor_thoracic_part_1	LTplL4SIPSPar
pectoralimajor_thoracic_part_2	LTplL5IliumPar
pectoralimajor_thoracic_part_3	ILptC5SIPSPar
pectoralimajor_thoracic_part_4	ILptC6SIPSPar
pectoralimajor_thoracic_part_5	ILptC7CIPar
pectoralimajor_clavicular_part_1	ILptC8CIPar
pectoralimajor_clavicular_part_2	ILptC9CIPar
pectoralimajor_clavicular_part_3	ILptC10CIPar

Table D.2.: Muscles of the AMS model created for the investigation of recruitment pattern of the back and abdominal muscles

Muscles of the upper body of the model	
pectoralimajor_clavicular_part_4	ILptC11CIPar
pectoralimajor_clavicular_part_5	ILptC12CIPar
pectoraliminor_1	LTptT1L1Par
pectoraliminor_2	LTptT2L2Par
pectoraliminor_3	LTptT3L3Par
pectoraliminor_4	LTptT4L4Par
rhomboideu1	LTptT5L5Par
rhomboideu2	LTptT6S1Par
rhomboideu3	LTptT7S2Par
serratuanterior_1	LTptT8S3Par
serratuanterior_2	LTptT9S4Par
serratuanterior_3	LTptT10SacrumPar
serratuanterior_4	LTptT11SacrumPar
serratuanterior_5	LTptT12SacrumPar
serratuanterior_6	PMT12I_TMPar
subscapulari1	PML1I_TMPar
subscapulari2	PML1T_TMPar
subscapulari3	PML2I_TMPar
subscapulari4	PML2T_TMPar
subscapulari5	PML3I_TMPar
subscapulari6	PML3T_TMPar
supraspinatu1	PML4I_TMPar
supraspinatu2	PML4T_TMPar
supraspinatu3	PML5_TMPar
supraspinatu4	PML5T_TMPar
supraspinatu5	QLC12_CIPar
supraspinatu6	QLL1_CIPar
teremajor_1	QLL2_CIPar

Table D.2.: Muscles of the AMS model created for the investigation of recruitment pattern of the back and abdominal muscles

Muscles of the upper body of the model	
teremajor_2	QLL3_CIPar
teremajor_3	QLL4_CIPar
teremajor_4	RA_Par
teremajor_5	OEC7_RSPar
teremajor_6	OEC8_RSPar
tereminor_1	OEC9_RSPar
tereminor_2	OEC10_RSPar
tereminor_3	OEC11_CIPar
tereminor_4	OEC12_CIPar
tereminor_5	OICI_C12Par
tereminor_6	OICI_C11Par
trapeziuscapular_part_1	OICI_C10Par
trapeziuscapular_part_2	OICI_RS1Par
trapeziuscapular_part_3	OICI_RS2Par
trapeziuscapular_part_4	OICI_RS3Par
trapeziuscapular_part_5	Transversus
trapeziuscapular_part_6	MFL1T8Par
Brachiali1	MFL1T9Par
Brachiali2	MFL1T10Par
TricepLH_1	MFL2T9Par
TricepLH_2	MFL2T10Par
TricepME_1	MFL2T11Par
TricepME_2	MFL3T10Par
TricepLA_1	MFL3T11Par
TricepLA_2	MFL3T12Par
Brach_rad_1	MFL4T11Par
Brach_rad_2	MFL4T12Par
Anconeu1	MFL5T12Par

Table D.2.: Muscles of the AMS model created for the investigation of recruitment pattern of the back and abdominal muscles

Muscles of the upper body of the model	
Anconeu2	SEL1T8Par
Pronator_terecaput_humeral_1	SEL1T10Par
Pronator_terecaput_humeral_2	SEL1T11Par
Pronator_terecaput_ulnare_1	SEL2T9Par
Supinator_humerupart_1	SEL2T10Par
Supinator_humerupart_2	SEL2T11Par
Supinator_ulna_part_1	SEL2T12Par
Supinator_ulna_part_2	SEL3T11Par
Pron_quadr_1	SEL3T12Par
Pron_quadr_2	SPL1T3Par
Extensor_Indicis	SPL1T4Par
Abductor_PolliciLongus	SPL1T5Par

E. Additional Results of Experimental Study of Muscle Fatigue Progress

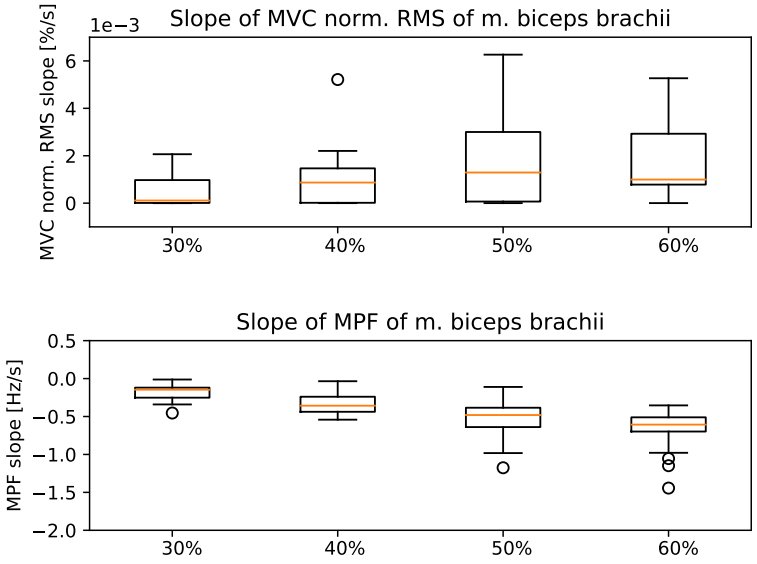

Figure E.1.: Slope of MVC normalized RMS from m. biceps brachii from isometric fatigue protocol (top); Slope of the MPF from m. biceps brachii from isometric fatigue protocol (bottom); both MVC normalized RMS and MPF derived from additional m. biceps brachii sensor

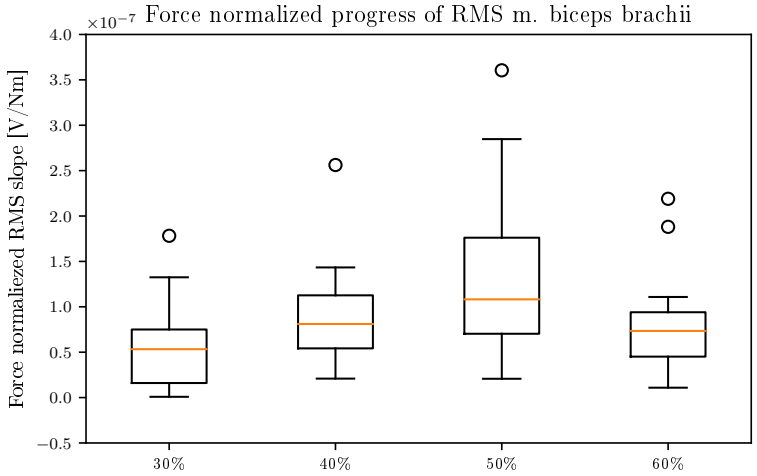

Figure E.2.: Slope of force normalized RMS of m. biceps brachii from isometric fatigue protocol derived from the additional sensor

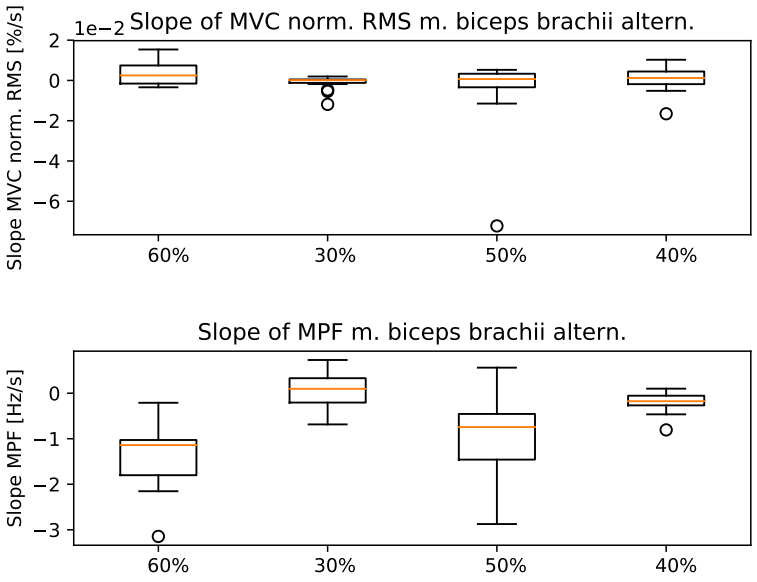

Figure E.3.: Slope of MVC normalized RMS from m. biceps brachii from alternating fatigue protocol (top); Slope of the MPF from m. biceps brachii from alternating fatigue protocol (bottom)

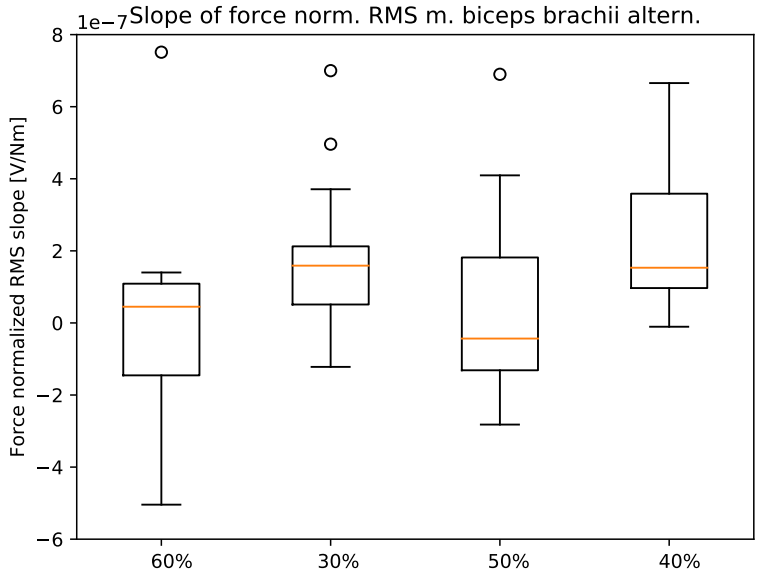

Figure E.4.: Slope of force normalized RMS from m. biceps brachii from alternating fatigue protocol

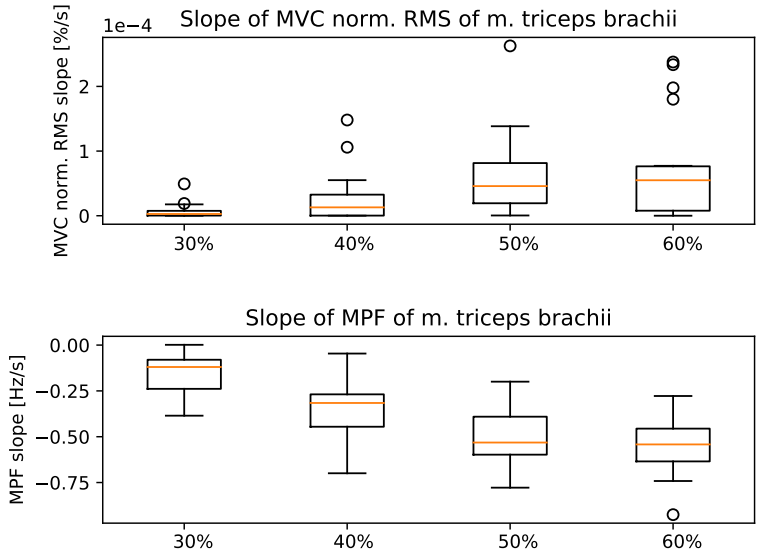

Figure E.5.: Slope of MVC normalized RMS from m. triceps brachii (top); Slope of the MPF from m. triceps brachii (bottom)

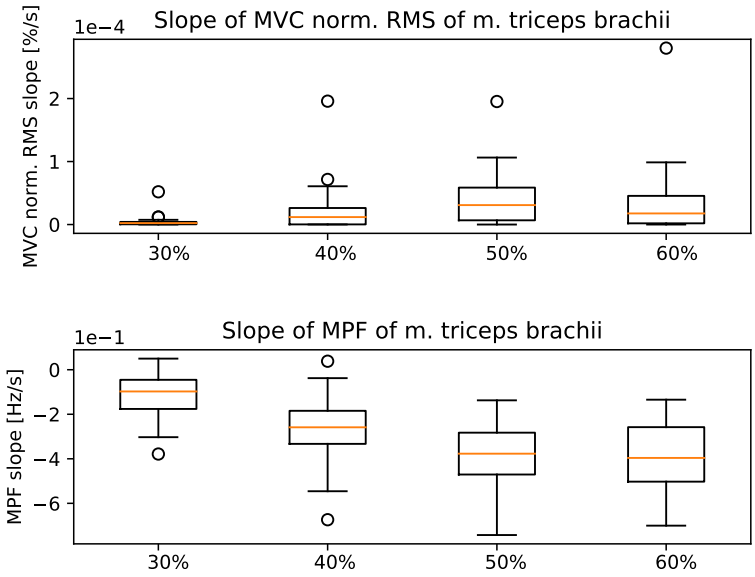

Figure E.6.: Slope of MVC normalized RMS from m. triceps brachii from isometric fatigue protocol (top); Slope of the MPF from m. triceps brachii from isometric fatigue protocol (bottom); both MVC normalized RMS and MPF derived from additional m. triceps brachii sensor

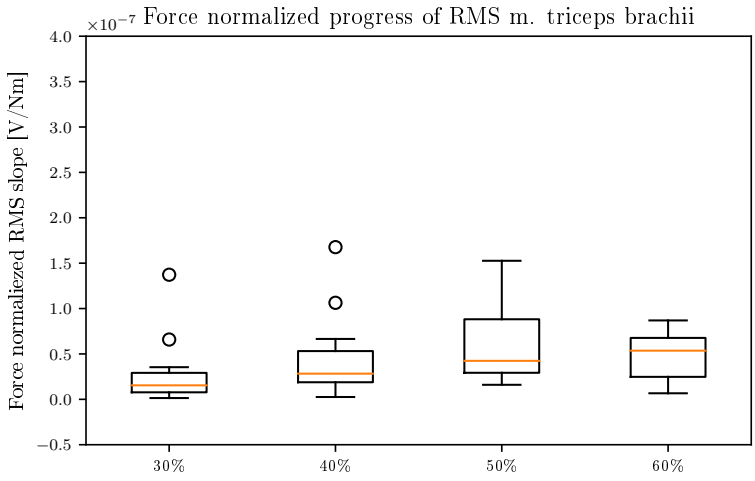

Figure E.7.: Slope of force normalized RMS from m. triceps brachii from isometric fatigue protocol

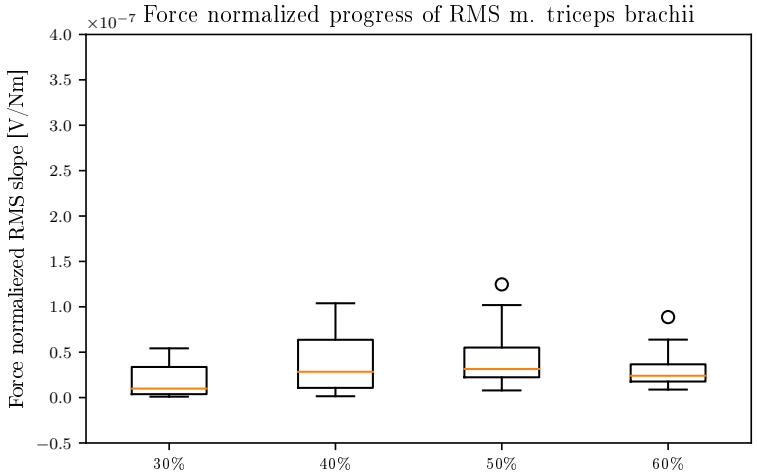

Figure E.8.: Slope of force normalized RMS of m. triceps brachii from isometric fatigue protocol derived from the additional sensor

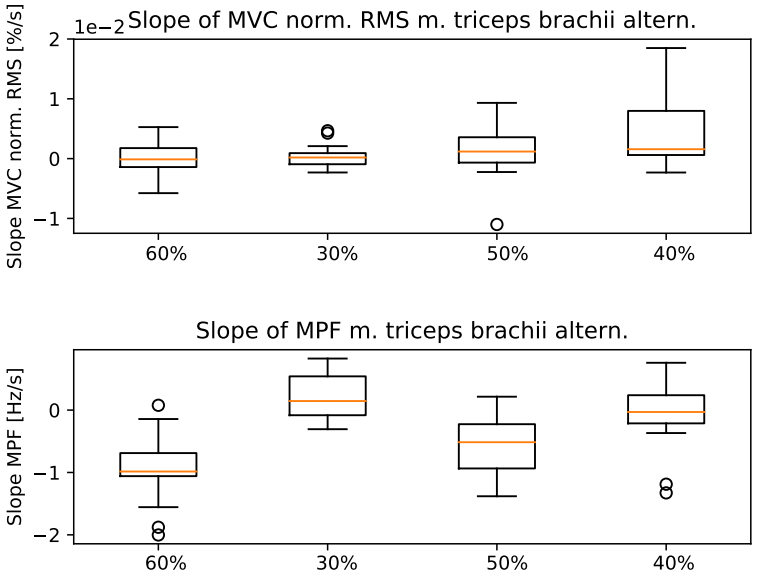

Figure E.9.: Slope of MVC normalized RMS from m. triceps brachii (top); Slope of the MPF from m. triceps brachii (bottom)

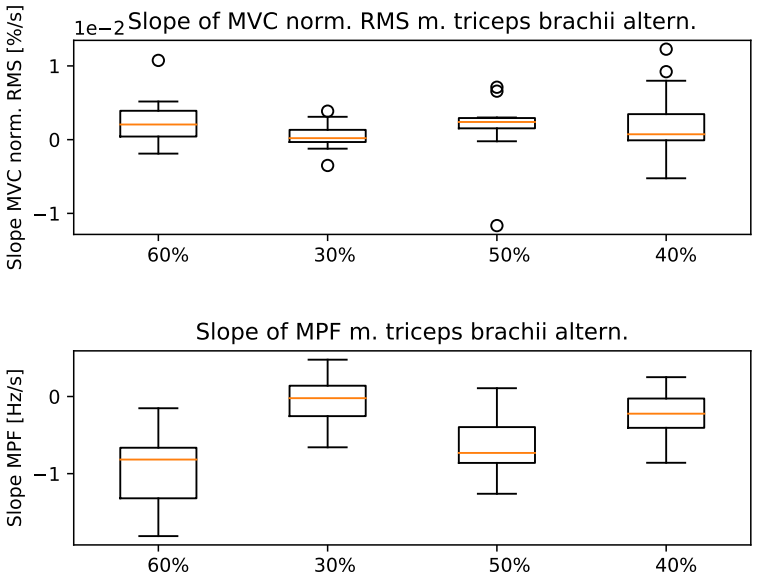

Figure E.10.: Slope of force normalized RMS of m. triceps brachii from isometric fatigue protocol derived from the additional sensor

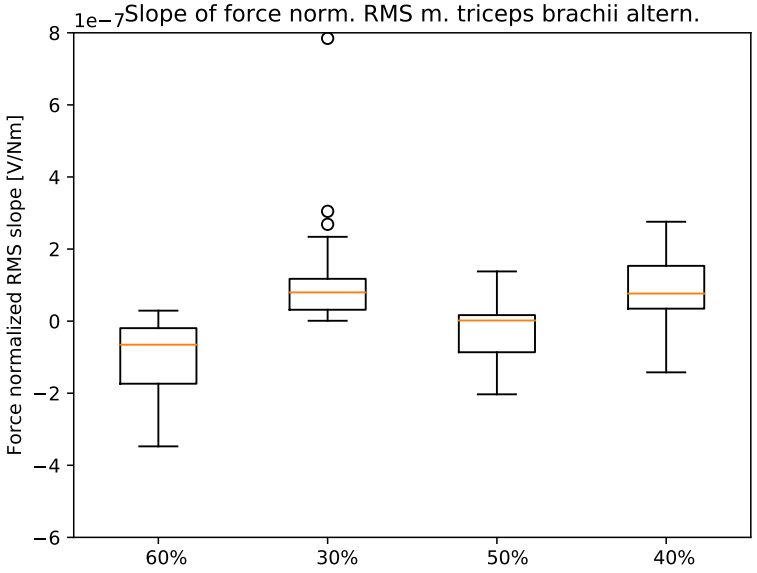

Figure E.11.: Slope of force normalized RMS from m. triceps brachii from alternating fatigue protocol

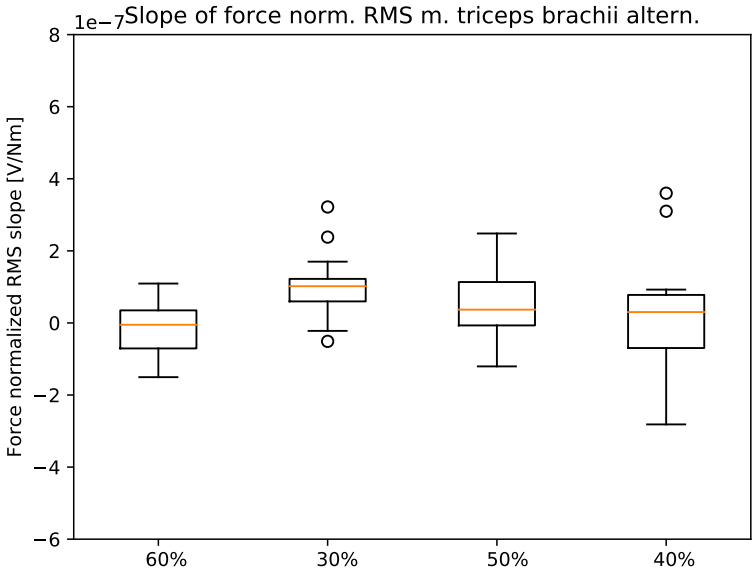

Figure E.12.: Slope of force normalized RMS from m. triceps brachii from alternating fatigue protocol

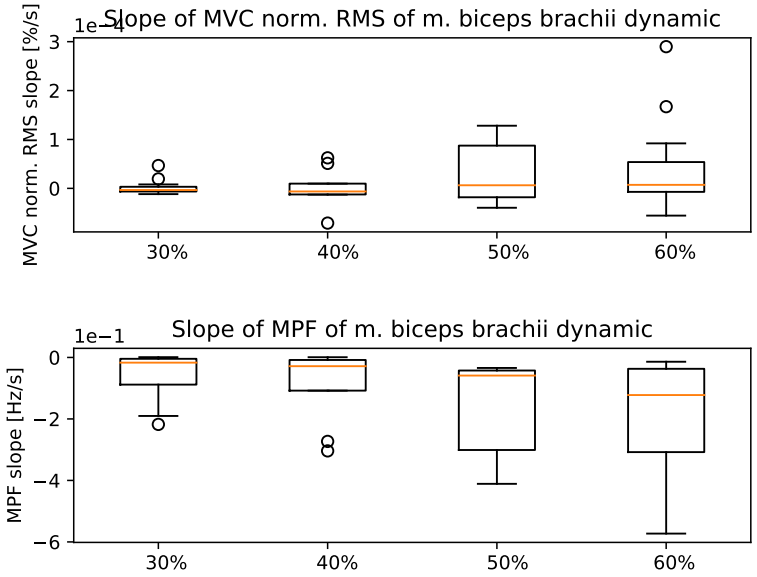

Figure E.13.: Slope of MVC normalized RMS from m. biceps brachii from dynamic fatigue protocol (top); Slope of the MPF from m. biceps brachii from dynamic fatigue protocol (bottom); both MVC normalized RMS and MPF derived from additional m. biceps brachii sensor

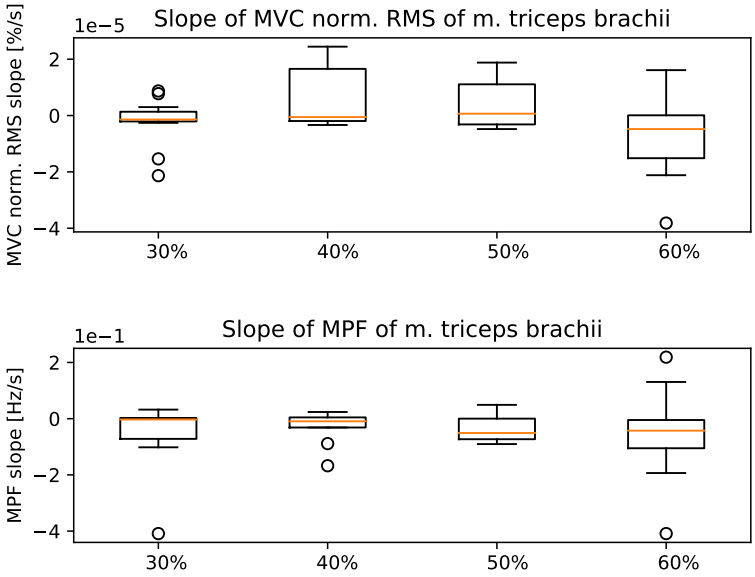

Figure E.14.: Slope of MVC normalized RMS from m. triceps brachii from dynamic fatigue protocol (top); Slope of the MPF from m. triceps brachii from dynamic fatigue protocol (bottom); both MVC normalized RMS and MPF derived from additional m. triceps brachii sensor

Lebenslauf
Simon Groß

// Persönliche Angaben

Geburtsdatum	14.04.1985, Straubing
Anschrift	Roter-Brach-Weg 42, 93049 Regensburg
Nationalität	deutsch
Familienstand	ledig, keine Kinder
Telefon	0160/8746798
E-Mail	simon-gross@outlook.de

// Ausbildung und Berufserfahrung

01/2014 – heute

Wissenschaftlicher Mitarbeiter
Labor für Biomechanik, OTH Regensburg

- Promotionsprojekt, Universität Regensburg: Muscle Fatigue in Musculoskeletal Numerical Models
  - Entwicklung von Algorithmen zur Erfassung von Muskelermüdung in numerischen Modellen
  - Entwickeln von Validierungsstrategien
  - Planung und Durchführung von experimentellen Studien
  - Programmieren von Auswertungstools
- Projektplanung sowie Betreuung von Mitarbeitern und Studenten
- Numerische Berechnung von Kontaktspannungen zwischen Knochen und Prothesen
- Numerische Festigkeitsanalyse von Prothesen
- Lehraufträge:
  - Musculoskeletal Computation (Mehrkörpersimulation)
  - Grundlagen der Programmierung (Matlab)
- Artikel:
  - Boning Up – ANSYS Software Simulates the Stresses and Strains on Bones of Individual Patients to Study a New Hip Implantation Method (ANSYS ADVANTAGE – Volume X, Issue 1, 2016)
  - FEA of the transiliacal internal fixator as an osteosynthesis of pelvic ring fractures In: Badnjevic A. (eds) CMBEBIH 2017. IFMBE Proceedings, vol 62. Springer, Singapore
- Konferenzbeiträge:
  - European Congress on Computational Methods in Applied Sciences and Engineering 2016 – *Simulating fatigue in musculoskeletal models using surface electromyography*
  - 23rd Congress of the European Society for Biomechanics 2017 – *Investigation of external load dependent static and dynamic muscle fatigue*
  - 8th World Congress of Biomechanics 2018 – *Combined experimental and numerical approach to investigate changes in muscle recruitment pattern of the back muscles during exhausting exercise*

03/2012 – 10/2013

Master of Science, Mechanical Engineering
OTH Regensburg

- Masterarbeit: FE Analysis of Stresses of the Pelvis during Side Impact

- Projektarbeit: Simulation of Material Test by Nakajima (FEM)
- Projektarbeit: Co-Simulation of a Six Degree of Freedom Manipulator to determine controlling algorithms and multi-sensory data fusion

10/2007 – 02/2012 **Bachelor of Engineering, Maschinenbau**
HS Regensburg

- Bachelorarbeit: Aufbau und Inbetriebnahme einer Electrospinning Apparatur zum Einsatz im Tissue Engineering
- Schwerpunkt: Konstruktion und Entwicklung
- Praktisches Studiensemester:
  Maschinenfabrik Reinhausen, Regensburg
  - Berechnung und Simulation von Schaltzeiten
  - Entwicklung von Prototypen Prüfmuster
  - Erstellen von 3D Konstruktionsmodellen
  - Erstellen von Zeichnungsableitungen (Solid Edge)
  - Verwalten von Modellen und Zeichnungen mit SAP

10/2006 – 07/2007 **Kurse Wirtschaftsinformatik**
Universität Regensburg

09/1995 – 07/2005 **Abitur**
Veit-Höser-Gymnasium, Bogen

// Weitere Qualifikationen

CAD Software	Solid Edge, Creo Elements
Simulations Software	LS Dyna, Ansys Classic, Ansys Workbench, AnyBody Modeling System, Recurdyn, MSC Adams
Messtechnik	Motion Capture (VICON), Kraftmessung (HBM Quantum), EMG Messungen (Delsys)
Programmiersprachen	Matlab, Python
Sprachen	Deutsch (Muttersprache), Englisch (Fließend in Wort und Schrift), Spanisch (Grundkentnisse)

SELBSTÄNDIGKEITSERKLÄRUNG

Ich, Simon Groß geboren am 14.04.1985 in Straubing erkläre hiermit, dass ich die vorliegende Arbeit ohne unzulässige Hilfe Dritter und ohne Benutzung anderer als der angegebenen Hilfsmittel angefertigt habe.
Die aus anderen Quellen direkt oder indirekt übernommenen Daten und Konzepte sind unter Angabe der Quelle gekennzeichnet. Insbesondere habe ich nicht die entgeltliche Hilfe von Vermittlungs- bzw. Beratungsdiensten (Promotionsberater oder andere Personen) in Anspruch genommen.
Die Arbeit wurde bisher weder im In- noch im Ausland in gleicher oder ähnlicher Form einer anderen Prüfungsbehörde vorgelegt.

Ort, Datum

eigenhändige Unterschrift
des Promovenden